INFORMATION TO USERS

This manuscript has been reproduced from the microfilm master. UMI films the text directly from the original or copy submitted. Thus, some thesis and dissertation copies are in typewriter face, while others may be from any type of computer printer.

The quality of this reproduction is dependent upon the quality of the copy submitted. Broken or indistinct print, colored or poor quality illustrations and photographs, print bleedthrough, substandard margins, and improper alignment can adversely affect reproduction.

In the unlikely event that the author did not send UMI a complete manuscript and there are missing pages, these will be noted. Also, if unauthorized copyright material had to be removed, a note will indicate the deletion.

Oversize materials (e.g., maps, drawings, charts) are reproduced by sectioning the original, beginning at the upper left-hand corner and continuing from left to right in equal sections with small overlaps.

Photographs included in the original manuscript have been reproduced xerographically in this copy. Higher quality 6" x 9" black and white photographic prints are available for any photographs or illustrations appearing in this copy for an additional charge. Contact UMI directly to order.

Bell & Howell Information and Learning
300 North Zeeb Road, Ann Arbor, MI 48106-1346 USA
800-521-0600

UMI®

PHYSICAL BEHAVIOR
OF
SUPERABSORBENT HYDROGELS
IN
SAND

by

Jaspreet Singh

Department of Chemical Engineering
McGill University
Montreal, Quebec
Canada

November 1997

A Thesis Submitted to the Faculty of Graduate Studies and Research
In Partial Fulfillment of the Requirements
For the Degree of
Doctor of Philosophy

National Library
of Canada

Acquisitions and
Bibliographic Services

395 Wellington Street
Ottawa ON K1A 0N4
Canada

Bibliothèque nationale
du Canada

Acquisitions et
services bibliographiques

395, rue Wellington
Ottawa ON K1A 0N4
Canada

Your file Votre référence

Our file Notre référence

0-612-44587-9

for Dilreen

It flashes, swells, and rises! One
More moment and it will be done.

Johann Wolfgang von Goethe
in Faust

The city of Jahilia is built entirely in sand... It is a sight to wonder at: walled, four-gated, the whole of it is a miracle worked by its citizens, who have learned the trick of transforming the fine white dune-sand of those forsaken parts, — the very stuff of inconstancy, — the quintessence of unsettlement, shifting, treachery, lack-of-form, — and have turned it, by alchemy, into the fabric of their newly invented permanence... The fortunes of the city of Jahilia are built on the supremacy of sand over water.

Salman Rushdie
in The Satanic Verses

Abstract

Swelling equilibrium and kinetics of two commercial superabsorbent gel particles —sodium polyacrylate spheres and polyacrylamide-co-potassium acrylate grains— were studied in water and in sand at room temperature. Equilibrium experiments involved swelling gel particles at different depths in saturated sand columns packed with different sand sizes. Kinetic experiments were performed in a two-dimensional cell; both gel particle size and sand particle size were varied. Water flow in gel-conditioned sand was also investigated in columns and the two-dimensional cells for different gel dosages.

The equilibrium swelling degree of gels in saturated sand was less than in water; decreasing sharply with depth in the first few centimeters, independent of sand particle size, then decreasing gradually with depth. A model was developed to describe equilibrium swelling in sand using the Flory model for polymer gels and a Cavity-Expansion model for frictional sand.

For individual gel particles the kinetic relationship between the fractional approach to equilibrium and the square root of time was sigmoidal for swelling in water and in saturated sand. This relationship was described by a model based on Fick's first law which accounted for the movement of the boundary of the gel and the time variation of the polymer volume fraction at the surface.

When water was distributed from the top of a uniform gel-conditioned bed, a gel layer formed on the surface. The gel particles, initially in the sand, were set free by the impact of the water. The released gel particles settled less rapidly than the denser sand particles. One minute after the initial disturbance of the dry sand-gel mixture, the water-borne particles settled on the surface to form a swelling gel layer.

In the water flow experiments the advance of the wetting front was impeded, while surface movement increased, with increasing gel dosages. Two models were developed to describe flow in gel-conditioned sand: Swelling Soil model and Instantaneous Equilibrium model. Both models were based on Darcy's law and accounted for the movement of solids.

Résumé

La cinétique et l'état d'équilibre lors du gonflement de particules de gel de deux superabsorbants commerciaux, le polyacrylate de sodium particules sphériques et l'acrylate de polyacrylamide-co-potassium acrylate en grains, ont été étudié à température ambiante dans un milieu composé de sable et d'eau. Pour étudier l'état d'équilibre un protocole expérimental a été mis en place utilisant des particules de gel ayant une capacité d'expansion. Les particules ont été placées a différentes hauteurs dans une colonne garnie saturée en sable de différentes tailles. Les expériences destinées à étudier la cinétique, ont été réalisées dans une cellule bidimensionnelle en faisant varier les tailles des particules de gel et de sable. L'écoulement de l'eau dans un milieu sablonneux mélangé avec des particules de gel a également fait l'objet d'une étude dans des colonnes et des cellules bidimensionelles pour différentes proportions de gel.

Le degré de gonflement des gels obtenu à l'équilibre dans du sable saturé a été inférieur a celui obtenu dans l'eau. Ce dernier s'avéra indépendant de la taille des grains de sable. La profondeur a une grande influence sur le degré qui a diminué partement dans les prémiers centimètres et graduellement ensuite. Un modèle été développé pour décrire l'equilibre d'expansion dans le sable, utilisant le modèle de Flory pour les gels de polymères et un modéle Cavity-Expansion pour du sable abrasif.

Pour chaque particule de gel, la relation cinétique entre l'approche fractionnelle vers l'équilibre et la racine carrée du temps a été sigmoïde pour un gonflement dans milieu eau sable saturé. Cette relation à été décrite par un modèle pour décrire basé sur la première loi de Fick qui tient en compte le mouvement de la surface du gel et la variation temporelle de la Fraction volumique en polymère à la surface.

Avec une alimentation en eau effectuée par le haut du lit une cauche de gel s'est formée à la surface. Les particules de gel, initialement dans le sable, ont été libérées par l'impact de l'eau. Ces dernières particules sédimentèrent moins rapidement que les grains de sable plus denses. Une minute après la perturbation initiale du mélange sable-gel, les particules suspendues dans l'eau se stablisèrent à la surface pour former une couche de particules gonflées.

Dans les expériences caractérisant l'écoulement de l'eau, la progression du front humide a été retardée en augmentant les proportions en gel. En même temps, le mouvement de la surface a augmenté. Deux modèles ont été développés pour décrire l'écoulement dans un milieu sablonneux contenant des particlues de gel: le modèle Swelling Soil et le modèle Instantaneous Equilibrium. Les deux modèles ont utilisé la loi de Darcy et ont tenu compte du mouvement de particules solides.

Acknowledgments

I would like to express my thanks to Professor Martin E. Weber for good advice on both *representing* and *intervening*. I extend my thanks to Professor Juan H. Vera for fruitful discussions. For their tremendous assistance, I would like to thank Ms. Anne Pirhoda, Ms. Pat Fong, Mr. Bill Habib, Mr. Ed. Siliauskas, Mr. A. Gagnon, Mr. Charles Dolan, and to the past and present members of the Gels/Separations research group at the Chemical Engineering Department. I am also indebted to the Brace Research Institute for financial support, to Professor Robert Bonnell (Department of Agricultural Engineering) for use of equipment and good discussions, to Dr. Maher Al-Jabari for critical comments, and to Mr. Arnaud Mercier for translating the abstract.

Contents

Nomenclature

Lower Case Letters

a	Ratio of horizontal to vertical pressure
c	Molar concentration of mobile ions inside the gel
c^*	Molar concentration of mobile ions in external solution
c_s	Molar electrolyte concentration in the gel
c_s^*	Molar electrolyte concentration in the external solution
e	Ratio of volume of voids to volume of solids
e_{max}	Maximum void ratio
e_{min}	Minimum void ratio
f	Phenomenological friction coefficient
f_g^o	Mass fraction of gel
g	Acceleration of gravity
k	Permeability coefficient
q	Overpressure on surface
r	Eulerian coordinate (radial)
r_c	Correlation coefficient
t	Time
t'	Modified time
t_K	Boundary time constant
u_i	Velocity of phase *i*
v_R	Polymer velocity at surface
m	Cartesian material coordinate
x_i	Mole fraction of component *i*
z_f	Fraction of monomeric units on gel

Upper Case Letters

D_m	Mutual diffusion coefficient
D_{eff}	Effective diffusion coefficient

NOMENCLATURE

D_i^*	Self diffusion coefficient of phase *i*
D_{col}	Diameter of column
D_r	Relative density
D_{soil}	Coefficient in Swelling Soil model
F	Fractional approach to equilibrium
G	Bulk modulus
ΔG	Change in Gibbs free energy
H	Depth; Height of the column
K	Parameter of gel elasticity
K_h	Hydraulic conductivity
M^{∞}	Mass of fully swollen gel
M^{o}	Mass of dry gel
M	Initial position of the surface of gel-conditioned sand
P_c	Cavity pressure
P_o	Pressure at gel surface; mean effective stress
P_{ext}	External pressure on gel
P_{atm}	Atmospheric pressure
Q	Mineralogy coefficient
R	Gas constant
R_o	Initial radius of gel sphere; Initial radius of spherical cavity
$R(t)$	Position of boundary at time *t*
T	Absolute Temperature
T_g	Glass Transition Temperature
V^{∞}	Volume of fully swollen gel
V^{o}	Volume of dry gel
V_s	Molar volume of solvent
V_m	Molar volume of the monomeric unit

Greek Letters

ϕ	Angle of friction
ϕ_r	Residual friction angle
ψ	Angle of dilation

NOMENCLATURE

α	$(1-\sin\phi)/(1+\sin\phi)$
β	$(2-\sin\psi)/(1+\sin\psi)$
ξ	$(R_c-R_o)/(R_o)$
ρ_i	Density of phase or component *i*
ρ_w	Density of water
ρ_s	Density of sand
γ	Specific gravity of sand
χ	Polymer-solvent interaction parameter
δ	Relative swelling ratio
σ	Stress
σ^*	Yield stress
ε	Strain
ε_i	Volume fraction of phase *i*
ε_i^o	Initial volume fraction of phase *i*
ω	Retardation factor
η, α	Parameters
μ_i	Chemical potential of component *I*
μ_c	Friction coefficient between constrained mass and wall
μ	Viscosity
ν	Number of ions into which the dissolved salt dissociates
φ_i	Volume fraction of phase *i* in the gel
φ_p^*	Normalized polymer volume fraction
φ_p^o	Polymer volume fraction at time zero
φ_p^∞	Polymer volume fraction at equilibrium
τ	Dimensionless time based on t and R_o
$\tau_{\kappa'}$	Dimensionless time constant based on t_κ and R_o
Φ	Ratio of final to initial gel mass or volume. Also, the ratio of initial to final polymer volume fractions.
Φ_t	Ratio of gel mass or volume at time t to dry gel mass or volume.
$\Phi_{H=0}$	Swelling ratio at zero depth.
Π	Osmotic pressure

NOMENCLATURE

Θ_i	Volume fraction of phase *i*
Ψ	Potential
Ω_{soil}	Coefficient in Swelling Soil model

List of Figures

List of Tables

Chapter 1

INTRODUCTION

Sandy soils have a low water holding ability. In addition, these soils, being largely located in semi-arid areas, receive limited rainfall. Studies indicate that water-absorbent polymer hydrogels, commonly known as superabsorbents, improve the water holding capacity of these soils (Anon, 1975; Moore, 1993). Traditionally, sandy soils have been conditioned by humus and clay to improve their agricultural potential. What makes superabsorbents different is their ability, even at very low dosages, to transform sand to water-rich topsoil in a few hours (Azzam, 1986).

1.1 SUPERABSORBENTS

Superabsorbent polymer hydrogels (Peppas 1986, Alamdal 1993, Gehrke 1994) are three-dimensional polymeric networks that swell in aqueous solutions. The network may be crosslinked either physically or chemically. In physically crosslinked gels, the network structure is formed by van der Waals forces, by hydrogen bonds or by ionic interactions. Because this crosslinking is weak, such gels dissolve in aqueous solutions. On the other hand, chemically crosslinked polymeric (ionic or non-ionic) networks do not dissolve in water. Superabsorbents belong to the latter category. To qualify as a superabsorbent, the dry material should spontaneously imbibe a minimum of 20 times its own weight of aqueous fluid while retaining its identity as a bead, a fiber, etc. (Brannon-Peppas, 1990). The hydrogel resulting from the transformation of the dry superabsorbent has sufficient integrity to resist flow and fusion with neighboring particles. The exact properties of a superabsorbent depend on the amount and type of polymer and crosslinker used.

Most superabsorbent polymer gels are hard or glassy when dry. When immersed in water, gels shift from the glassy state to the rubbery state due to water absorption. Above the glass transition temperature, T_g, a polymer is in the rubbery state, i.e. it is soft and elastic and can be easily deformed. Below T_g, a polymer is in the glassy state; stiff and hard and difficult to deform. A rubbery polymer readily changes its configuration in response to the stresses induced by penetrant molecules because, above T_g, thermal energy is available for doing so. Since glassy polymers deform with difficulty, their sorption behavior differs from that of rubbery polymers. For superabsorbent gels the transition from the glassy to the rubbery state usually occurs very early in the course of swelling.

Several reviews, articles and symposium series are available on superabsorbents. Buchholz (1994-a) described new superabsorbent polymers, ways to optimize absorption and the design of the shape of polymer particles: wrinkled, irregular, clusters, granules, fibers, rods, spheres. In a separate paper, Buchholz (1994-b) discussed several applications of superabsorbents, mentioned methods of synthesis, and listed the analytical techniques used to characterize them.

1.2 SOIL

Soil is a porous medium composed of solid grains and an interstitial pore space that usually contains air and aqueous phases. The solid particles are various organic and inorganic materials. The organic matter consists of plant and animal residues, whereas the inorganic minerals may be quartz, feldspar, colloidal silicates, etc.

SOIL MATRIX

The solids form the matrix or 'skeleton' of the soil. The soil matrix may or may not be rigid. The particle type (clay, sand, or silt), particle size distribution, and particle-to-particle cohesion determine the behavior of the soil matrix by influencing the shape, size and volume fraction of soil pores.

SOIL WATER

Sandy soils do not hold water well and much of the water passes down through the soil. Water that moves downward and is not held by the soil is called *gravitational water*. Silt loams and silts hold the most available water (*capillary water*) for plant growth even though much of the total water is unavailable. As the clay content of soil increases, the soils hold more water, however, much of the water (*hygroscopic water*) is held so tightly that plants cannot absorb it. A sandy soil may contain about 5 kg of water per 100 kg of oven-dried solid phase, whereas a clay soil may contain more than 5 times as much water.

1.3 SUPERABSORBENT —OR GEL— CONDITIONED SOILS

Although the properties of superabsorbents have been known since the 1930s, only in the 1960s did commercial development begin, first for disposable diapers. The addition of superabsorbents to soils was first made possible in 1951 with the introduction of hydrolyzed polyacrylonitrile (HPAN) under the trade name Krilium (Swanson, 1953). Inspite of good results, it was soon realized that using HPAN was uneconomical, even at low dosage. The recent popularity of superabsorbents for use in soils is primarily due to a new generation of materials with better physico-chemical properties and lower cost. Most commercially available superabsorbents for use in soils belong to three main categories:

- crosslinked sodium or potassium polyacrylates
- crosslinked polyacrylamide containing ionogenic groups, most often in the form of polyacrylic acid, poly(methacrylic acid), or their alkali metal salts.

- natural polymers like cellulose, starch, lignin, dextran, alginates, etc. modified by grafting synthetic hydrophilic polymers, like polyacrylamide, polyacrylonitrile or polyacrylic acid.

Superabsorbent gel particles distributed in sandy soil produce the following changes. They

- increase water holding capacity
- decrease water infiltration
- decrease water evaporation
- improve aeration
- reduce erosion and water run off

Consequently, these translate into

- less expenditure on irrigation
- stronger, larger plants with more extensive root systems
- earlier seed emergence and crop maturity
- more efficient water utilization by plants
- more response to fertilizers and to new crop varieties
- less plant disease related to poor soil aeration

Superabsorbent conditioned sandy soils may approach the desirable physical, chemical, bacteriological and agronomical properties of arable lands. The stability of gel-conditioned soils was found to be almost 4-fold that of clay soil, because gel-conditioned soils are free of shrinkage, cracking and crust formation (Azzam, 1980; Blodgett, 1993). In addition, superabsorbent conditioning of sandy soils may decrease water evaporation and transpiration rates below those of clay soils.

Superabsorbents-in-soil help plants make better use of fertilizers according to studies by Azzam *et al.* (1983, 1985). In addition, bacteriological fertility becomes significantly higher which causes marked increase in germination, plant growth and development in superabsorbent-conditioned sandy soils.

Superabsorbents induce *artificial aggregation* in sand (Azzam, 1980), which unlike clay is not cohesive. The number and size of water-stable aggregates increases with the rate of application. Moreover, gel treated soil promotes growth of soil bacteria, reduces compaction of soil, prevents crust formation, imparts friability, and controls erosion. Aggregation of soil particles may be due to hydrogen-bonding association or polymer bridging. Superabsorbents in soil are, in a way, a replacement for natural aggregating agents in healthy soils, for instance, polysaccharides, proteins, etc.

Superabsorbents may also alleviate major problems associated with traditional irrigation methods such as canal irrigation, which causes excessive salinity and accumulation of harmful chemicals in soils. Because superabsorbents depend on rainfall, and not artificial irrigation techniques, continued use of these materials may not change the chemical composition of soils.

Azzam (1986) showed that gel additives even at a dosage of 50 to 140 $kg.ha^{-1}$ provide a productivity in sandy soils at a level obtainable by treatment with 20 % (of the order of hundreds of tons per hectare) alluvial deposits. He also suggested that the presence of plants in the soil improves the superabsorbent efficiency. There are also indications that gel-conditioning is more economical than drip irrigation (Azzam, 1985).

Prospects for large scale use of superabsorbent materials under field conditions depend on

- the availability of raw material.
- safety of the product.
- economic feasibility.
- biodegradability or gel longevity.

While this work was in progress several small companies began to sell superabsorbents for soil applications. These companies are highly visible on the internet and are advertising superabsorbents as, "authoritative material for use with trees, shrubs, flower beds, turf, forestry, hydromulching, by landscape architects, landscapers, nurserymen, greenhouse operators, reclamation, forestry and engineering firms."

1.4 SUPERABSORBENTS IN GAS, WATER, AND SOIL

Most studies on superabsorbents-in-soil have focused on the changes brought about in the overall bulk properties of the gel conditioned soils, for instance, water holding capacity. On the other hand, extensive experimental, theoretical and modeling studies exist in the area of superabsorbents-in-water. Some studies carried out on superabsorbents-in-gas have also been reported.

SUPERABSORBENTS-IN-GAS

Claims have been made regarding the use of superabsorbents for cultivation without liquid irrigation. Azzam (1983) argued that the hygroscopic nature of gels makes them suitable for application to arid lands which lie near the sea coast where humidity exceeds 70 %. Although this proposal seems reasonable, gel particles swell very little in humid air, e.g., Kazanskii (1992) reported a swelling degree as low as 3-3.5g/g at 99% relative humidity as opposed to 500 g/g when the same gel was immersed in water.

SUPERABSORBENTS-IN-WATER

Dry superabsorbents absorb 20-1000 times their weight of water or aqueous solutions. Extensive literature exists on gel swelling experiments (Flory, 1979; Illavsky et al., 1982, 1985; Gehrke, 1994).

The work done on superabsorbents-in-water indicates that water absorption and release characteristics are affected by the choice of ionizable functional group, specific crosslinking agent, level of crosslinking, polymer amount and backbone sequence, and gel fabrication method. In addition, the shape of the superabsorbent material has an influence, e.g. spheres swell faster than slabs or cylinders.

SUPERABSORBENTS-IN-SOIL

Three reviews, coming from diverse areas such as polymer chemistry (Kazanskii and Dubrovskii, 1992), soil management (Azzam, 1980) and horticulture (Orzolek, 1993), summarize progress in the field. Most reports of experimental work on superabsorbents-in-soils (Al-Omran *et al.*, 1987, 1991; El-Shafei *et al.*, 1992) suggest that superabsorbents:

- cause swelling of the soil matrix
- reduce the effective mean pore radius
- decrease water penetrability
- decrease hydraulic conductivity

Azzam (1985) reported a decrease in bulk density and an increase in voids caused by application of polyacrylamide gels. He proposed that the size distribution of the soil pores was shifted from water draining pores towards smaller water retaining capillaries. This increases the water retention and decreases the evaporation rates in sandy soils, thus imparting clay like properties.

1.5 THIS WORK

Soils host a variety of complex biological, physical and chemical processes as shown in the topmost triangle in Figure 1.1. This thesis was confined to the physico-chemical aspects. No attempt was made to study the absorption of the gel-retained water by plants. The system was composed of three main constituents: superabsorbent gel, water, and sand matrix. Real soils are composed of clay, and sand, and organic matter. In this work silica sand was used instead of a soil because sand has the lowest possible water holding capacity. In addition, it provided a system free of the swelling effects of clay. Three areas were investigated: equilibrium swelling, kinetics of swelling, and flow through gel-conditioned sand.

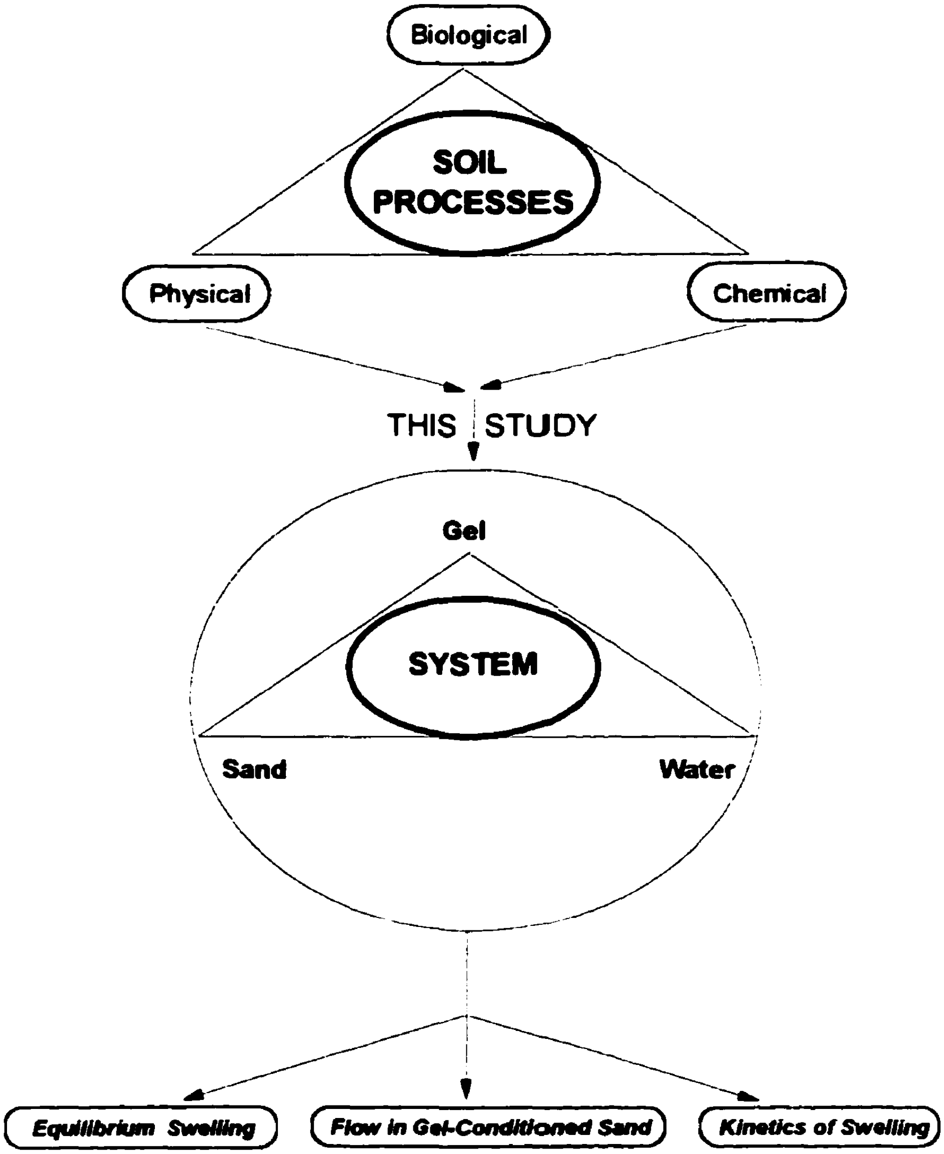

FIGURE 1.1. Conceptual framework of this study.

1.6. LIST OF POSSIBLE EXPERIMENTAL VARIABLES

A large number of independent variables might affect swelling of superabsorbent particles in sand. The variables may be classified under 5 headings:

(1) Sand Variables
  - composition
  - shape
  - size distribution

(2) Gel Variables
  - material
  - shape
  - size distribution

(3) Interaction Variables
  - dosage of gel
  - initial gel distribution in sand
  - initial bulk density distribution
  - initial soil water distribution

(4) Water Variables
  - initial pH
  - initial salt content
  - feed water composition

(5) Run Variables
  - cyclic/single process
  - initial sand depth
  - sand column dimensions
  - method of supplying water
  - method of removing water

In this work, the effects of sand size, gel material, gel size, gel distribution, and gel dosage were studied.

1.7. OBJECTIVES

1. To measure and model the equilibrium swelling of individual superabsorbent particles in water and in water-saturated sand.
2. To measure and model the kinetics of swelling of individual superabsorbent particles in water and in water-saturated sand.
3. To measure and model the effect of superabsorbent conditioning on the flow of water in sand.

1.8. ORGANIZATION OF THE THESIS

Chapter 2 describes the superabsorbents and reports experiments involving equilibrium in water and in saturated sand. An equilibrium swelling model from polymer science is combined with a cavity expansion model from soil science to describe the experimental data. In Chapter 3, the technique used to visualize gel particles in sand is described along with experiments involving the kinetics of swelling in water and in saturated sand. A moving boundary model for free swelling in water is extended to include large gel volume changes in water and in saturated sand. Chapter 4 reports experiments on flow of water into superabsorbent-conditioned sand. It describes the mechanism of formation of a gel layer at the surface. Two models are developed to describe this flow. Finally, the conclusions, contributions to knowledge, relevance of this study to agricultural applications, and recommendations for further work are presented in Chapter 5.

Chapter 2

EQUILIBRIUM SWELLING

2.1. INTRODUCTION

This chapter describes equilibrium swelling of gel particles in sand. The guiding question for this chapter is, How different is the equilibrium swelling degree of superabsorbents in sand from that in water. First, experiments involving equilibrium swelling of the selected superabsorbents are described and discussed. Next, Flory's equilibrium swelling model from polymer science is presented along with a cavity expansion model from soil science. Finally, the two models are combined to describe the experimental data. This chapter also includes a section that introduces the gel materials and the sand type used throughout the course of the study.

2.2. EXPERIMENTAL

2.2.1 DEFINITIONS

The swelling ratio of the gels is defined as

$$\Phi = \frac{M^{\infty}}{M^{\circ}} \qquad (2.1)$$

where M^{∞} and M^{0} are the fully swollen and dry masses of the gel particle, respectively. For constant and equal densities of the solvent and the polymer phases, the above is the same as the equilibrium volume ratio

$$\Phi = \frac{V^{\infty}}{V^{\circ}} \qquad (2.2)$$

where V^{∞} and V^{o} are the fully swollen and dry volumes of the gel, respectively.

2.2.2 SUPERABSORBENT MATERIALS

For gel experiments in sand, the gels must have high absorption capacity, high rate of absorption, and high strength. In addition, their residual monomer content must be low and the gel particles must maintain their integrity throughout the course of swelling experiments. The two materials described in Table 2.1 were used in this work.

TABLE 2.1. Superabsorbent Materials.

NAME	CHEMICAL NAME	CHEMICAL STRUCTURE	PARTICLE SIZE / SHAPE
STOCKOSORB (AP® 40K, 41K) Manufacturer: Stockhausen Greensboro, USA	Crosslinked polyacrylamide-co-potassium acrylate	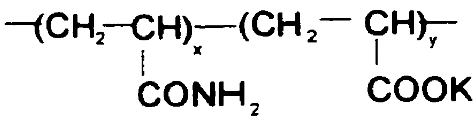 $-(CH_2-\underset{CONH_2}{CH})_x-(CH_2-\underset{COOK}{CH})_y-$	1000-2000 μm Granular
SUMITOMO (AQUA KEEP® J-440) Manufacturer: Sumitomo Co. Osaka, JAPAN	Crosslinked sodium polyacrylate	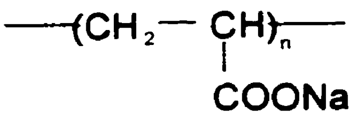 $-(CH_2-\underset{COONa}{CH})_n-$	500-800 μm Spherical

STOCKOSORB GELS are irregular granules produced by grinding lumps of the dry, solid polymer. According to the manufacturer, the gels have a specific gravity approximately equal to 1. These gels were used as received. The chemical structure of the gels, shown in Table 2.1, has *x* to *y* ratio equal to 1.5.

SUMITOMO GELS are crosslinked spheres produced by emulsion polymerization. According to the manufacturer, the gels have a specific gravity approximately equal to 1. These gels are supplied as dry aggregates about 750 μm in size. Each aggregate comprises several spheres and swells to about 5-9 mm in distilled water. From a fully swollen aggregate, it is easy to separate the individual spheres, most of which are 1 mm in size or larger. By swelling a number of 10 g batches of Sumitomo gel, it was possible to separate single spheres 5 mm or larger, which were then used for swelling experiments.

2.2.3 SAND

Silica sand was obtained from *A&C Ltd. (Montreal, Quebec)* and narrowly sieved into 4 average particle sizes: 720 μm, 475 μm, 300 μm, and 190 μm as listed in Table 2.2.

TABLE 2.2. Sand sizes.

FRACTION #	AV. DIAMETER, μm	MIN. DIAMETER, μm	MAX. DIAMETER, μm
1	720	595	841
2	475	354	595
3	300	250	354
4	190	125	250

Sand was used as received from the supplier and not washed. Dry sand, as received, was packed into a Plexiglas column, 30 cm high and 6.9 cm in diameter, with a perforated bottom with holes smaller than the sand size. Distilled water was distributed from the top of the column and allowed to drain through the bottom. The drained water was collected in a 500 ml container. In this water dry gel particles were swollen. Particles were also swollen in an equal volume of fresh distilled water. After equilibration, the mass of the gel particles, was measured to ± 0.1 mg with an electronic microbalance. The swelling ratio of the gels in the water drained through the sand and distilled water was identical within ±1%. Therefore, sand was used as received from the supplier and not washed.

2.2.4 PROCEDURE

PRETREATMENT

Each gel particle was dialyzed for 24 hours in distilled water to remove unreacted monomers and oligomers trapped in the network. The water was replaced every 8 hours. The gels so obtained were dried at room temperature and stored in 50 ml sealed glass bottles. Following drying, the weight of each gel particle, was measured to ± 0.1 mg with an electronic microbalance.

SWELLING IN WATER

The swelling experiments were performed at room temperature in a Plexiglas column, 60 cm high and 6.9 cm in diameter, filled with distilled water. Dry gel particles in tea bags were suspended at different levels. Each tea bag was tied to a long string which was held by a stand at the top of the column. The free end of the string, which hung beneath the tea bag, was attached to 1 cm diameter steel sphere to maintain the depth of the tea bag inside the column. After 12 hours, which is approximately six times the time required for the gels to reach equilibrium size, the tea-bags were removed quickly and opened to recover the swollen gel particles. The excess surface water on the gel particles was blotted with a J-cloth and the particles were weighed to ± 0.1 mg with an electronic microbalance. The reproducibility of the experimental results was determined by swelling 10 replicates in distilled water. The 95% confidence interval values of swelling ratio for Stockosorb and Sumitomo gels were 550 ± 7.4 and 170 ± 2.3 , respectively, or about ±1.3% for both gels.

SWELLING IN SAND

Equilibrium swelling experiments were performed at room temperature in a Plexiglas column, 60 cm high and 6.9 cm in diameter, as shown in Figure 2.1. The column had a perforated bottom with 100 μm diameter holes to support the sand. The column was sectioned at three different levels: 2 cm, 28 cm, and 54 cm from the top. Three Plexiglas rings, with O-rings attached to their inner sides, held the column sections together. Dry sand of a given mesh size was packed into the column in the increments of 5 cm right to the top. Three gel particles were placed at 1 cm, at 30 cm, and at 55 cm from the top as the column was packed with dry sand and their locations were marked on the outer wall of the column. Next, distilled water was distributed from the top of the column and allowed to drain through the bottom. This step removed air entrapped inside the column. The column was then placed inside a larger column, 70 cm high and 12 cm in diameter, filled with distilled water. The water level in the outer column was maintained at the same level as the sand surface in the inner column, thus ensuring saturation of the sand. After 12 hr, which is approximately 3 times the time required by gels to reach equilibrium size, the sectioned column was removed and dismantled in stages to recover the swollen gel particles from each of the three levels.

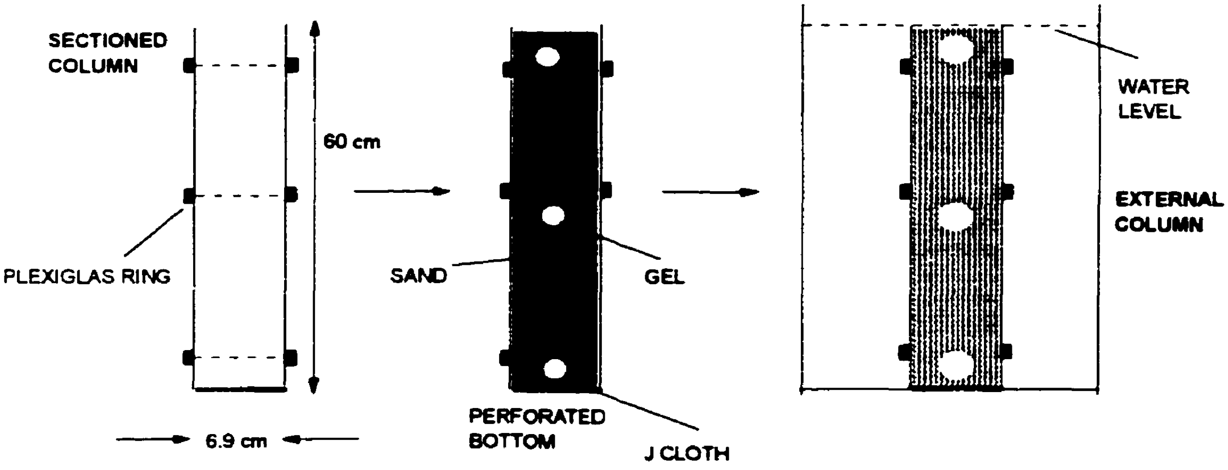

FIGURE 2.1 Schematic setup of the equilibrium swelling sectioned column experiments.

The particles swollen 55 cm below the surface were removed before those at 30 cm which, in turn, were removed before those at 1 cm. The column was dismantled as follows: The Plexiglas ring sealing the bottom and the middle sections was slipped down to expose the seam in between the bottom and the middle sections of the column. A thin steel plate was pushed through the seam to separate the lower section of the column of sand. The steel plate became the new base for the column, thus preventing sand and water from flowing out. Next, a sharp hollow stainless steel cylinder of 1 cm diameter external diameter, 0.99 cm internal diameter, and 3 cm long was inserted inside the bottom section, along the marks labeling the location of the gels, to scoop out sand samples containing the swollen gel particles. The top of the cylinder was then gently tapped to extrude the sample which was collected on a J-cloth. The sand cylinder was then gently spread out until the gel particle was found.

During this stage, the gel particles required careful handling because the potential for damage was high. Although encountered rarely, some gel particles deteriorated physically as evidenced by the appearance of large cracks or by fragmentation into smaller particles. Such particles were discarded. Extreme care was taken to prevent physical damage to a gel particle while locating, handling, washing, and transferring it. The above procedure was repeated to recover the other gel particles from the remaining sections.

Adhering to the recovered gel particles was a layer of sand particles which could not be removed by simply shaking the gel particles. The sand on each gel particle was removed by placing the sand-covered gel particle on a J-cloth, and washing it quickly with distilled water. The wash procedure took less than 5 seconds. Some water was absorbed by the gel during washing, but the amount absorbed was no more than 3% of the particle weight. The approximate weight gain of 3% was determined by washing sand-free partially swollen gel particles, which were 50% of their equilibrium swelling ratio. Following washing, the mass of each gel particle, was measured to ± 0.1 mg with an electronic microbalance.

The weight of water absorbed was reduced by 3% to account for absorption during washing.

The reproducibility of the experimental results was determined by swelling 10 replicates in distilled water saturated 190 μm sand at 1 cm depth. The 95% confidence interval values of swelling ratio for Sumitomo and Stockosorb gels were 385 ± 8.3 and 146.2 ± 3.4 , respectively. Due to the nature of sand, the confidence interval is wider here than in case of gels swollen in distilled water [Sumitomo: ±2.2% (sand) vs ±1.3% (water) of the mean; Stockosorb: ±2.3% (sand)) vs ±1.3% (water) of the mean].

2.2.5 RESULTS

Hydrostatic pressure has a weak effect on the equilibrium swelling behavior of both gels in water. Figure 2.2 shows the swelling ratio as a function of depth below the surface of distilled water. The gels swelled the most at the top of the column: Φ was 550 for the Sumitomo gel and 170 for the Stockosorb gel. With increasing depth, the swelling ratio decreased, but the decrease was less than 13% at 55 cm depth.

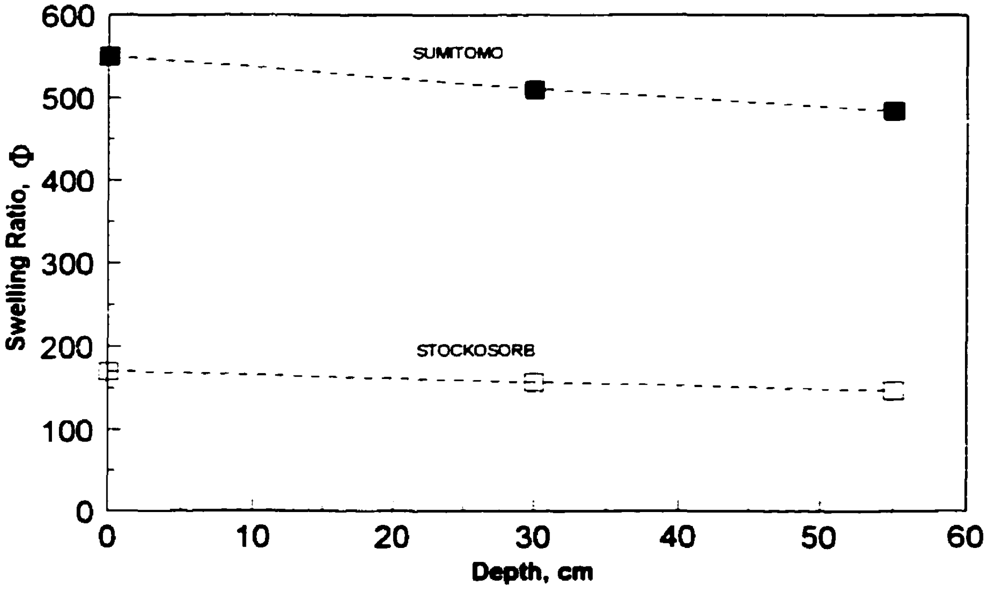

FIGURE 2.2 Swelling ratio (Φ) as a function of depth for Sumitomo (■) and Stockosorb (□) gels in a water column. The dashed lines are drawn to guide the eye.

When swollen in saturated sand, the two gels behaved differently. Figures 2.3 and 2.4 show the swelling ratio as a function of depth and sand size for Sumitomo and Stockosorb gels, respectively. At the surface of sand, i.e. at zero depth, the gels attained swelling degrees identical to those for free swelling in water. However, for gels buried in saturated sand the swelling ratio decreased rapidly with depth in the first few centimeters. This behavior is attributed to the resistance of sand to shearing through friction between the particles. Both Sumitomo and Stockosorb gels exhibited this precipitous drop in swelling ratio; although the Stockosorb gels experienced a larger drop. The particles buried at depths of 30 cm and 55 cm swelled less than gels close to surface, however the drop in swelling ratio between the depths of 1 cm and 55 cm was relatively small.

Figures 2.3 and 2.4 reveal that the drop in gel swelling ratio in the first few centimeters was independent of the diameter the of the sand particles. At increasing depths, however, the swelling ratio became a function of sand particle diameter, with smaller sand sizes giving lower swelling ratios. Once again, the frictional nature of sand is responsible for this effect. Smaller sand particles have more particle-to-particle contacts per unit volume of saturated sand than the larger particles thus resisting movement more as the gel swells. Sumitomo gels absorb about 3 times as much water as Stockosorb gels, both in water and in saturated sand. This is largely due to the higher ionic content of the Sumitomo gel.

The results described above involved swelling of initially dry gel particles in saturated sand. Another way to arrive at an equilibrium is to swell the gel particles in water and, when fully swollen, to transfer them to saturated sand where they will shrink to an equilibrium size. Figures 2.5 and 2.6 show the swelling ratio for this different path to an equilibrium for Sumitomo and Stockosorb gels, respectively. Subsequently these experiments are referred to as shrinking experiments. In both figures, the equilibrium swelling ratio is plotted as a function of depth and sand size. For larger sand particle diameters, both

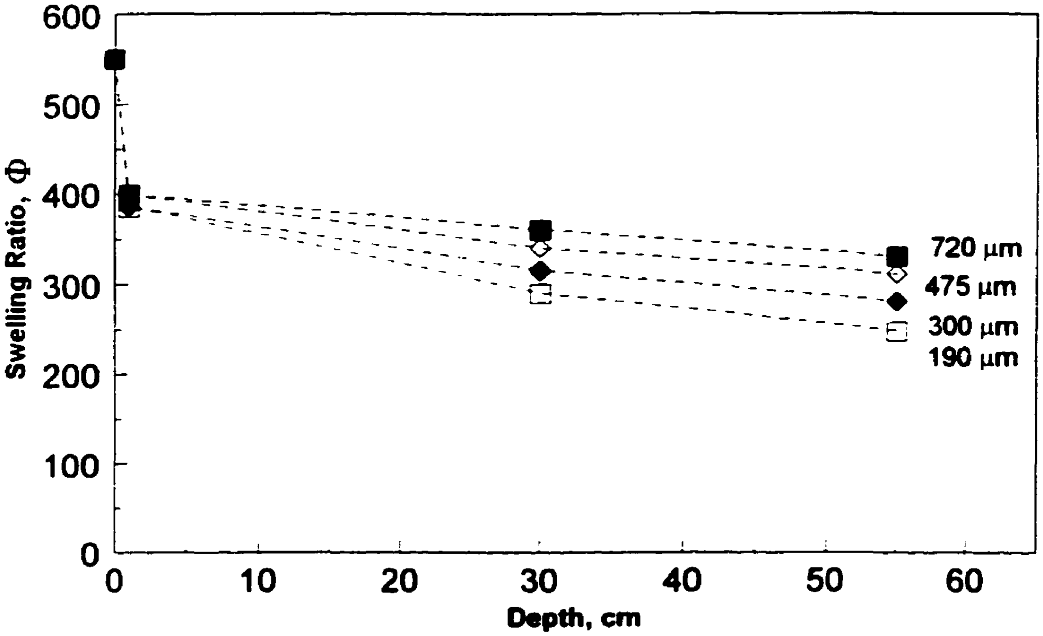

FIGURE 2.3 Swelling ratio (Φ) as a function of depth and sand particle size for Sumitomo gels swelling in a saturated sand column. Sand size: 720 (■), 475 (◊), 300 (◆), 190 μm (□). The dashed lines are drawn to guide the eye.

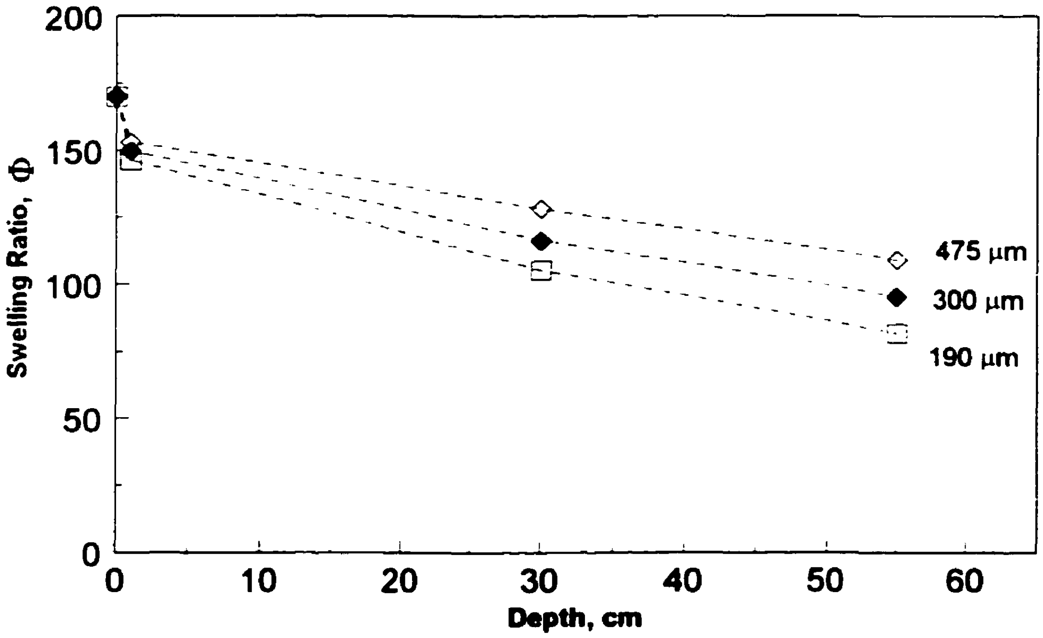

FIGURE 2.4 Swelling ratio (Φ) as a function of depth and sand particle size for Stockosorb gels swelling in a saturated sand column. Sand size: 475 (◊), 300 (◆), 190 μm (□). The dashed lines are drawn to guide the eye.

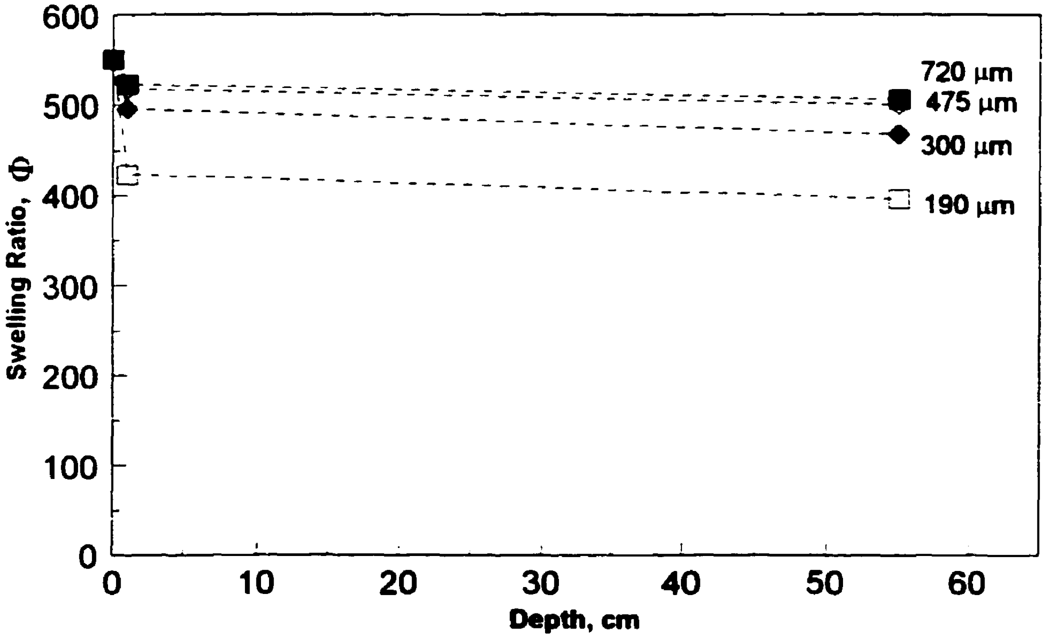

FIGURE 2.5 Swelling ratio (Φ) as a function of depth and sand particle size for Sumitomo gels shrinking in a saturated sand column. Water swollen gels (Φ=550) were placed inside the column. Sand size: 720 (■), 475 (◊), 300 (◆), 190 μm (☐). The dashed lines are drawn to guide the eye.

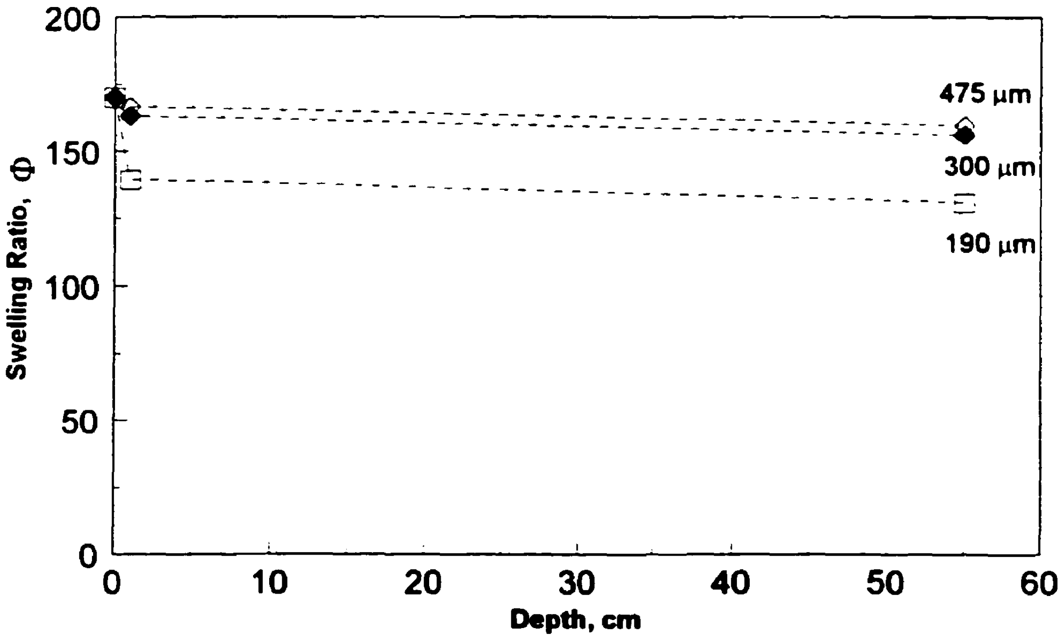

FIGURE 2.6 Swelling ratio (Φ) as a function of depth and sand particle size for Stockosorb gels shrinking in a saturated sand column. Water swollen gels (Φ=170) were placed inside the column. Sand size: 475 (◊), 300 (◆), 190 μm (☐). The dashed lines are drawn to guide the eye.

Sumitomo and Stockosorb gels shrank less than 10% of their water swollen size at all depths. In contrast, for smaller sand particle diameters, both gels shrank approximately 25% of their water swollen size at all depths.

The swelling and shrinking of the two gel types in 475 μm saturated sand are compared in Table 2.3. From Table 2.3 and Figures 2.3-2.6 it is clear that shrinking is not the reverse of swelling. However, similar forces are responsible for making swelling and shrinking different. The swelling of dry gel particles is reduced because of shear forces. The shrinking of swollen particles is also reduced by shear forces or by what is known in soil science as arching (Terzaghi, 1943).

TABLE 2.3. Comparison between Sumitomo and Stockosorb Φ values for gels swollen at different depths in saturated sand (475 μm).

DEPTH (cm)	Φ			
	SUMITOMO		STOCKOSORB	
	swelling	shrinking	swelling	shrinking
0	550	550	170	170
1	400	520	150	167
30	330	-	125	-
55	310	500	109	160

Arching may be understood by considering the following: If one part of the support of sand starts to yield while the remainder stays in place the sand adjoining the yielding part begins to move out of its original position. The relative movement within the sand is opposed by a shearing resistance. Since the shearing resistance tends to keep the yielding mass in its original position, it reduces the pressure on the yielding part of the support and increases the pressure on the adjoining stationary part. This transfer of pressure from a yielding mass of soil onto adjoining stationary parts is arching.

Due to arching the shrinkage of swollen gel particles in sand is significantly reduced. A shrinking gel particle equilibrates at a Φ value much higher than an identical dry particle which swells inside sand in the absence of arching. This effect is subsequently referred to as the cavity-effect.

Figures 2.5 and 2.6 suggest arching is a function of sand particle size. However, contrary to expectations, fine sand yields lower swelling ratios, due to less arching, or less transfer of pressure from a yielding mass of soil onto adjoining stationary parts. This result, although not well understood is in agreement with the investigations of Vollmy on the cavity-effect in sand (1937).

Additional swelling and shrinking experiments were performed to indicate the effect of overburden pressure. A portion of the saturated sand column was replaced by a steel cylinder of equal weight, as shown in Figure 2.7. The weight of the steel cylinder, 6.89 cm in diameter and 13.7 cm in length, was 4 kg, which was equal to the weight of 55 cm deep saturated sand. For swelling experiments in saturated sand and equivalent top-loaded columns, the swelling ratio in the top-loaded columns was reduced by 40%. However, for shrinking experiments in saturated sand and equivalent top-loaded columns, there was little change in the swelling ratio. The swelling ratios in sand columns and top-loaded columns are compared in Table 2.4.

The differences in Φ for swelling experiments are due to the unusual behavior exhibited by most granular materials when they are held inside a cylindrical container with height at least three times the diameter (Handy, 1985). Because of the contact forces between grains and static friction with the sides of the container, the container walls support a large part of the weight. Thus the pressure head for a granular material does not depend on height in the manner it does for a liquid (see Equation 2.17). This effect, commonly known as "silo effect" or "bin effect" is a manifestation of arching. For gel swelling in the top-loaded column experiment, the silo effect is virtually absent because the gel particle is located only 1 cm beneath the sand surface. Since the column walls support little weight, a greater mean effective stress is generated, thus reducing the value of the gel swelling ratio, Φ.

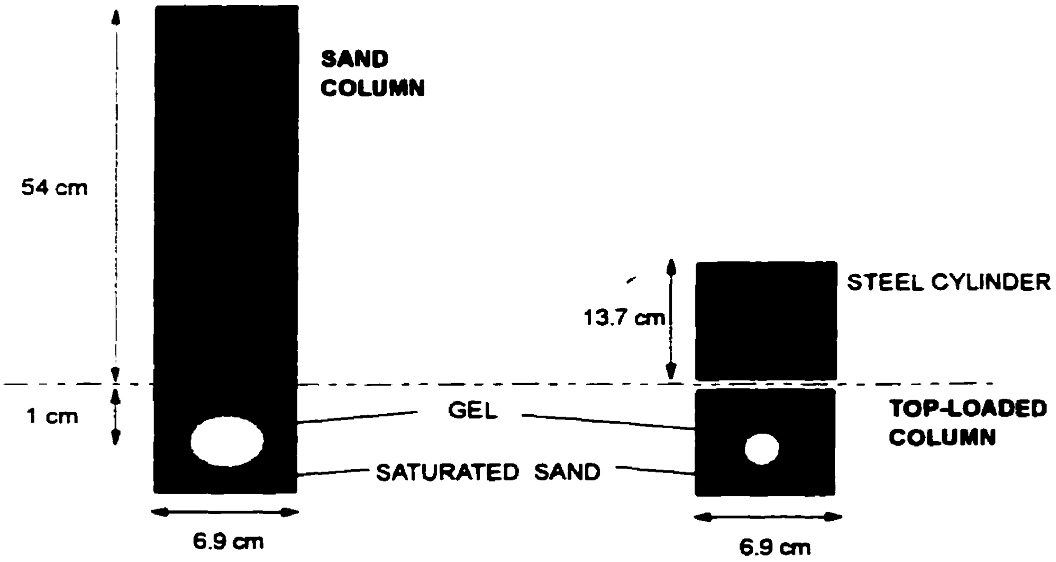

FIGURE 2.7 Schematic diagram showing the saturated sand column and the equivalent top-loaded column made by replacing the saturated sand column above the marked level by a steel cylinder of equal weight

TABLE 2.4. Comparison of swelling ratio for swelling and shrinking inside a sand column and an equivalent top-loaded column for Stockosorb gels (Φ in water at 1 atm=170). Gels inside the sand column were placed at 55 cm depth.

SAND SIZE (μm)	Φ			
	SWELLING		SHRINKING	
	TALL SAND COLUMN	TOP-LOADED COLUMN	TALL SAND COLUMN	TOP-LOADED COLUMN
474	109	70	160	159
300	95	60	156	156
190	82	52	131	128

Similarly for gel shrinking in the top-loaded column experiment, the silo effect is virtually absent because the gel particle is located only 1 cm beneath the sand surface. Despite the absence of silo effect, a water swollen gel particle in top-loaded shrinking experiments has a similar equilibrium size when shrinking in sand at 1 cm. This is ascribed to the cavity-effect. When the water swollen gel particle is placed in a sand column or an equivalent top-loaded column the mean effective pressure above the cavity, in which the gel rests, is less than the hydrostatic pressure. Due to arching, the pressure from above the cavity is deflected to adjoining parts of sand and eventually to the column walls thereby reducing the compressive force on the gel particle.

2.3. THEORETICAL

2.3.1 MODELS FOR GEL SWELLING

Most models which describe swelling equilibria of superabsorbent-solvent systems are extensions of those for non-crosslinked polymer solutions. For a detailed review, see Sassi *et al.* (1992) and Vasheghani-Farahani (1991). These models can be categorized as follows:

- Lattice model of Flory
- Lattice model with rewritten ionic terms
- Lattice model with non-Gaussian distribution and polymer charges
- Lattice model with holes
- Quasi-chemical lattice model

Most models describe swelling of polyelectrolyte gels at equilibrium in terms of the minimization of the Gibbs free energy of the gel. The free energy change, ΔG, corresponding to gel volume change is the sum of four contributions:

$$\Delta G = \Delta G_{mix} + \Delta G_{elastic} + \Delta G_{ion} + VP_{ext} \qquad (2.3)$$

where ΔG_{mix} is the contribution due to mixing of pure solvent with an initially pure, amorphous, unstrained network. $\Delta G_{elastic}$ is the contribution due to rubber elastic configurational changes of the gel structure. ΔG_{ion} is the contribution due to mixing of ions with the solvent. The fourth contribution, VP_{ext}, is present only if an external pressure, P_{ext}, above the pressure of the swelling medium, is applied to the gel whose swollen volume is V.

Using standard thermodynamic relations, it is possible to obtain from Equation 2.3 the following relation (Siegal, 1994):

$$\Pi = \Pi_{mix} + \Pi_{elastic} + \Pi_{ion} + P_{ext} \tag{2.4}$$

where Π is the swelling pressure, which is zero at equilibrium, and Π_{mix} , $\Pi_{elastic}$, and Π_{ion} are the mixing, elastic, and ionic swelling pressures, respectively.

This work uses the lattice model of Flory. This model does not describe all polymer-solvent phenomena, for instance, it is unable to predict LCST volume transitions observed in certain gels. Despite its predictive limitations the above model was used in this work because it is the simplest treatment available to describe gel swelling.

2.3.2 FLORY MODEL FOR GEL SWELLING

In the Flory model (Flory, 1953) the expression for polymer/solvent mixing comes directly from his lattice-based polymer solution theory:

$$\Pi_{mix} = \frac{RT}{V_s}\left[\ln(1-\varphi_p) + \varphi_p + \chi\varphi_p^2\right] \tag{2.5}$$

where: φ_p = polymer volume fraction inside the gel

χ= polymer-solvent interaction parameter

V_s = molar volume of the solvent

R= ideal gas constant

T= absolute temperature

The elastic term comes from his theory of rubber elasticity. This term assumes the deformations to be Gaussian.

$$\Pi_{elastic} = RTK\left[\varphi_p^{1/3} - \frac{\varphi_p}{2}\right] \tag{2.6}$$

where K, the parameter of gel elasticity, is related to effective number of chains in the gel network, the molar volume of solvent, and the dry volume of the gel.

The ionic term is derived assuming ideal Donan equilibria for a dilute solution.

$$\Pi_{ion} = RT\left[(c - c^{*})\right] \tag{2.7}$$

where: c = molar concentration of mobile ions inside the gel

c^{*} = molar concentration of mobile ions in the external solution

This term is usually expanded to take the following form (Gehrke, 1986)

$$\Pi_{ion} = RT\left[\frac{z_f \varphi_p}{V_m} + v(c_s - c_s^{*})\right] \tag{2.8}$$

where: z_f = the fraction of monomeric units on the gel which are ionized

V_m = molar volume of a monomeric unit.

c_s = molar electrolyte concentration in the gel

c_s^{*} = molar electrolyte concentration in the external solution

ν = the number of ions into which the electrolyte dissociates

For swelling in distilled water, in the absence of electrolytes, the ionic term simplifies to

$$\Pi_{ion} = RT\left[\frac{z_f \varphi_p}{V_m}\right] \tag{2.9}$$

The fourth term is present only if an external pressure, P_{ext}, above the pressure of the swelling medium is applied to the gel. For gels swelling inside water at atmospheric pressure, P_{atm},

$$P_{ext} = (P_o - P_{atm}) \tag{2.10}$$

where P_o is the pressure at the gel surface.

2.3.3 MODELS FOR CAVITY EXPANSION

The origins of the cavity expansion theory go back to 1945 when Bishop *et al.* (1945) derived equations for quasi-static expansion of cylindrical and spherical cavities in metals. The first application to soils was by Chadwick in 1959. Hopkin's (1960) extensive review of the expansion of spherical cavities in elastic-plastic materials covers in detail the mathematical models as well as the problems which motivated the models. Forrestal and Luk (1988) refined the theory to describe spherical cavity expansion in compressible elastic-plastic solids.

Cavity expansion theory has found several applications in granular media and soil mechanics problems. It was first used in geotechnical problems to interpret *in situ* measurement of soil properties with the pressuremeter (Gibson and Anderson, 1961).

2.3.4 CAVITY EXPANSION IN SANDS

Cavity expansion in sands was modeled by Hughes *et al.* (1977) for cylindrical cavities. The description was extended to include spherical cavities by Withers *et al.* (1989) whose results for a spherical cavity are used here.

DESCRIPTION: An unbounded three-dimensional medium of sand contains a single spherical cavity as shown schematically in Figure 2.8. Initially the radius of the cavity is R_o and a mean effective pressure, P_o, acts throughout the sand, which is assumed to be homogeneous. The pressure inside the cavity, P_c , where $P_c > P_o$, causes the cavity to expand to a new radius R_c .

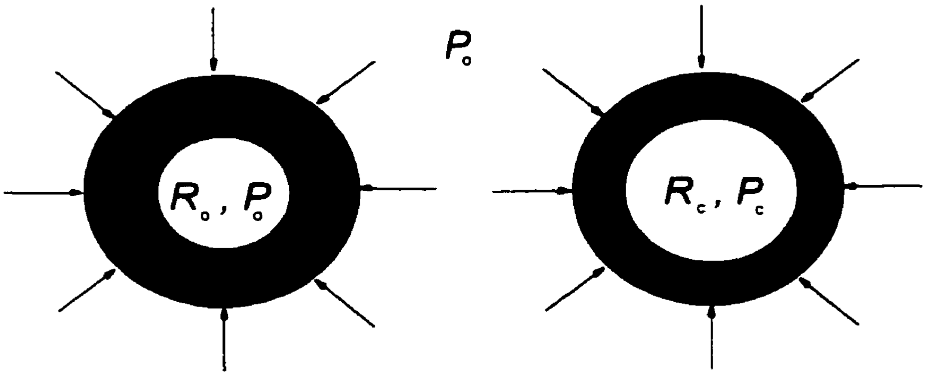

FIGURE 2.8 Geometry of cavity inside sand.

ASSUMPTIONS: The sand is modeled as an isotropic elastic-perfectly plastic material. It behaves elastically and obeys Hooke's law until the onset of yielding as shown in Figure 2.9. In the figure, stress, σ, is defined as a force per unit area of a section through a mass, and strain, ε, is defined as change in length per unit length in a given direction.

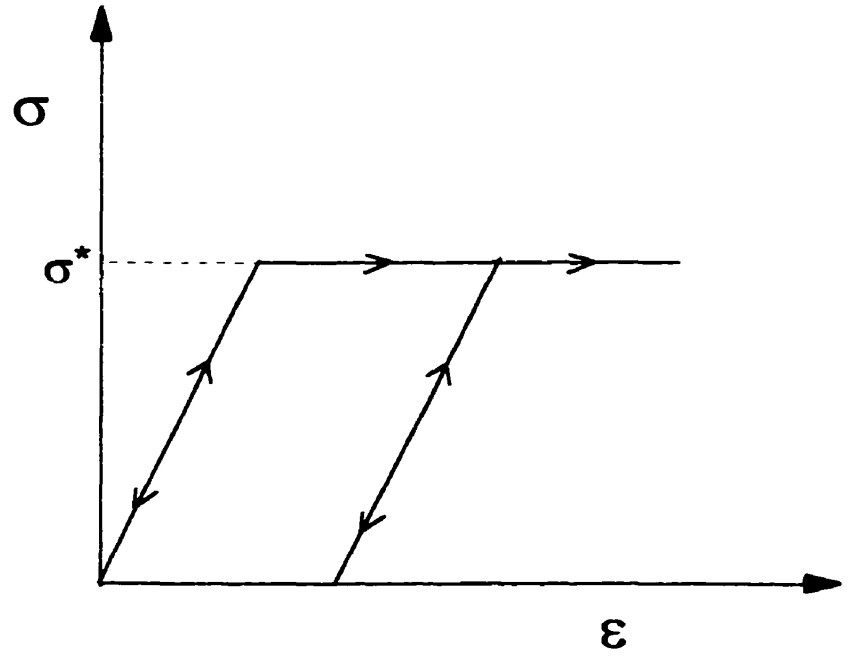

FIGURE 2.9 Idealized elastic-perfectly plastic stress-strain behaviour.

As shown, sand first behaves elastically for stress σ smaller than yield stress σ^*, then becomes perfectly plastic when σ reaches σ^*. The difference between plastic and elastic strains is that the former are irrecoverable. Elastic strains, ε, on the other hand, return to zero if the load is removed.

The properties of the sand are defined by the angle of friction ϕ, the angle of dilation ψ, and the shear modulus G.

The friction angle of sands is influenced by slip, rolling, and packing. During shear, sand grains can slip against one another, leading to friction. If grains rotate or roll during shear, this also causes friction. These factors are, in turn, influenced by size, shape and surface roughness of the particles.

Another cause of friction is grain fabric or the extent of packing. Consider sand in a column with grains closely packed together with little space left in between. As shear starts, the sand particles will tend to ride one over the other, resulting in dilation. The denser the packing, the greater the dilation. This volume change during shear is called *dilatancy* and has a very important effect on shear strength because a considerable amount of shearing energy is used to cause dilation. On the other hand, if sand is loose and all particles have the same diameter, there is no tendency for dilation. Contraction may occur and friction is due only to slip and rotation between grains. Grain packing for one particular sand can be evaluated by means of the initial void ratio. Friction due to grain slipping and rotation is referred to as residual friction. It depends on the size, shape and surface roughness, which are intrinsic characteristics of a particular sand. Dilatancy, on the other hand, depends on the state -dense or loose- of the packing of sand.

A rough idea about the friction is obtained by making a sand-pile. When the pile builds up to steeper than the friction angle, it starts to collapse. Generally, small sized particles, particles with low sphericity, particles with non-uniform distribution, and particles with higher surface roughness have a higher friction angle.

The shear modulus depends on the Young's modulus and the Poisson ratio for a given material. The typical values of shear modulus for metals and soils are 20-80 GPa and 0.01-10 MPa, respectively. The shear modulus of soils is influenced by a number of factors, like size, shape, type of soil particles, water content, density, void ratio, stress history, applied shear stress, degree of sample disturbance, testing conditions, amplitude and direction of stress changes (Bardet, 1997). Generally, everything else being the same, the shear modulus increases with decreasing water content and decreasing particle size.

EQUATIONS (Withers *et al.*, 1989)

The cavity expansion pressure is given by

$$P_c = P_{atm} + \left[\frac{3(P_o - P_{atm})}{1+2\alpha}\right]\left[\frac{\{2G/(P_o - P_{atm})\}(1+\beta)(1+2\alpha)}{3(1-\alpha)}\xi + \frac{(2-\beta)}{3}\right]^{2(1-\alpha)/(1+\beta)} \tag{2.11}$$

where

$$\alpha = \frac{1-\sin\phi}{1+\sin\phi} \tag{2.12}$$

$$\beta = \frac{2-\sin\psi}{1+\sin\psi} \tag{2.13}$$

$$\xi = \frac{R_c - R_o}{R_o} \tag{2.14}$$

2.3.5 FLORY-CAVITY MODEL

The Flory-Cavity Model combines the Flory model for swelling equilibrium of gels and the Cavity Expansion model for sand. The external pressure in the Flory model is replaced by the cavity expansion pressure given by Equation 2.11

$$P_{ext} = P_c - P_{atm} \tag{2.15}$$

The cavity expansion pressure is a function of shear modulus, friction angle, dilation angle, mean effective pressure acting on the gel surface, and initial radius of the gel.

2.4. COMPARISON OF EXPERIMENTS WITH MODELS

SWELLING IN WATER

The Flory model (see Section 2.3.2) was fitted to the experimental data for equilibrium swelling in water by taking P_o as the local hydrostatic pressure:

$$P_o = P_{atm} + H\rho_w g \tag{2.16}$$

where *H* is the depth, ρ_w is the density of water, and *g* is the acceleration due to gravity. Figure 2.10 shows the results of adjusting the gel elasticity parameter, *K*, to fit the data for each gel. The best fit values were 0.16 and 0.14 g/cm^3 for the Sumitomo and Stockosorb gels, respectively. The figure shows that the Flory model provides a good fit to the experimental data for swelling in water. The fitted values of *K* compare well with literature values which lie in the range 0.001-1 g/cm^3 (Vasheghani-Farahani, 1990). The closeness of the two *K* values suggests that the crosslink content was similar for the Sumitomo and Stockosorb gels.

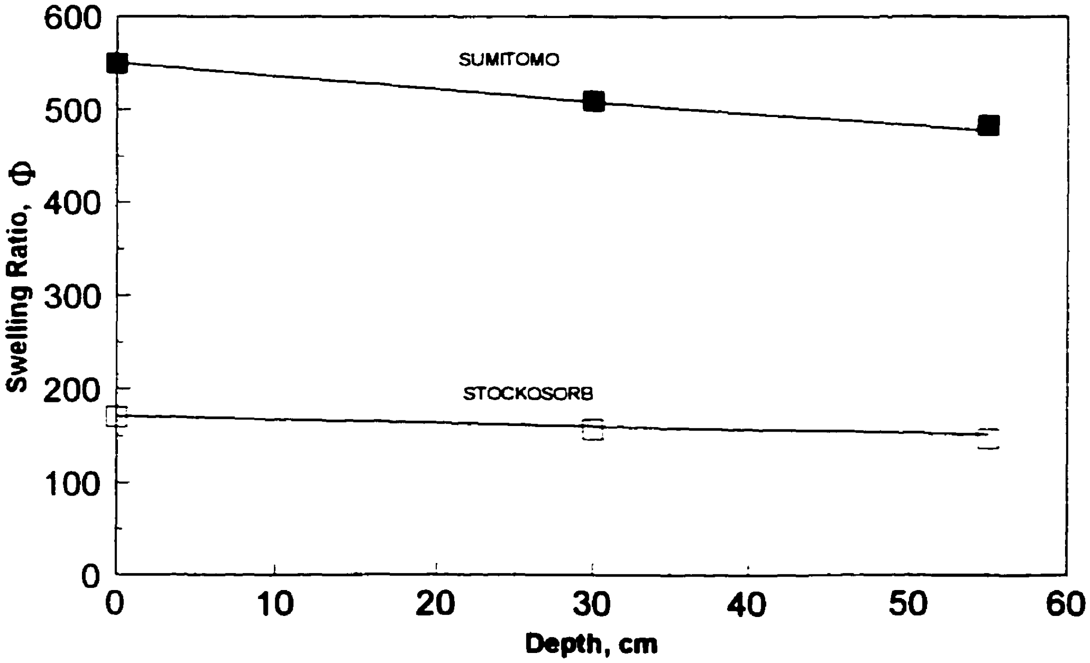

FIGURE 2.10 Best fit of Flory model to the swelling data for Sumitomo (■) and Stockosorb (□) gels in water. Curves are for *K* = 0.16 (Sumitomo) and *K*=0.14 (Stockosorb).

SWELLING IN SAND

The Flory-Cavity model (see Section 2.3.5) was fitted to the swelling data for Sumitomo and Stockosorb gels. The gel-elasticity parameter, K, was fixed at the value obtained by fitting the Flory model to the data for swelling in water. The hydrostatic pressure term, Eq. 2.16, was replaced by the following expression which relates the mean effective pressure acting on the gel surface, P_o, to the column diameter and height (Jacobson, 1958)

$$P_o = P_{atm} + \frac{D_{col}(\rho_s - \rho_w)g}{4a\mu_c}\left[1 - \exp\left(-a\mu_c \frac{4H}{D_{col}}\right)\right] + q\exp\left(-a\mu_c \frac{4H}{D_{col}}\right) \tag{2.17}$$

where: D_{col} = diameter of the column

H= height of the column

q= overpressure on the surface of sand

ρ_s = density of sand

ρ_w = density of water

g = acceleartion due to gravity

a= ratio of horizontal to vertical pressure

μ_c= frictional coefficient between contained mass and wall

The above formula was developed by Janseen (1895) to incorporate the phenomenon of arching in order to compute silo pressure. With increasing height or column diameter, Eq. 2.17 approaches a limit pressure.

For the purposes of fitting, $a\mu_c$ was equal to 0.17 (Bulson, 1985). The friction angle, ϕ, was estimated from the correlations published by Bolton (1986):

$$\phi = \phi_r + 3(D_r(Q - 4.6) - 1) \tag{2.18}$$

where D_r is the relative density, Q is the mineralogy coefficient (for quartz Q=10) and ϕ_r is the residual friction angle or friction angle independent of relative density. The relative density, D_r, is

$$D_r = \frac{e_{\max} - e}{e_{\max} - e_{\min}} \tag{2.19}$$

here e is the void ratio which is equal to the ratio of volume of voids to volume of solids, e_{max} is the maximum void ratio and e_{min} is the minimum void ratio. According to Lamb and Whitman (1979) for standard Ottawa sand $e_{max} = 0.8$ and $e_{min} = 0.5$. For both sand particle sizes e was experimentally determined to be approximately equal to 0.67.

The residual friction angle in Equation 2.18 was computed according to results published by Koerner (1970):

$$\phi_r = 36^\circ \quad \text{for} \quad 200 > \text{av. sand dia.} > 60\,\mu m \tag{2.20a}$$

$$\phi_r = 32^\circ \quad \text{for} \quad 600 > \text{av. sand dia.} > 200\,\mu m \tag{2.20b}$$

The dilation angle was given by (Bolton, 1986)

$$\psi = \frac{\phi - \phi_r}{0.8} \tag{2.21}$$

The shear modulus, G, which was the only fitted parameter. According to the soil science literature, G is a function of P_o (Bardet, 1997). It was assumed to vary with P_o according to:

$$G = \gamma\left(P_o - P_{atm}\right)^{\varepsilon} \tag{2.22}$$

where γ and ε are constants. The two constants were estimated by minimizing the following objective function:

$$\Im = \sum_{i=1}^{n}\left[\Phi_i^{\exp} - \Phi_i^{\text{model}}\right]^2 \tag{2.23}$$

where n is the number of experimental points. Since G is the same for a given sand size, 7 data points were used: 3 for Sumitomo and 3 for Stockosorb in sand columns and one for Stockosorb in the top-loaded column.

Figure 2.11 shows that the Flory-Cavity Model provides a good fit to the experimental data for swelling in sand. The best fit values of γ were equal to 3.5 MPa and 2 MPa for 190 μm and 474 μm sand sizes, respectively. The exponent ε was equal to 1.5 for both sand sizes. As expected, the finer sand particle size is associated with a higher value of G.

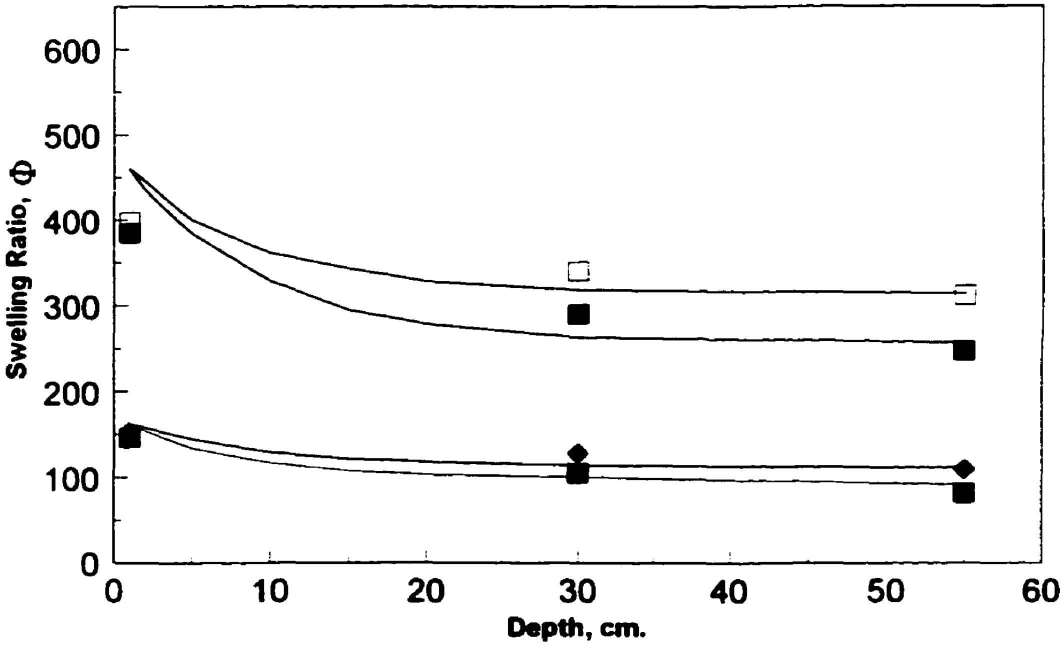

FIGURE 2.11 Best fit of Flory-Cavity model to the swelling data for Stockosorb gels in saturated sand column. Sumitomo [Sand size: 475 (□), 190 (■) μm], Stockosorb [Sand size: 475 (◊), 190 (◆)μm].

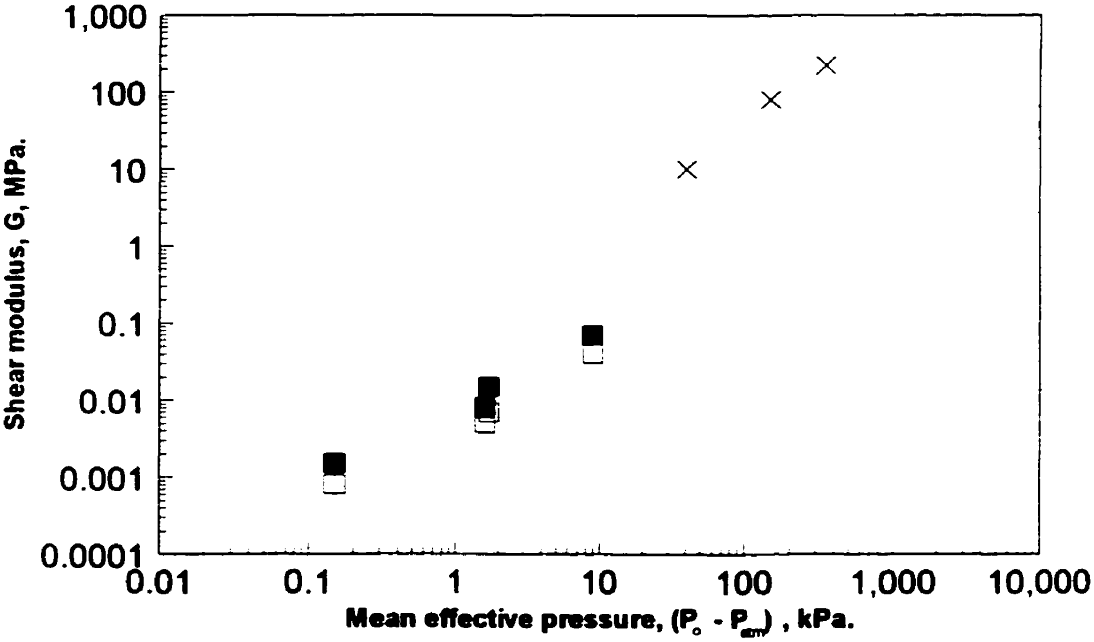

FIGURE 2.12 Variation of shear modulus, G, with mean effective pressure, (P_o - P_{atm}), as reported in literature (×) (Arulmoli et al., 1992) and as obtained by fitting the Flory-Cavity model to Stockosorb swelling in 190 μm (■) and 475 μm (□) water-saturated sand.

The values of G reported in literature are for higher pressures than those involved in the present experiments. Figure 2.12 shows the G values reported in the literature (Bardet, 1997) and the G values obtained by fitting the Flory-Cavity model to each individual Stockosorb experimental point including the point for the top-loaded column experiment. The literature values are for unsaturated sand whereas the fitted values are for saturated sand which has a tendency to lower the value of G (Bardet, 1997).

The values of the three parameters in Flory-Cavity Model were varied to determine the sensitivity of Φ to each one of the parameters. A 25% increase in the values of ϕ, G, and ψ caused the swelling ratio, Φ, to decrease by 12%, 5%, and 3%, respectively.

2.5. FLORY-CAVITY MODEL PREDICTIONS FOR DIFFERENT DIAMETER COLUMNS

Next, the Flory-Cavity model was used to predict swelling ratios in columns of different diameters. The predictions were made using Equations 2.4, 2.11, 2.15, and 2.17 and with the values of parameters identical to their literature values or to the fitted values reported in the previous section.

The ratio of the swelling ratio, Φ, to the value of swelling ratio at zero depth, $\Phi_{H=0,}$ is defined as the relative swelling ratio, δ.

$$\delta = \frac{\Phi}{\Phi_{H=0}} \tag{2.24}$$

This ratio is always less than or equal to 1. Figures 2.13 shows the relative swelling ratio, δ, as a function of the column depth predicted for different column diameters for Stockosorb gels. The gels swell the most at shallow depths for a given column diameter. With increasing depths, gel swelling decreases rapidly followed by a gradual approach to a limiting value. At a fixed depth, increasing column diameter decreases swelling. At shallow depths, gels swell relatively independent of column diameter.

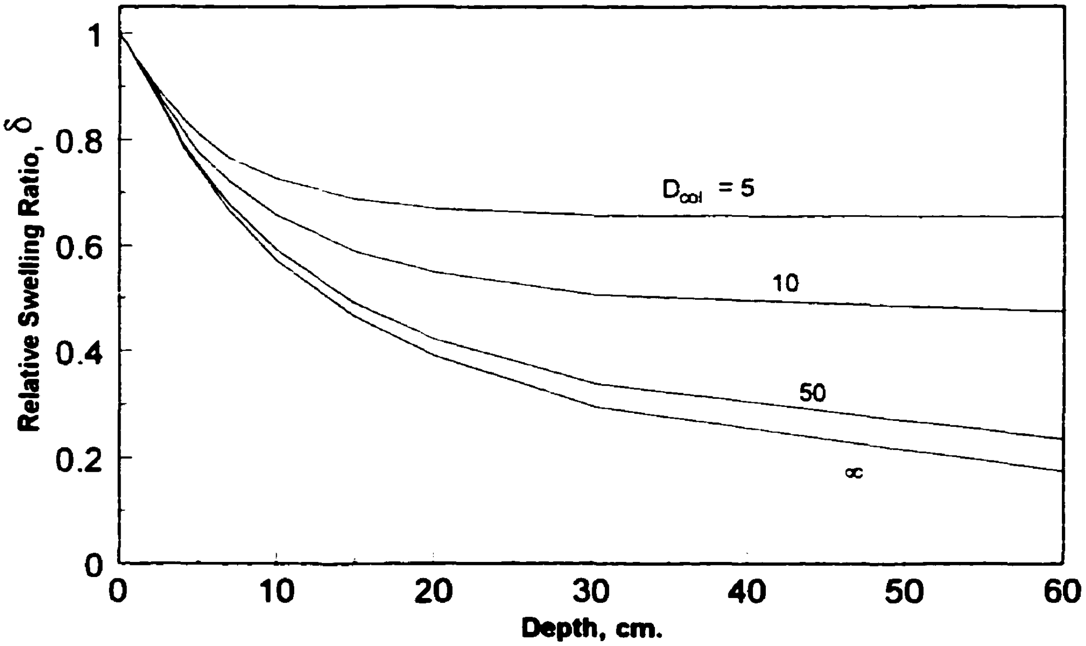

FIGURE 2.13 Relative swelling ratio, δ, of Stockosorb gels in water saturated sand as a function depth, *H*, in cm. The numbers on the curves are the column diameter, D_{col}, in cm.

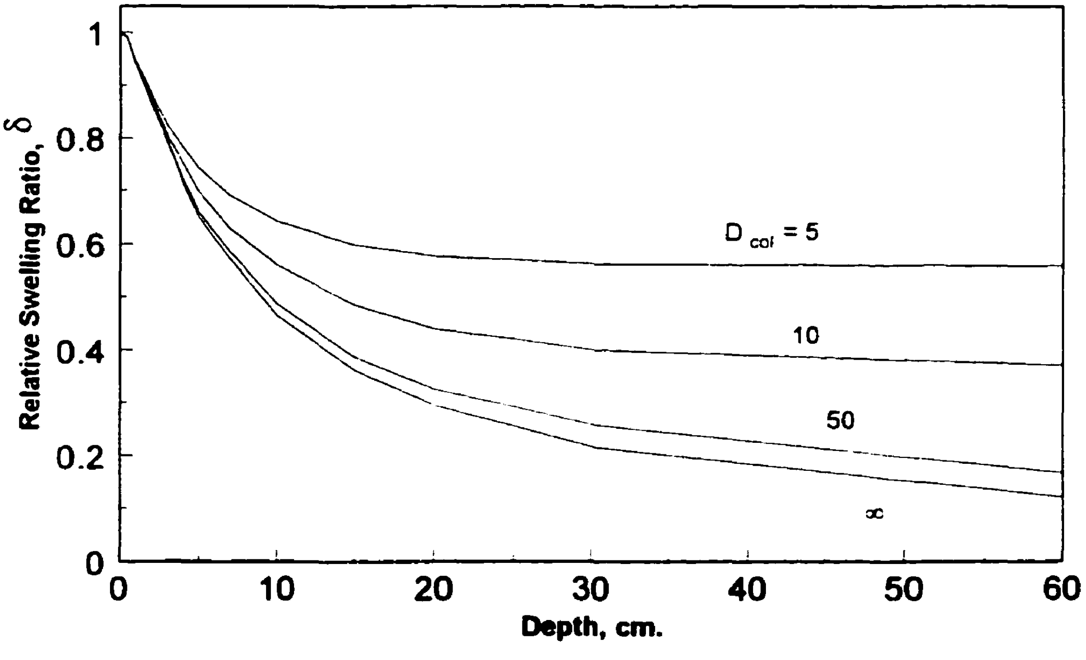

FIGURE 2.14 Relative swelling ratio, δ, of Sumitomo gels in water saturated sand as a function depth, *H*, in cm. The numbers on the curves are the column diameter, D_{col}, in cm.

Figure 2.14 shows the predicted swelling behavior of Sumitomo gels. Although the results are similar to those for Stockosorb gels, Sumitomo gels undergo a larger drop in the value of δ for a given depth and column diameter. This is ascribed to their higher ionic, which is 40% higher than Stockosorb gels. Because gels with higher ionic content swell more, they create a larger cavity in sand. This generates a higher value of strain in Equation 2.14, which in turn increases the frictional force the gel encounters in sand, or P_c in Equation 2.11, thereby reducing its relative swelling ratio.

These predictions are useful to extend the results of this work to gels swelling in fields, assumed as a column of infinite diameter. If the plant roots reach 30 cm beneath the surface in a sandy field, the theoretically derived curves of Figures 2.13 and 2.14 give δ values of approximately 0.3 and 0.2 for Stockosorb and Sumitomo gels, respectively. These δ values correspond to swelling ratios of 50 and 110 for Stockosorb and Sumitomo, respectively.

Chapter 3

KINETICS OF SWELLING

3.1. INTRODUCTION

Previous work on kinetics focused on free swelling of gels in water or in aqueous solutions. The kinetics of swelling in granular media, and in sand in particular, have not been studied largely because it is difficult to observe gels in opaque sand columns. As demonstrated in the last chapter, equilibrium swelling in sand is less than in water because of the resistance to gel expansion caused by the friction between sand particles. The guiding question for this chapter was, How different are the swelling kinetics of superabsorbent gels in sand from those in water.

In the following sections, models available for describing the kinetics of gel swelling are described. A moving boundary model for gel swelling is extended to include a time variable boundary condition. Next, the technique used to visualize gel particles in sand is described along with experiments on the kinetics of gel swelling in water and in sand. And finally, the model is fitted to the experiments.

3.2. THEORETICAL

3.2.1. MODELS FOR KINETICS OF FREE SWELLING

The experimental swelling data for many gels undergoing large volume changes exhibit a sigmoidal shape when plotted as the fractional approach to equilibrium versus the square root of time. Subsequently this plot is called the swelling curve. Most simple models describing the kinetics of gel volume change fail to predict the sigmoidal shape of the swelling curve. The models may be divided into three categories:

(A) FIXED BOUNDARY FICKIAN DIFFUSION MODEL: The Fickian diffusion model applies Fick's laws to the distribution of solvent in a gel sample during swelling or collapse (Buckley and Burger, 1962). The movement of the gel boundary, an important feature of large volume change, is not taken into account. These models predict that the fractional approach to equilibrium increases linearly with the square root of time up to roughly 0.4 and that the swelling curve, the fractional approach to equilibrium vs square root of time, is not sigmoidal even if the diffusion coefficient is a function of composition.

(B) COLLECTIVE DIFFUSION MODELS: These models, developed by Tanaka and coworkers (Tanaka and Fillmore, 1979; Li and Tanaka, 1990), treat the swelling of a gel as the expansion of a network driven by a gradient of stress. These models describe small volume changes, but they fail to predict the sigmoidal swelling curves resulting from large volume change. Furthermore, the parameters estimated by fitting these models to data may be unrealistic (Komori and Sakamoto, 1989).

(C) NON-FICKIAN DIFFUSION MODELS: Sigmoidal experimental swelling curves are often taken to indicate non-Fickian behavior. Deviations from the fixed boundary Fickian behavior are usually attributed to some of the following phenomena:

- variable surface concentration.
- a history dependent diffusion coefficient.
- stresses between parts of the gel swollen to different extents.
- polymer relaxation.

The first three have been discussed by Crank (1951), while the last has been modeled by Berens and Hopfenberg (1978) and Joshi and Astarita (1979). Although these models predict the swelling curves for large volume changes reasonably well, they are subject to three objections: (i) they do not allow for the movement of the gel boundary, (ii) they require three or more parameters to fit experimental data, and (iii) the diffusion coefficients may show unusual composition dependence, e.g. a maximum at an intermediate composition.

3.2.2 MOVING BOUNDARY FICKIAN DIFFUSION MODELS

Recent experimental and theoretical studies of the kinetics of volume change have demonstrated the importance of boundary motion (Rossi and Mazich, 1991; Mazich *et al.*, 1992; Rossi and Mazich, 1993). Singh and Weber (1996) described the kinetics of one-dimensional gel swelling and collapse for large or small volume change of spheres, cylinders and slabs. They computed swelling curves using a constant value of diffusion coefficient. For slabs their computed swelling curves were initially linear for all Φ-values, while for cylinders and spheres, the swelling curves were linear for values of Φ below 2.5, but sigmoidal for values above 2.5.

GEL VOLUME CHANGE MODEL FOR SPHERES:

Singh and Weber (1996) modeled one-dimensional gel volume change as isothermal motion of a polymer phase (p) and a solvent phase (s). Each element of volume contains polymer at a volume fraction φ_p and solvent at a volume fraction φ_s , where

$$\varphi_p + \varphi_s = 1 \qquad (3.1)$$

For a sphere, assuming that the phases have constant densities, the continuity equation for each phase is

$$\frac{\partial \varphi_i}{\partial t} = -\frac{1}{r^2}\frac{\partial}{\partial r}\left(r^2 \varphi_i \mathbf{u}_i\right) \qquad (3.2)$$

where t is the time, $\mathbf{u}_i$ is the linear velocity of phase i, and the product $\varphi_i\mathbf{u}_i$ is the volumetric flux density or the volume of phase i crossing a stationary unit area in unit time.

The volumetric flux density is separated into two contributions: a diffusive flux and a convective flux.

$$\varphi_i \mathbf{u}_i = -D_m \frac{\partial \varphi_s}{\partial r} + \varphi_i \left(\varphi_p \mathbf{u}_p + \varphi_s \mathbf{u}_s \right) \tag{3.3}$$

where D_m is the mutual diffusion coefficient.

The surface of the gel at $r=R$ separates the polymer from the external solution. This interface moves at a velocity $\mathbf{v}_R$, which is equal to the polymer velocity at the surface.

$$\mathbf{v}_R = \frac{dR}{dt} = \mathbf{u}_p \big|_R \tag{3.4}$$

This equation is referred to subsequently as the interface equation.

VOLUME CHANGE EQUATIONS:

Combining Equations 3.1-3.4 gives the following gel diffusion equation

$$\frac{\partial \varphi_p}{\partial t} = \frac{1}{r^2} \left[\frac{\partial}{\partial r} \left(D_m \, r^2 \frac{\partial \varphi_p}{\partial r} \right) \right] \tag{3.5}$$

and the following interface equation

$$\frac{dR}{dt} = -\frac{D_m}{\varphi_p} \frac{\partial \varphi_p}{\partial r} \bigg|_{r=R} \tag{3.6}$$

INITIAL AND BOUNDARY CONDITIONS:

The initial polymer volume fraction is uniform at φ_p^o and at the surface of the gel sphere the polymer volume fraction achieves its equilibrium value, φ_p^∞ , instantaneously upon exposure to the solvent:

$$\text{at} \quad t = 0, \quad \varphi_p = \varphi_p^\circ \quad \text{for} \quad 0 \le r \le R \tag{3.7}$$

$$\text{at} \quad r = R, \quad \varphi_p = \varphi_p^\infty \quad \text{for} \quad t > 0 \tag{3.8}$$

The remaining boundary condition for Equation 3.5 arises from symmetry:

$$\text{at} \quad r = 0, \quad \frac{\partial \varphi_p}{\partial r} = 0 \quad \text{for} \quad t \ge 0 \tag{3.9}$$

The initial condition for Equation 3.6 is at $t = 0 \quad R = R_o$ (3.10)

where R_o is the initial radius of the sphere.

DIMENSIONLESS VOLUME CHANGE EQUATIONS:

Dimensionless time, distance, volume fraction and interface position are defined as follows:

$$\tau = \frac{D_m t}{R_o^2} \tag{3.11}$$

$$z = \frac{r}{R} \tag{3.12}$$

$$\theta = \frac{\varphi_p^{\circ} - \varphi_p}{\varphi_p^{\circ} - \varphi_p^{\infty}} \tag{3.13}$$

$$Z = \frac{R}{R_o} \tag{3.14}$$

Assuming that D_m is a constant, Equations 3.5 to 3.10 have the following dimensionless forms

$$\frac{\partial \theta}{\partial \tau} = \frac{z}{Z}\left(\frac{dZ}{d\tau}\right)\frac{\partial \theta}{\partial z} + \frac{1}{Z^2}\left[\frac{2}{z}\left(\frac{\partial \theta}{\partial z}\right) + \frac{\partial^2 \theta}{\partial z^2}\right] \tag{3.15}$$

$$\frac{dZ}{d\tau} = [\Phi - 1]\frac{1}{Z}\left.\frac{\partial \theta}{\partial z}\right|_{z=1} \tag{3.16}$$

subject to

at $\tau = 0, \quad \theta = 0 \quad$ for $\quad 0 \le z \le 1$ (3.17)

at $z = 1, \quad \theta = 1 \quad$ for $\quad \tau > 0$ (3.18)

at $z = 0, \quad \dfrac{\partial \theta}{\partial z} = 0 \quad$ for $\quad \tau > 0$ (3.19)

at $\tau = 0, \quad Z = 1$ (3.20)

where

$$\Phi = \frac{\varphi_p^{\circ}}{\varphi_p^{\infty}} \tag{3.21}$$

Equations 3.15 through 3.21 show that θ is a function of τ, z and Φ, while Z is a function of τ and Φ.

FRACTIONAL APPROACH TO EQUILIBRIUM FROM THE MODEL

The volumetric fractional approach to equilibrium, F, is given by

$$F = \frac{V - V^{\circ}}{V^{\infty} - V^{\circ}} \tag{3.22}$$

where V is the gel volume at time t, V° is the initial gel volume and V^{∞} is the equilibrium (final) gel volume. The volumetric fractional approach to equilibrium and the mass fractional approach to equilibrium are identical if the polymer and the solvent phases have equal densities. Since the volume of the polymer is the same in the initial and final states, Φ may also be written as the ratio of final to initial volumes:

$$\Phi = \frac{V^{\infty}}{V^{\circ}} \tag{3.23}$$

Combining Equations 3.14, 3.22 and 3.23 yields

$$F = \frac{Z^3 - 1}{\Phi - 1} \tag{3.24}$$

For constant D_m, the fractional approach to equilibrium is a function only of the dimensionless time τ and the volume ratio, Φ.

3.3. EXPERIMENTAL

3.3.1 DEFINITIONS

FRACTIONAL APPROACH TO EQUILIBRIUM:

The fractional approach to equilibrium, $F(t)$, was calculated from

$$F = \frac{M^t - M^{\circ}}{M^{\infty} - M^{\circ}} \tag{3.25}$$

where

M^t ≡ Mass of gel at time t;

M° ≡ Initial mass of gel ($t = 0$);

M^∞ ≡ Equilibrium mass of gel ($t \to \infty$);

SWELLING RATIO (Φ_t):

The time dependent swelling ratio of the gels was defined as

$$\Phi_t = \frac{M^t}{M^\circ} \tag{3.26a}$$

For constant and equal densities of the solvent and the polymer phases, which is true for both Sumitomo and Stockosorb gels (see Section 2.2.2).

$$\Phi_t = \frac{V^t}{V^\circ} \tag{3.26b}$$

where V^t and V^o are the volumes of the gel at time = t and time = 0, respectively. At equilibrium, Φ_t equals Φ.

3.3.2 EXPERIMENTAL PROCEDURES

SWELLING IN WATER

The experiments involved determination of transient weight changes of gel particles at room temperature in 50 ml of quiescent distilled water. The approach to equilibrium was followed by removing the gel from the solution periodically, blotting the excess water with a J-cloth, weighing it, and then returning it to the water.

Using this procedure, the complete swelling curve for highly swelling gels was generated. Earlier attempts to measure swelling kinetics by Ogawa et al. (1993) were not successful. Instead of swelling individual beads, they swelled sodium polyacrylate particles of 100-250 μm diameter collectively in tea bags immersed in water. The tea bags were periodically removed from the water, then weighed. Their experiments did not provide a complete kinetic analysis, because the gels equilibrated within 1.5 minutes.

Figures 3.1 and 3.2 show the reproducibility of swelling data in water for Stockosorb and Sumitomo gels, respectively. The data are plotted as the swelling ratio, Φ_t, versus the time in minutes, *t*. Each figure shows data for two dry gels with identical radius: 0.76 mm (Stockosorb) and 0.33 mm (Sumitomo). The figures indicate good reproducibility for both gel types.

SWELLING IN SAND

Swelling-in-sand experiments were performed in a "two-dimensional" cell because it allowed visual observation of the gel particles as they grew. Gels were observed swelling in sand in a rectangular Plexiglas vessel with inside dimensions of 50 cm high, 30 cm wide, and 7 mm thick. The thickness was chosen to permit good images of the gel particles to be recorded. The bed had a perforated bottom to support the sand and to allow air to leave and water to drain. Dry sand of a given mesh size was packed into the bed in increments of 5 cm and the bed was tapped 3 times after each increment. Two gel particles, spaced 2 cm apart, were placed adjacent to the front wall, at a level 1 cm below the surface of the sand. Two types of experiments were performed: the first with saturated sand and the second with the addition of a fixed volume of water. A schematic illustration of the experimental technique is shown in Figure 3.3

For the saturated sand experiments, prior to each set of measurements the bed was placed inside a water reservoir with water level maintained at the same height as the sand surface inside the bed. Water from the reservoir immediately entered the bed from the bottom and moved upwards as a horizontal wetting front due to capillary action. The time when the front crossed the gels was marked as time zero. Approximately every 5-10 minutes thereafter, the bed was raised above the reservoir for 5 seconds for video-recording using rear illumination. After 5 seconds of video-recording, the bed was lowered back to its original position. Raising the bed above the water provided a sharper contrast between the gels and the surrounding sand by desaturating the bed briefly. This procedure was used because in a saturated bed the boundary between swelling

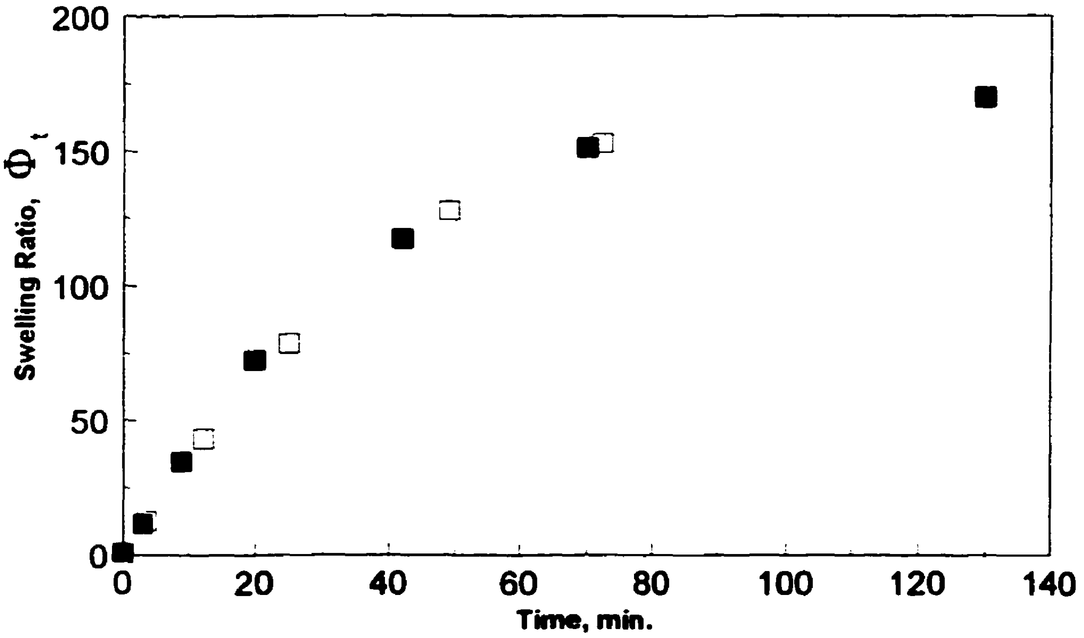

FIGURE 3.1. Replicate swelling profiles for Stockosorb gels in water. Dry radius equal to 0.76 mm. Sand size: 190 μm. Depth: 1 cm.

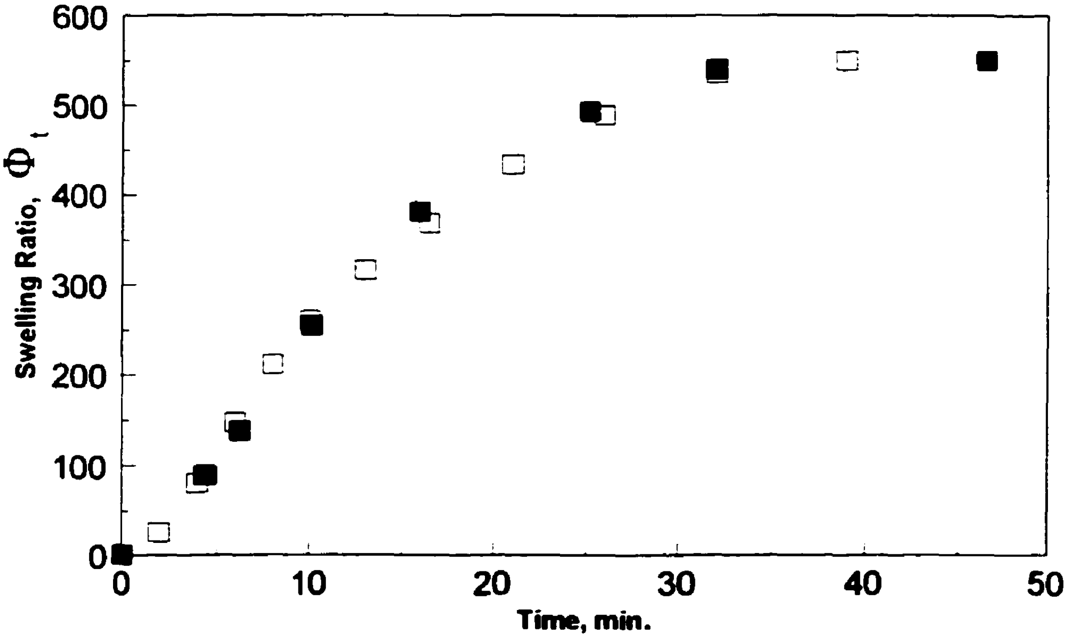

FIGURE 3.2. Replicate swelling profiles for Sumitomo gels in water. Dry radius equal to 0.33 mm. Sand size: 190 μm. Depth: 1 cm.

gel particle and the surrounding sand is fuzzy, since light transmission through sand increases with increasing moisture content. Repeated desaturation and resaturation did not alter the gel swelling kinetics. This was determined by swelling identical gels in 90% and 100% water saturated sand. Furthermore, this will become clearer in Section 3.6.3 which shows that gels swelling in saturated sand and in sand with a fixed volume of water applied yield identical diffusion coefficients. At the end of each experiment the bed was opened, the gel particles isolated, washed quickly to remove adhering sand, and weighed.

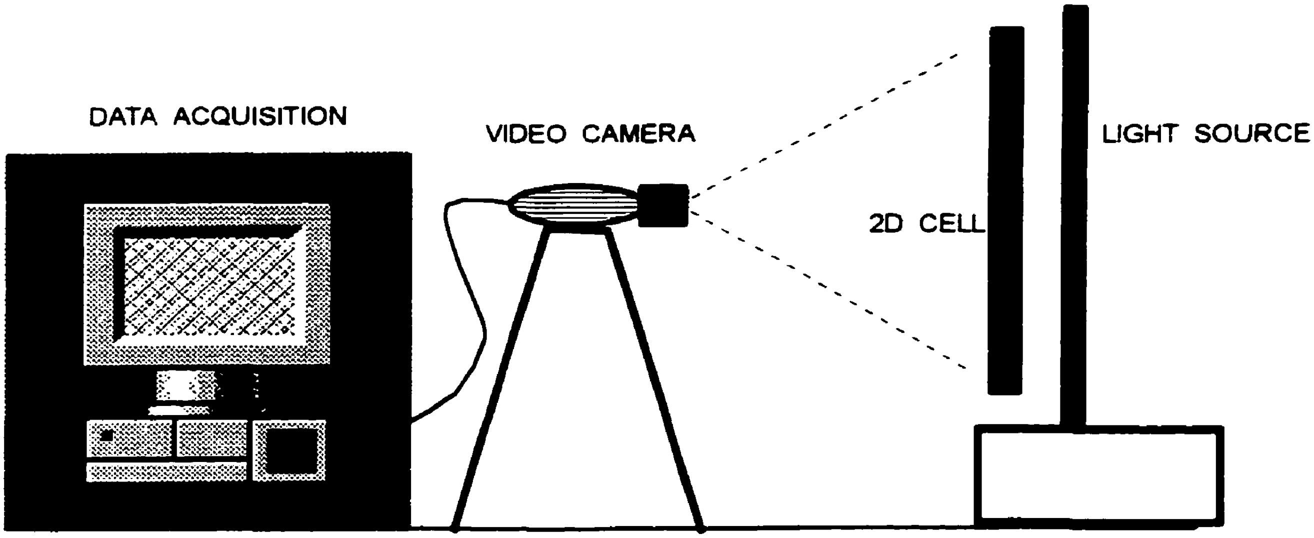

FIGURE 3.3. Schematic setup of the two-dimensional cell along with the digital image acquisation and analysis system.

For the sand with fixed volume of water experiments, prior to each set of measurements a liter of water was added to the top of the bed through a distributor which dispersed it evenly over the cross-sectional area of the bed. A horizontal wetting front was formed which moved downwards without fingering. It took less than a minute for the water front to reach the bottom. The time at which the front crossed the gels inside the bed was marked as time zero. The complete history of swelling was video recorded with the help of rear illumination. At the end of each experiment the bed was opened, the gel particles recovered, washed, and weighed.

The video images were captured by a video capture card (Video Blaster RT 300), digitized, and transferred to a 486 PC. Sigmascan software was used to analyze the images. Raw images were processed to clarify the boundaries of the swelling gel particles. The time history of typical Stockosorb gels swelling in sand is shown in Figure 3.4. The region displayed in the photographs is 3 cm wide. The approximate final gel diameters were 6.5 and 7 mm for the left and the right particle, respectively. The visible gel area was correlated to the gel mass inside the bed. Separate calibration curves were required for water-saturated sand experiments and for fixed-volume-of-water experiments. The curves were obtained by following procedures identical to the ones described above, with one difference: instead of waiting for the gels to equilibrate, the cell was opened when the gel particles acquired a given size. Different experiments were performed for different final gel sizes. Figures 3.5 and 3.6 show the calibration curves for gels in water-saturated sand experiments and in fixed-volume-of-water experiments, respectively. The data points are the mean values of three replicates in 190 μm sand size. The dotted lines are linear regressions. The calibration curves changed within ±1% for different sand sizes.

Figures 3.7 and 3.8 show the reproducibility of swelling data in water saturated sand in the two-dimensional cell for Stockosorb and Sumitomo gels, respectively. The data are plotted as the swelling ratio, Φ_t, versus the time in minutes, t. Each figure shows data for two dry gels with identical radii: 0.76 mm (Stockosorb) and 0.36 mm (Sumitomo). The figures indicate good reproducibility for both gel types, however, the data exhibited more scatter than the data obtained for swelling in water.

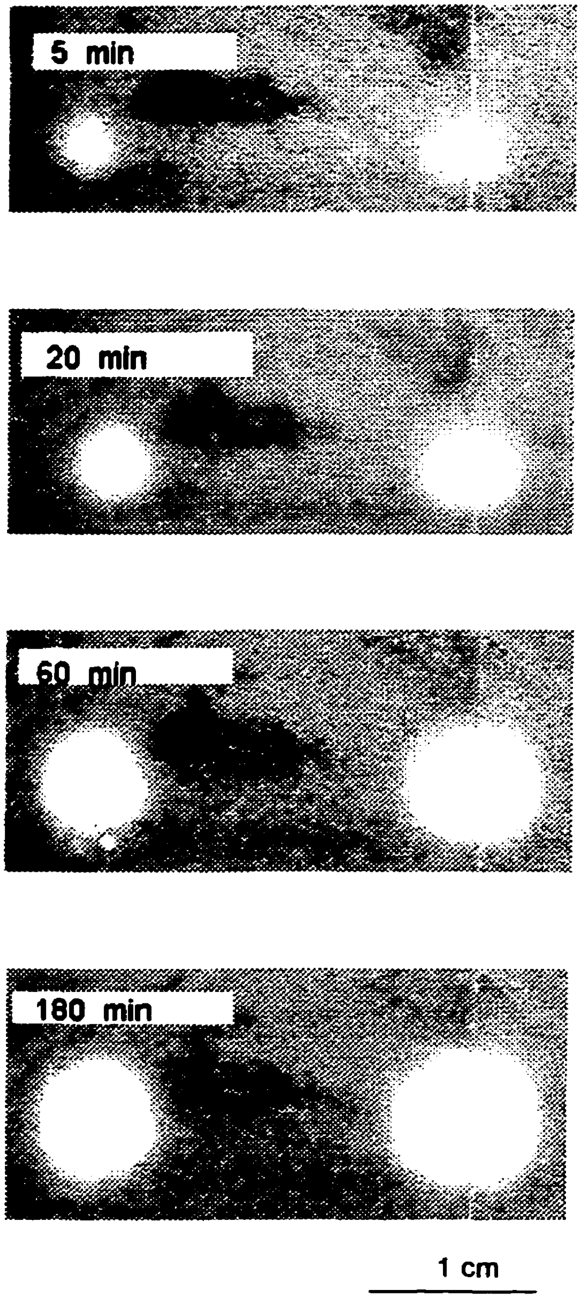

FIGURE 3.4. Images of two Stockosorb gels swelling adjacent to each other inside a two-dimensional cell at 5, 20, 60, and 180 minutes. Sand size: 190 μm. Depth: 1 cm.

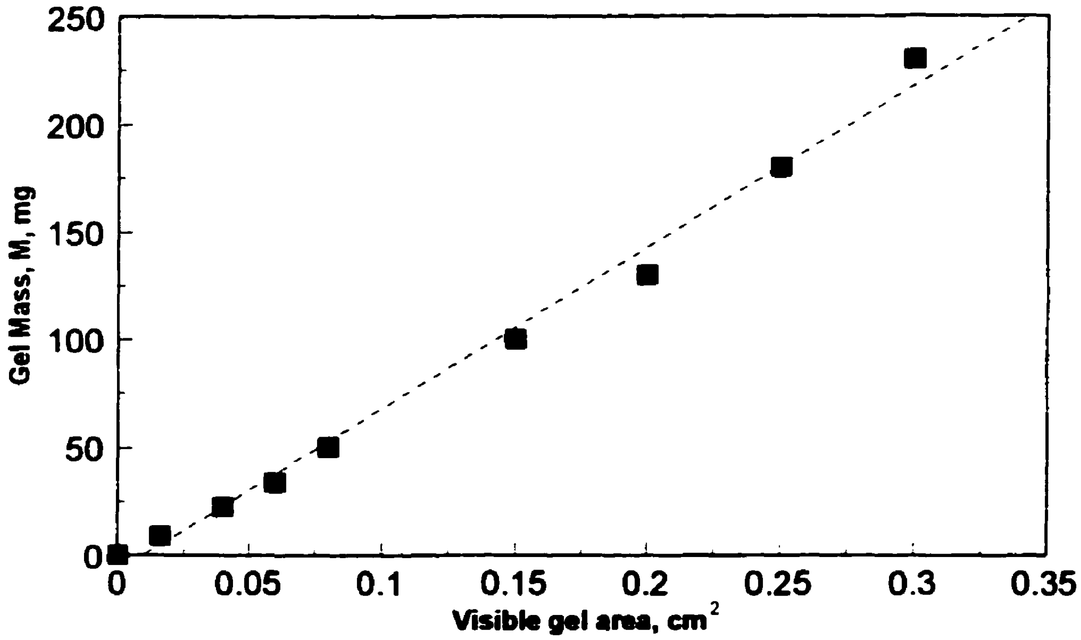

FIGURE 3.5. Calibration curve for two-dimensional cell experiments involving water-saturated sand. Sand size: 190 μm.

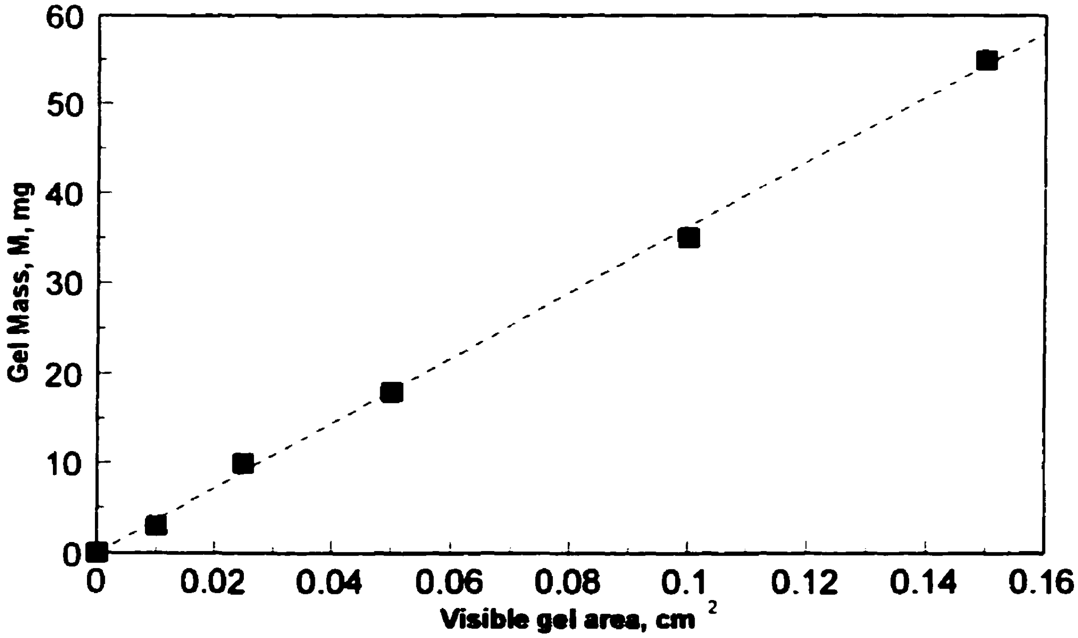

FIGURE 3.6. Calibration curve for two-dimensional cell experiments involving swelling of gels in sand with a fixed-volume-of-water. Sand size: 190 μm.

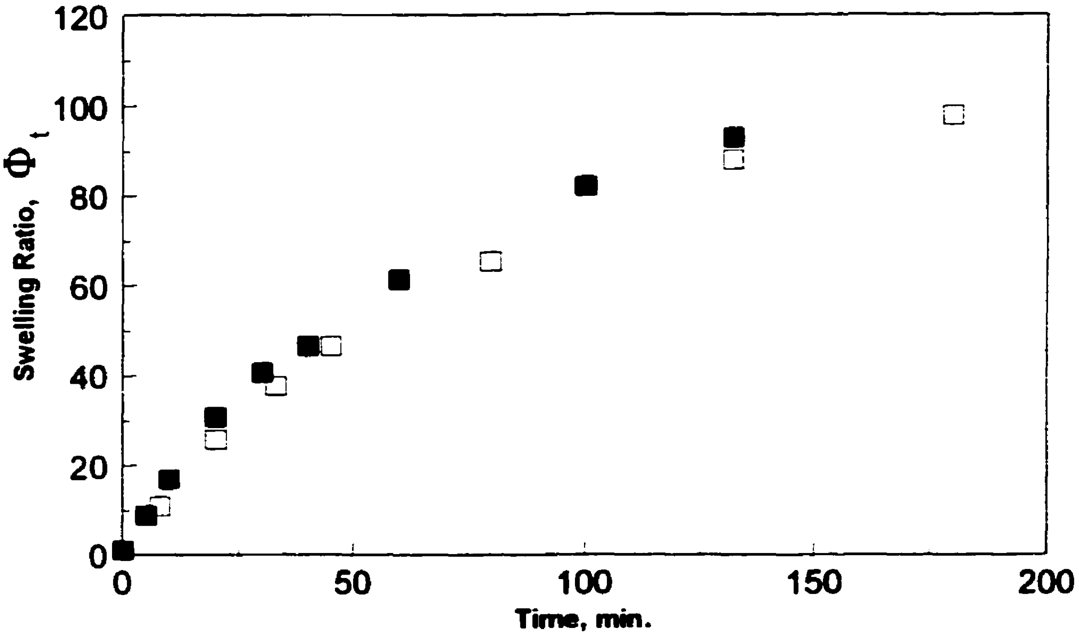

FIGURE 3.7. Replicate swelling profiles for Stockosorb gels in water saturated sand. Dry radius equal to 0.76 mm. Sand size: 190 μm. Depth: 1 cm.

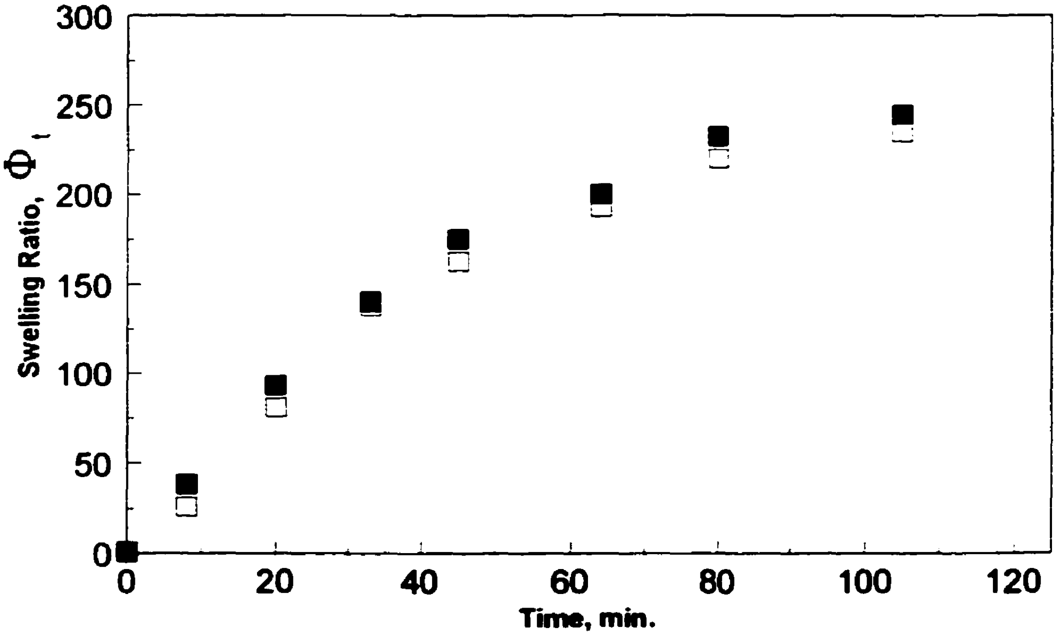

FIGURE 3.8. Replicate swelling profiles for Sumitomo gels in water saturated sand. Dry radius equal to 0.36 mm. Sand size: 190 μm. Depth: 1 cm.

3.3.3. RESULTS

SWELLING IN WATER

Figure 3.9 shows the swelling data for Stockosorb and Sumitomo gels in water plotted as the swelling ratio, Φ_t, versus the time in minutes, t. The Sumitomo gel had a larger final swelling ratio and a faster equilibration.

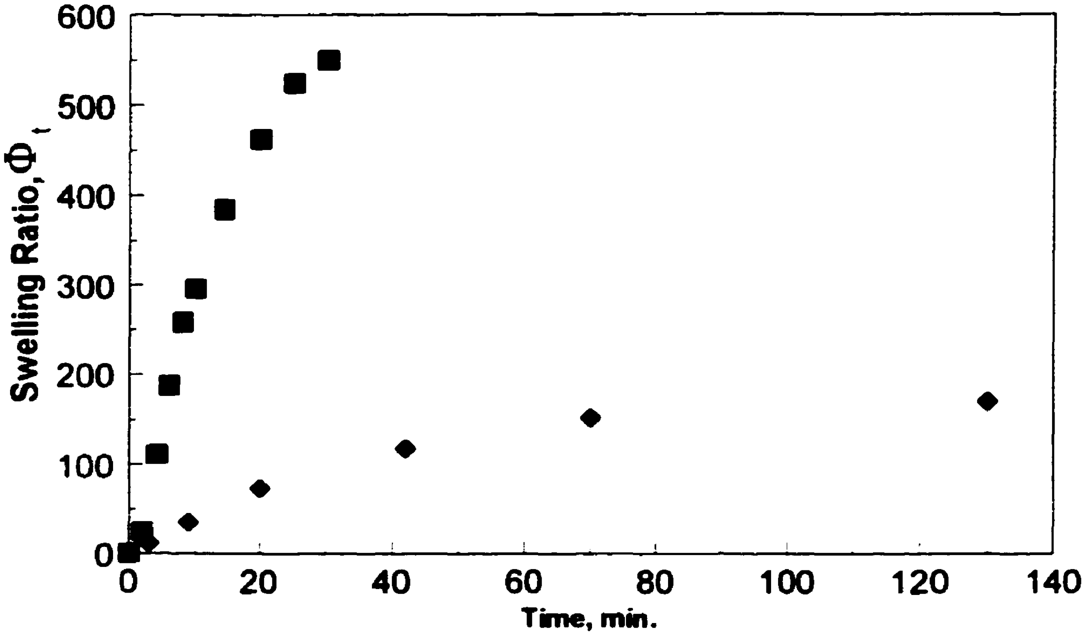

FIGURE 3.9. Swelling ratio as a function of time in water for Stockosorb gel (◆) (Φ = 170) with dry radius equal to 0.76 mm and Sumitomo gel (■) (Φ = 550) with dry radius equal to 0.28 mm.

Figure 3.10 shows the swelling curves for Stockosorb gels in water, i.e. the fractional approach to equilibrium, F, versus the square root of time in minutes, $\sqrt{t}$. Data for four otherwise identical dry gels with radii of 0.62, 0.66, 0.76, and 0.89 mm are shown. All curves were sigmoidal in shape. Swelling was slow during the early stages, accelerated over the middle range of F values, and slowed as equilibrium was approached. The smallest radius yielded the fastest equilibration. Figure 3.11 shows these data as the fractional approach to equilibrium, F, versus the square-root of a modified time, $\sqrt{t'}$, where

$$t' = \frac{t}{R_\circ^2} \qquad (3.27)$$

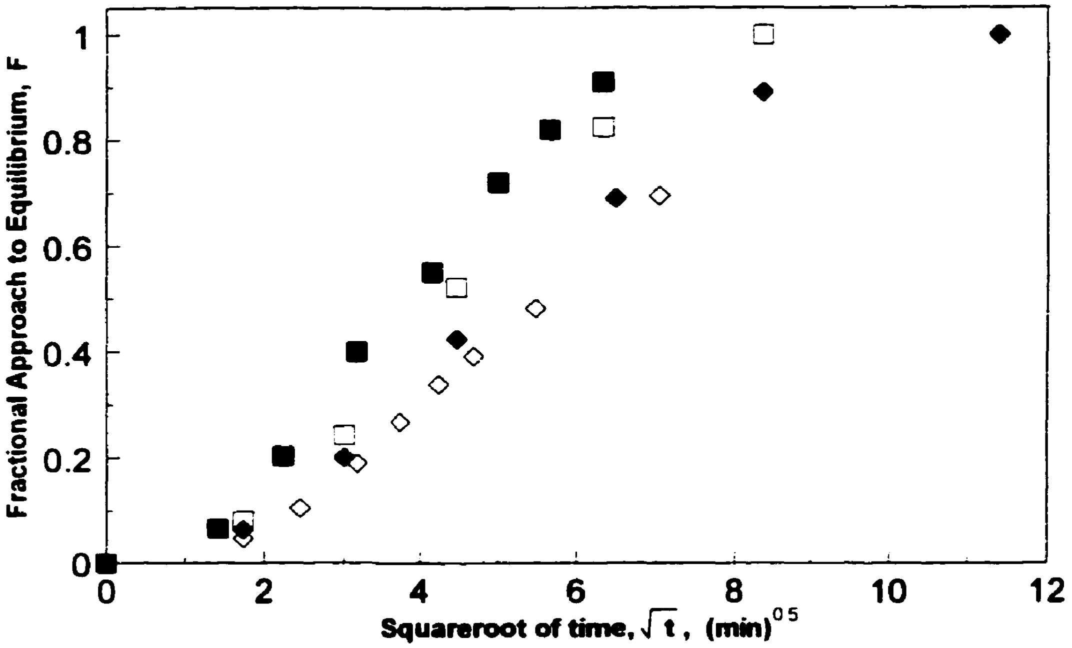

FIGURE 3.10. Swelling curves for Stockosorb gels (Φ = 170) in water. Dry radii equal to 0.62 (■), 0.66 (□), 0.76 (◆), and 0.89 (◇) mm.

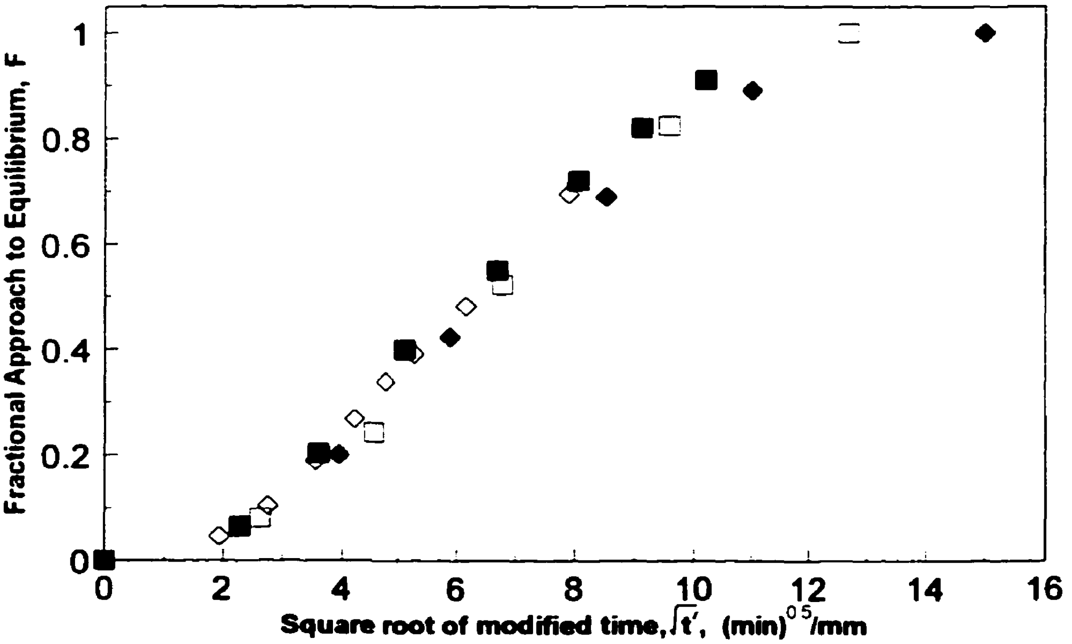

FIGURE 3.11. Modified-time swelling curves for Stockosorb gels (Φ = 170) in water. Dry radii equal to 0.62 (■), 0.66 (□), 0.76 (◆), and 0.89 (◇) mm.

and R_0 is the radius of the gel particle at time zero. Plotting the data in this manner brings the swelling data together for different sizes.

Figure 3.12 shows the swelling curves for Sumitomo gels in water. Data for three gel particles with radii of 0.28, 0.33, 0.35 mm are shown. Sumitomo gels also exhibited sigmoidal swelling curves. Initially the swelling curves were close, but they separated around F equal to 0.7 with the smallest particle approaching the equilibrium the most quickly. When these data are plotted as F versus $\sqrt{t'}$, as shown in Figure 3.13, the data do not come together.

SWELLING IN SAND

In Chapter 2 it was shown that the equilibrium swelling ratio of a gel expanding inside a saturated sand column was less than the equilibrium swelling ratio of the same gel immersed in water. A further drop in swelling ratio is expected when a gel particle is swollen in the two-dimensional cell owing to the wall effect. Table 3.1 compares the swelling ratios of Stockosorb and Sumitomo gels swelling inside the column and the cell in water and in saturated sand. Inside the water cell the swelling ratio of Stockosorb dropped by 5% of its value inside a column, whereas Sumitomo gels experienced no drop. In contrast,

TABLE 3.1. Comparison of Φ values in column (6.9 cm inner diameter) and cell (0.7 cm thickness) for Sumitomo and Stockosorb gels swollen in water and in saturated sand (190 μm) at a depth of 1 cm.

GEL	Φ			
	IN WATER		IN SATURATED SAND	
	COLUMN	CELL	COLUMN	CELL
STOCKOSORB	170	161	146	100
SUMITOMO	550	550	385	250

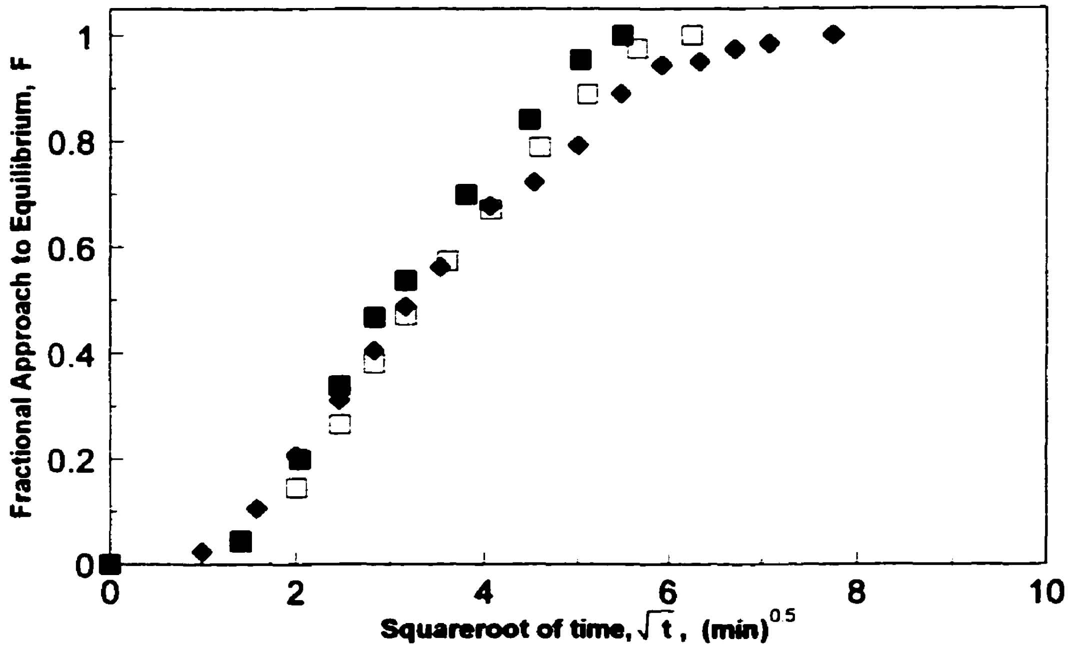

FIGURE 3.12. Swelling curves for Sumitomo gels (Φ = 550) in water. Dry radius equal to 0.28 (■), 0.33 (□), and 0.35 (◆) mm.

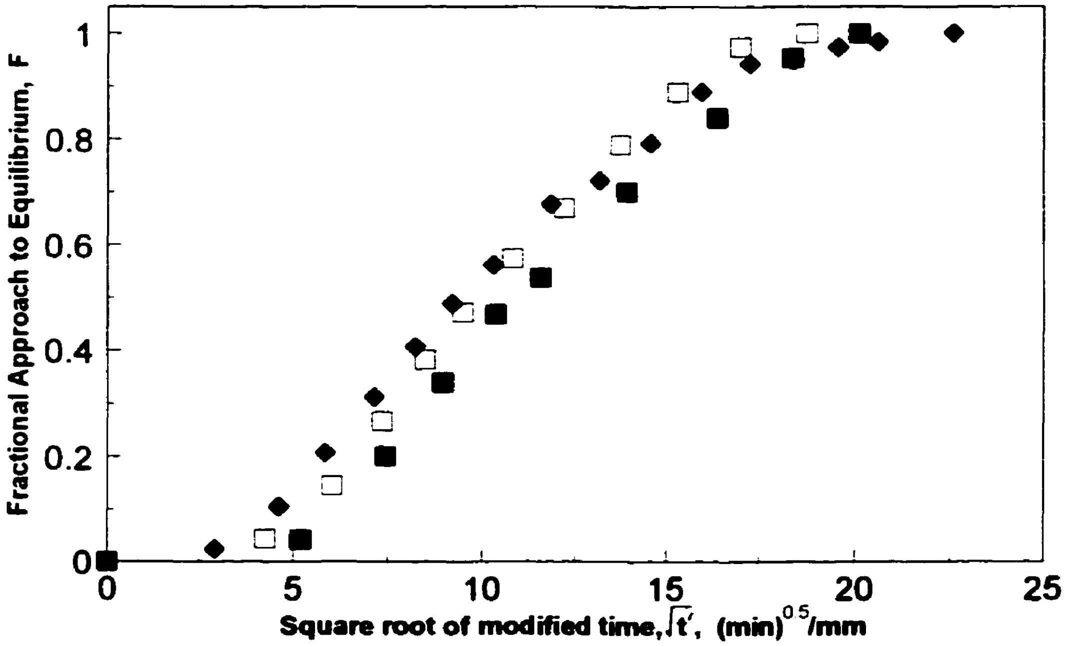

FIGURE 3.13. Modified-time swelling curves for Sumitomo gels (Φ = 550) in water. Dry radii equal to 0.28 (■), 0.33 (□), and 0.35 (◆) mm.

inside the water-saturated sand cell, the swelling ratio dropped roughly by 50% of its value inside a column for both gels. This is a significant drop in the swelling ratio, however, in situations involving sand in fields, the drop in swelling would be less than the drop experienced inside the cell because of the absence of wall effect. The cell experiments are also useful to obtain knowledge of retardation of swelling kinetics in sand when compared to water. The kinetics of gel swelling in fields are expected to lie in between their kinetics in water and in two-dimensional cells.

Figure 3.14 shows the swelling curves for two Sumitomo gel particles in saturated sand. The mean dry grain size was 0.19 mm. The curves resemble the sigmoidal curves for swelling in water.

Figure 3.15 shows the swelling curves for two Stockosorb gel particles in saturated sand of 0.19 mm mean grain size. The curves are similar to those of the Sumitomo gels. Figure 3.16 shows the swelling of Stockosorb gel particles with R_o=0.76 mm in saturated sands of two different sizes: 0.19 mm and 0.48 mm. The swelling kinetics were not affected by sand grain size. This result complements the result for swelling equilibrium of gels buried close to the sand surface. It was demonstrated in Chapter 2 that the equilibrium swelling degree for gel particles close to surface was independent of the sand particle size.

Figure 3.17 compares the swelling of Stockosorb gels in water and in saturated sand. The swelling curves for sand lie to the right of those for water. This seems inconsistent with the theoretical predictions of the model described in Section 3.2.2 (Singh, 1996): For gels with the same diffusion coefficient, the swelling curves for low Φ values lie to the left of those associated with higher Φ. This discrepancy is resolved later in Section 3.6.3.

The results described above are for experiments performed with saturated sand. The situation inside a bed which received a fixed-volume-of-water from above is different. In the fixed-volume-of-water experiments gel particles did not attain their maximum swelling capacity. Swelling ceased, much earlier, because

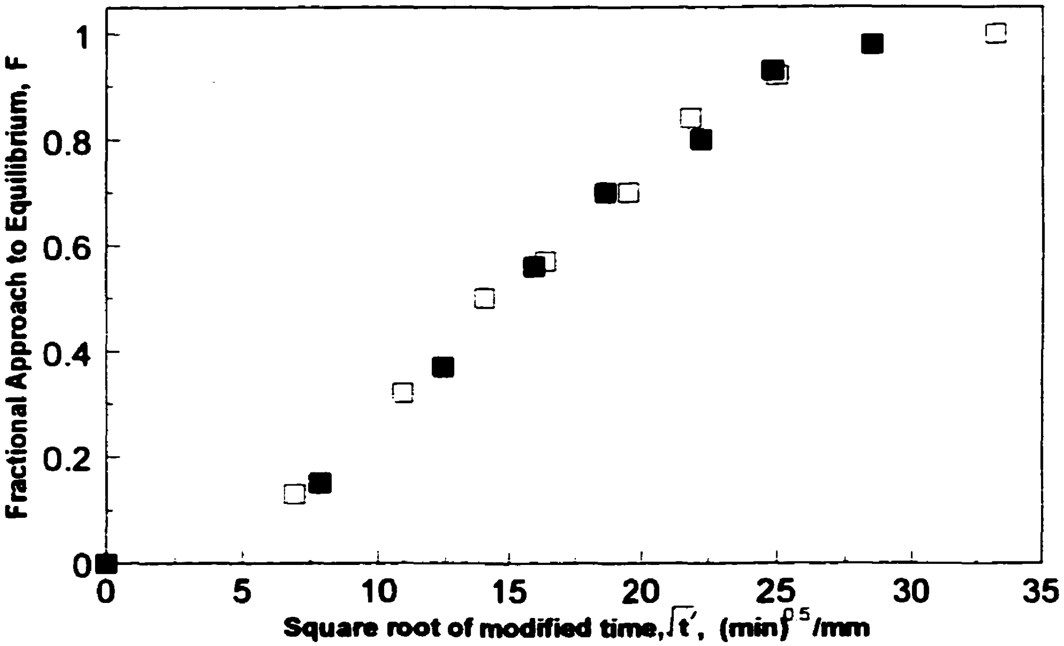

FIGURE 3.14. Modified-time swelling curves for Sumitomo gels in 0.19 mm saturated sand. Dry radius equal to 0.36 (■) and 0.41 (☐) mm. Depth = 1 cm where Φ = 250.

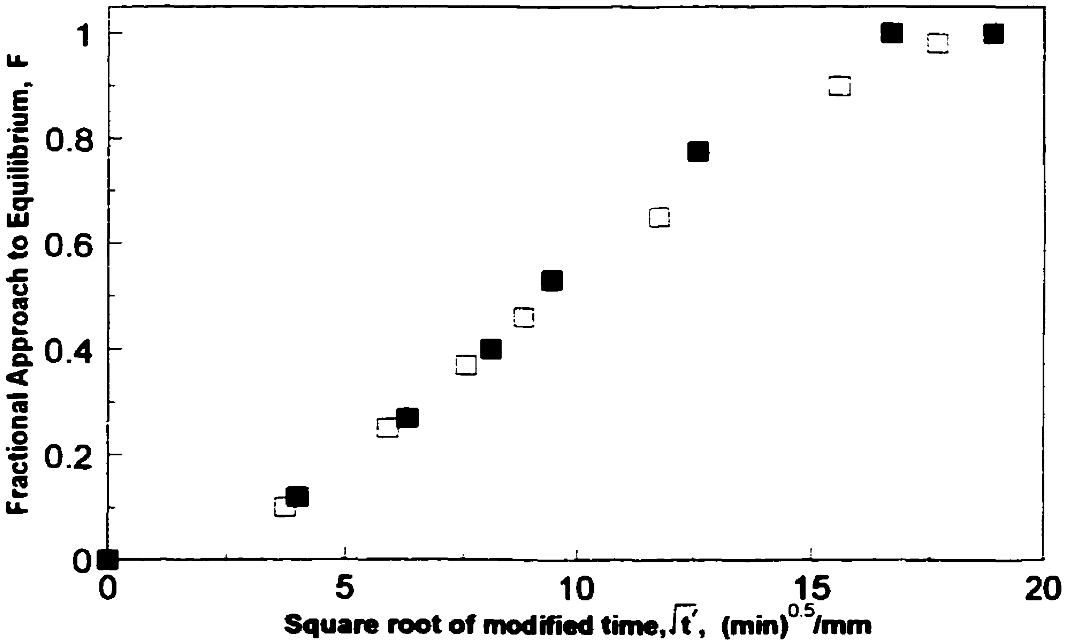

FIGURE 3.15. Modified-time swelling profiles for Stockosorb gels in 0.19 mm saturated sand. Dry radii equal to 0.71 (■) and 0.76 (☐) mm. Depth = 1 cm where Φ = 100.

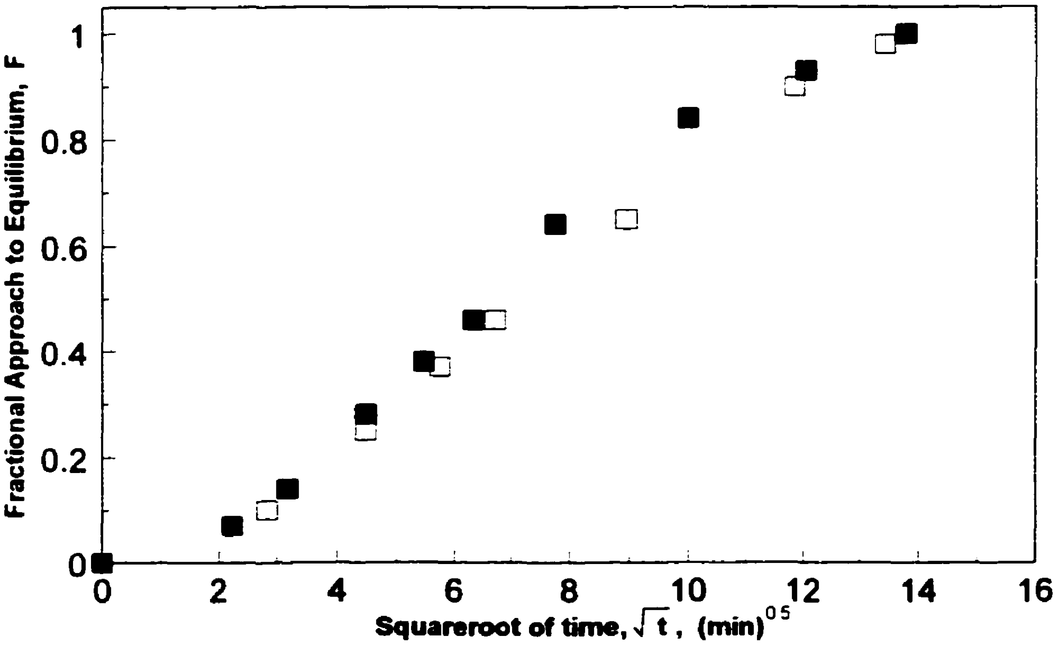

FIGURE 3.16. Modified-time swelling curves for Stockosorb gels (Φ = 100) in 0.48 mm (■) and 0.19 mm (□) saturated sand. Dry radius equal to 0.76 mm. Depth = 1 cm where Φ = 100.

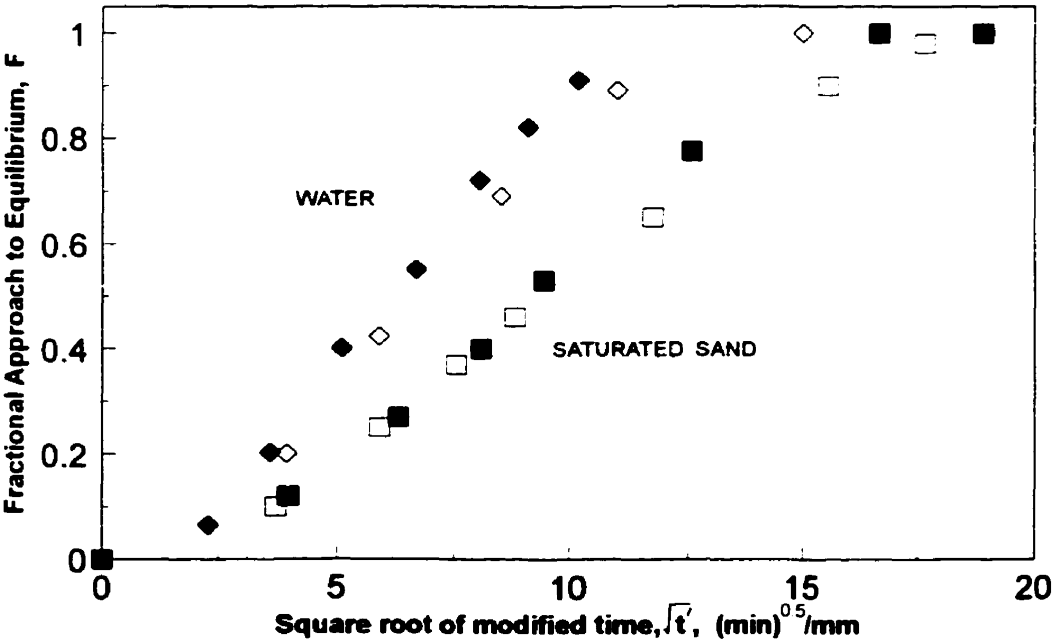

FIGURE 3.17. Comparison of modified-time swelling curves in water and in saturated sand (0.19 mm) at a depth of 1 cm. [Water: gel dry radius = 0.71 (■) and 0.76 (□) mm, Φ = 170; Saturated Sand: gel dry radius = 0.62 (◆) and 0.76 (◇) mm, Φ = 100]

of the limited supply of water. Figure 3.18 shows the swelling behavior of Stockosorb gels as F versus $\sqrt{t}$. The swelling ratio dropped to Φ=27.7 from its value of Φ=100 in saturated sand. However, despite a drop in the swelling ratio, the shape of the swelling curve was sigmoidal. This is in agreement with the predictions of the gel volume change model described in Section 3.2.2: The swelling curves for lower Φ lie to the left of those for higher Φ.

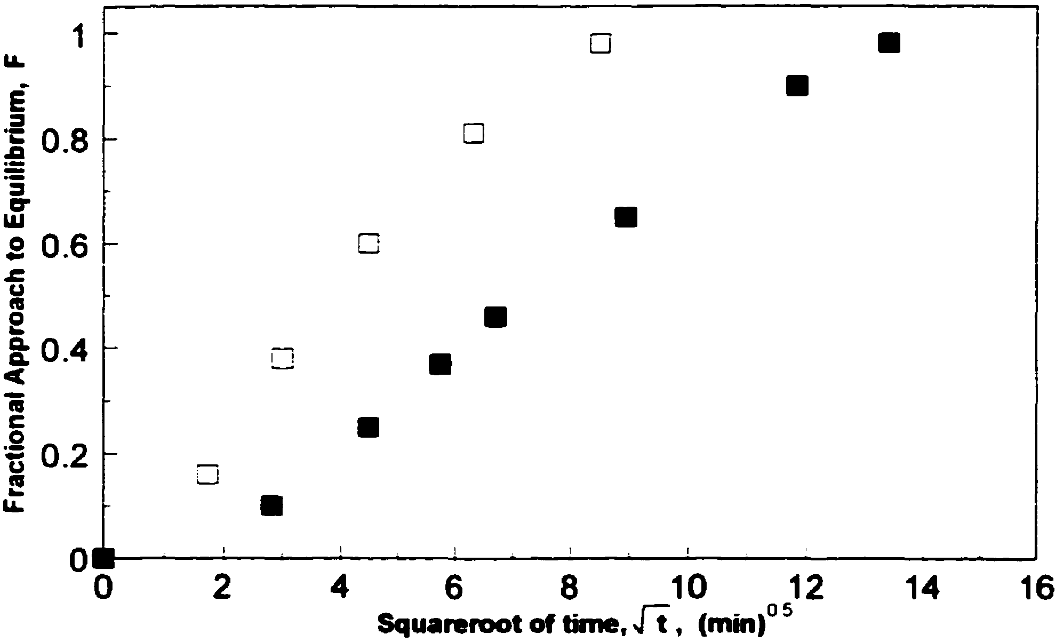

FIGURE 3.18. Comparison of swelling curves in water-saturated sand (■), Φ = 100, and sand with a fixed-volume-of-water added (□), Φ = 27.7, at a depth of 1 cm. Sand dia. = 0.48 mm. Dry gel particle diameter=0.76 mm.

3.4. EXTENSION OF THE GEL VOLUME CHANGE MODEL

Previous work has shown that the numerical computations of the model equations for spheres with a constant D_m (Section 3.2.2) predict swelling curves which are linear for small values of Φ, but sigmoidal for $\Phi \geq 2.5$ (Singh, 1996). However the experimental swelling data exhibit a more pronounced sigmoidal shape than the model predicts. Use of a composition-dependent D_m does not improve the fit.

SURFACE RELAXATION

Because the experimental swelling curves are not well described in terms of gel boundary movement or a variable D_m, the model was extended by making the surface boundary condition time-dependent. If the surface equilibrium is established at a finite rate the shape of the swelling curve is modified. A simple form of time variation of surface polymer volume fraction is postulated:

$$\varphi_p\big|_{r=R} = \varphi_p^{\circ} - (\varphi_p^{\circ} - \varphi_p^{\infty})(1 - e^{-t/t_\kappa}) \tag{3.28}$$

This first order process is described by a new parameter, t_κ, the boundary time constant. In dimensionless form

$$\theta\big|_{z=1} = \left(1 - e^{-\tau/\tau_\kappa}\right) \tag{3.29}$$

where τ_κ is the dimensionless boundary time constant:

$$\tau_\kappa = \frac{t_\kappa D_m}{R_\circ^2} \tag{3.30}$$

This makes the fractional approach to equilibrium in Eq. 3.24, a function of the dimensionless time τ, the volume ratio, Φ, and the boundary time constant, τ_κ.

The time variable surface boundary condition reflects the finite time required for the disentanglement of the polymer network. For $\tau_\kappa \ll 1$, the surface relaxation is much faster than the diffusive transport and the swelling proceeds as if there were instantaneous achievement of equilibrium at the surface. When $\tau_\kappa \gg 1$, there is essentially no variation of polymer volume fraction inside the gel during the swelling process.

For the special case of $\tau_\kappa \gg 1$, the time variation of surface polymer volume fraction is identical to the time variation of polymer volume fraction of the gel. Therefore, Equation 3.28 acquires the following form

$$\varphi_p = \varphi_p^{\circ} - (\varphi_p^{\circ} - \varphi_p^{\infty})(1 - e^{-t/t_\kappa}) \tag{3.31}$$

Combining Equations 3.14, 3.21, 3.24, and 3.31 yields

$$F = \frac{1 - \exp\left(-\tau/\tau_\kappa\right)}{\Phi - (\Phi - 1)\left(1 - \exp\left(-\tau/\tau_\kappa\right)\right)} \tag{3.32}$$

3.5. MODEL PREDICTIONS WITH CONSTANT D_m AND t_κ

When the gel boundary moves, it is no longer possible to derive analytical solutions of the equations even for a constant diffusion coefficient. The model equations were solved numerically by the finite difference method of Sparrow and Chuck (1984) for spheres. An implicit scheme was used for the gel diffusion equation and an explicit scheme for the interface equation. The discretization, and the convergence and accuracy of the numerical computations are discussed in Singh (1993). Results are presented here as the fractional approach to equilibrium, *F*, versus the square root of dimensionless time, $\sqrt{\tau}$.

Figures 3.19 and 3.20 show volume change curves for $\Phi=1$ and $\Phi=100$, respectively, for several values of τ_κ. The curves for $\Phi=1$ represent water uptake without change in gel volume; i.e. the solution for Fickian diffusion in a sphere. In both figures, when τ_κ equals 0.001, the swelling curve essentially merge with the curve for no relaxation, i.e., the curve for $\tau_\kappa = 0$, which is the solution with the dimensionless surface polymer volume fraction rising instantaneously to 1. With increasing τ_κ, the sigmoidal portion becomes more pronounced and swelling is slower. When τ_κ equals 10, the swelling curve approaches the curve for the relaxation dominated process i.e., Equation 3.32.

Figures 3.21, 3.22 and 3.23 show the concentration profiles for $\Phi=100$ at several dimensionless times, τ, for different τ_κ values. The dimensionless polymer volume fraction is plotted against the dimensionless radius r/R_o. Figure 3.21 shows the concentration profiles for $\tau_\kappa = 0.001$. With increasing time, the dimensionless radius increases from 1 towards a final value of 4.64. Because the surface relaxation is much faster than the diffusive transport, swelling proceeds almost as if the dimensionless surface polymer volume fraction reached its equilibrium value instantaneously. At short times, there exist sharp gradients near the moving boundary. Figure 3.22 shows the concentration profiles for several τ values for $\tau_\kappa=0.1$, where, because of relaxation, the surface polymer volume fraction does not rise instantaneously to 1. The concentration

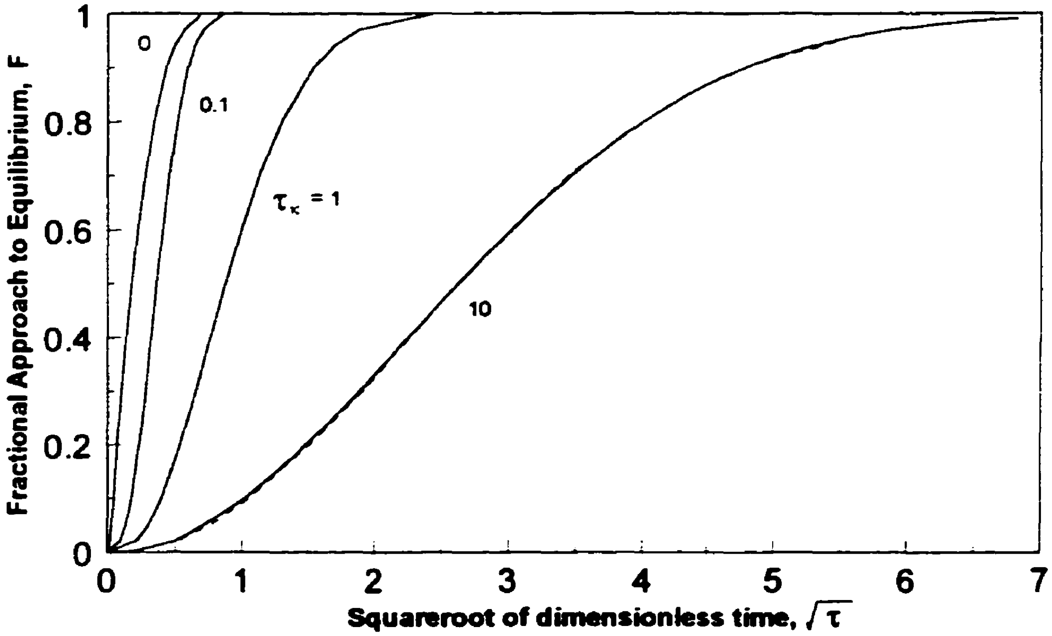

FIGURE 3.19. Swelling curves for spheres with constant D_m for different values of τ_κ for Φ=1. The dotted line is the solution of τ_κ>>1 limiting case as presented in Equation 3.32.

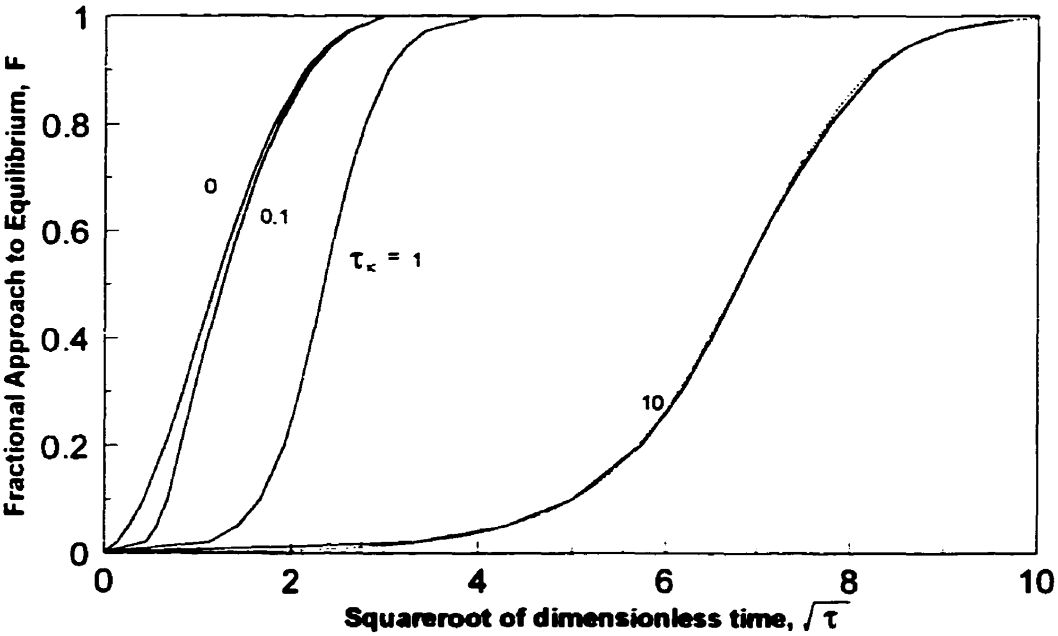

FIGURE 3.20. Swelling curves for spheres with constant D_m for different values of τ_κ for Φ =100. The dotted line is the solution of τ_κ>>1 limiting case as presented in Equation 3.32.

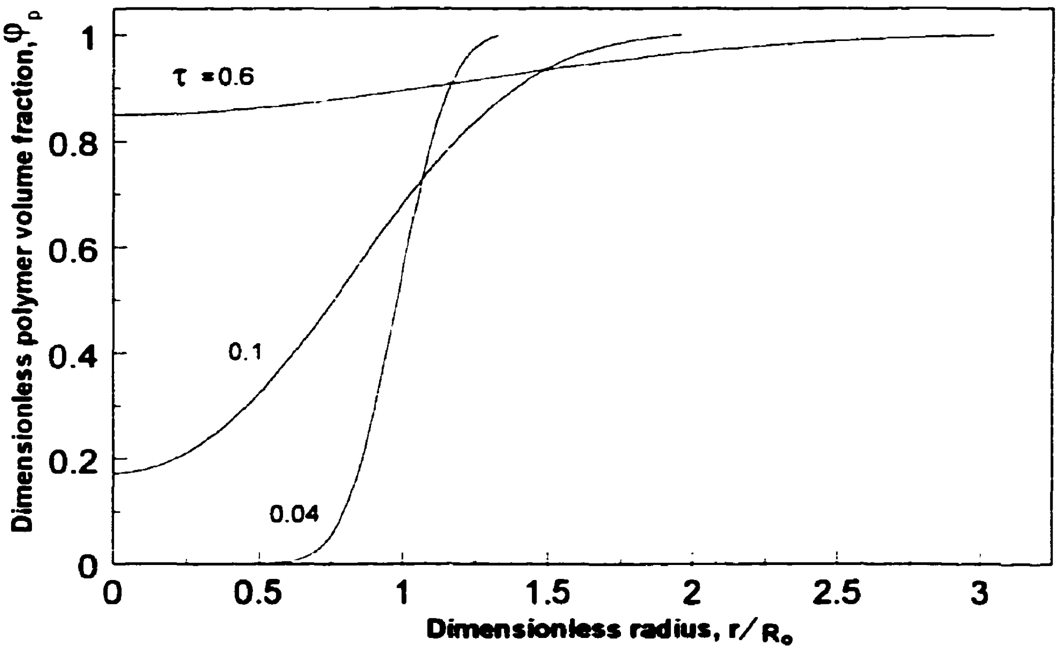

FIGURE 3.21. Concentration profiles for spheres at various dimensionless times, τ, for relaxation time constant τ_κ equal to 0.001. (Φ=100)

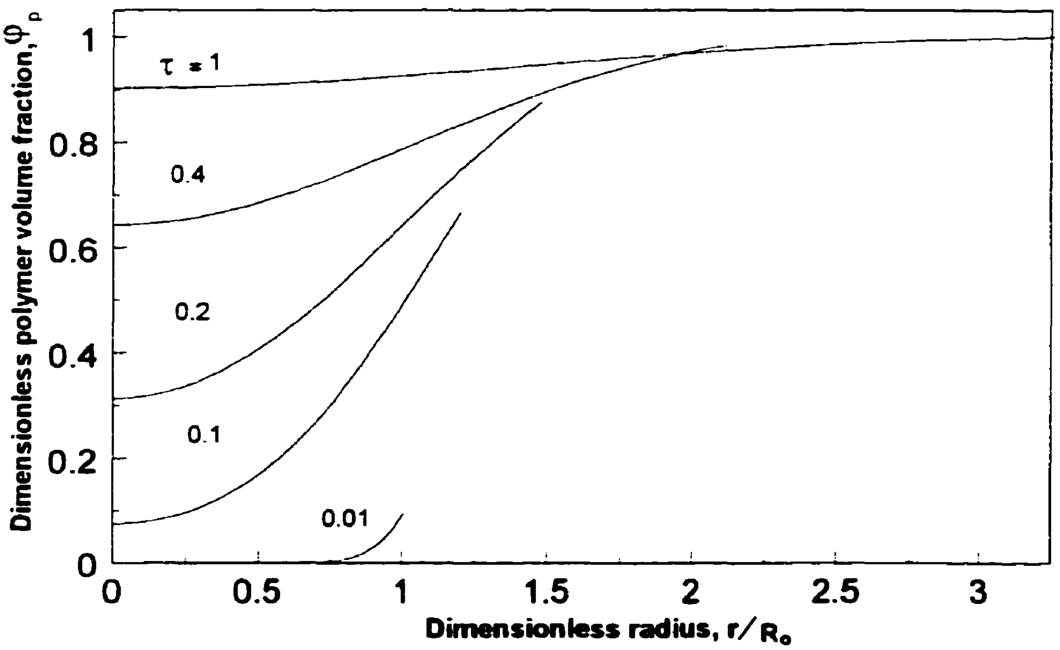

FIGURE 3.22. Concentration profiles for spheres at various dimensionless times, τ, for relaxation time constant τ_κ equal to 0.1. (Φ=100)

gradient near the moving boundary is less sharp than for $\tau_\kappa = 0.001$. Finally, Figure 3.23 shows the concentration profiles for $\tau_\kappa = 10$. In this case, relaxation is much slower than diffusion, thus there is essentially no spatial variation of polymer volume fraction inside the gel.

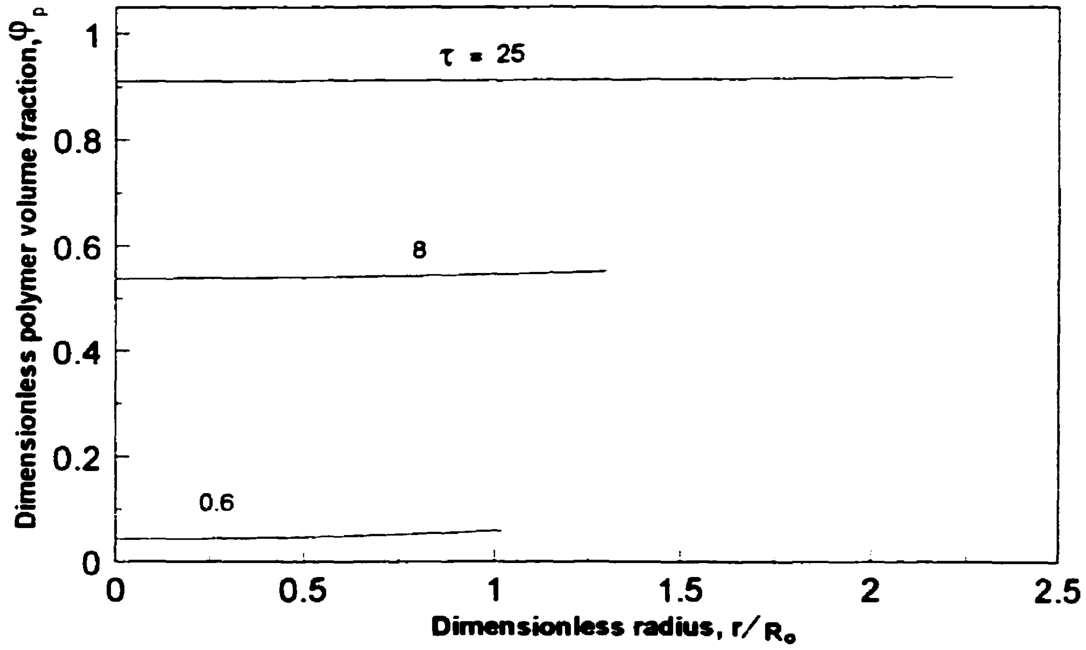

FIGURE 3.23. Concentration profiles for spheres at various dimensionless times, τ, for relaxation time constant τ_κ equal to 10. (Φ=100)

3.6. COMPARISON OF EXPERIMENTS WITH MODEL

3.6.1 ESTIMATION OF THE PARAMETERS

The two unknowns in the model are the diffusion coefficient, D_m, and the relaxation time constant, t_κ. These parameters were estimated by minimizing the following objective function:

$$\Im = \sum_{i=1}^{n}\left[F_i^{\text{exp}} - F_i^{\text{model}}\right]^2 \qquad (3.33)$$

where n is the number of experimental points.

A PASCAL program OPTIM, which uses Powell's method of conjugate directions (Press et al., 1989), was used to obtain the unconstrained minimum of the objective function. The goodness of fit of the model to the experimental points was measured by the following correlation coefficient, r_c

$$r_c = \sqrt{1 - \frac{\sum_{i=1}^{n}\left[F_i^{exp} - F_i^{model}\right]^2}{\sum_{i=1}^{n}\left[F_i^{exp} - F^{av}\right]^2}} \tag{3.34}$$

where F_{av} is the average value of experimental points.

3.6.2 FITTING THE MODEL TO DATA FOR GEL SWELLING IN WATER

The volume change model for constant D_m with t_κ=0 and Φ=550 was fitted to the Stockosorb data for a sphere with a radius of 0.62 mm as shown in Figure 3.24. The dotted curve on the left is the best fit, which was obtained with D_m = 9.2×10^{-10} m^2/s. The correlation coefficient was equal to 0.941. Since the experimental swelling curve was more sigmoidal than the fitted curve, t_κ was adjusted along with D_m . The solid curve represents the best fit, which was obtained with D_m = 1.0×10^{-9} m^2/s and t_κ =24 s (or τ_κ = 0.06) and gave a correlation coefficient of 0.984. This is a better fit during both the initial and the final phases of swelling, which are not well fitted with t_κ =0. With these best fit values, the solid curve on the right was computed for a 0.76 mm radius gel sphere. The prediction is satisfactory given that these data were not used in fitting parameters.

Figure 3.25 is a similar plot for Sumitomo gels. The curve on the left was obtained by fitting the model to experimental points for a sphere with an initial radius of 0.28 mm. The best fit values were D_m = 8.3×10^{-10} m^2/s and t_κ=24 s. The correlation coefficient was equal to 0.962. With the best fit values, the curve on the right was computed for a 0.35 mm radius gel sphere.

The value of t_κ was equal to 24 s for both Stockosorb and Sumitomo gels. The boundary time constant, t_κ, reflects the time required for disentanglement

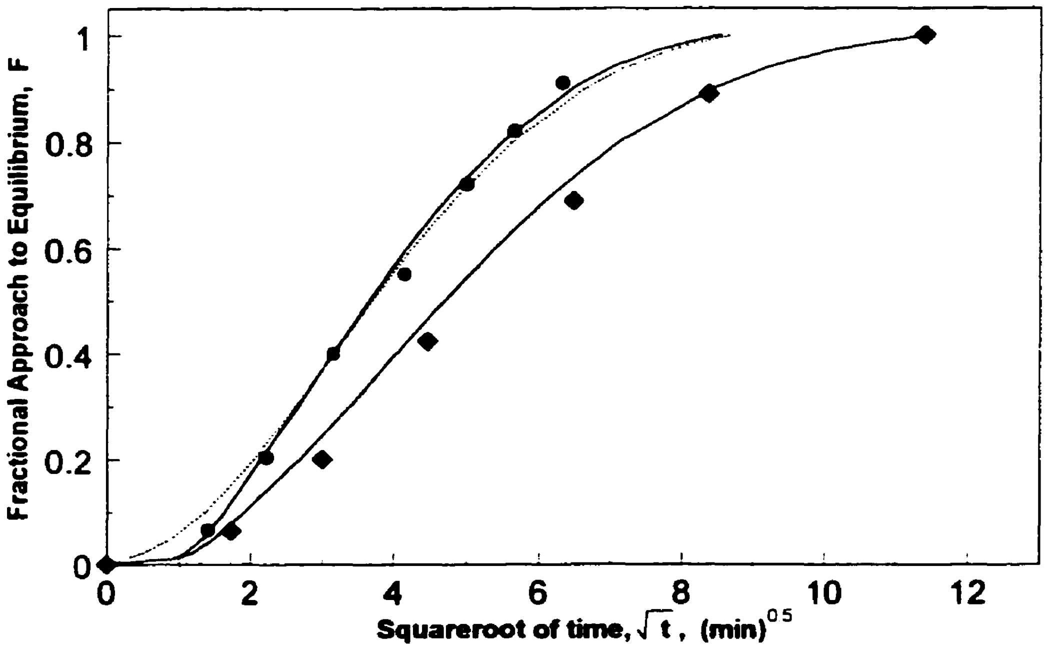

FIGURE 3.24. Best fits of model (the two curves on left) to the swelling data for Stockosorb gels in water [Φ = 170]. Dry gel radius = 0.62 mm (•). D_m=9.2×10^{-10} m^2/s, t_κ=0 (dotted curve); D_m=1.0×10^{-9} m^2/s, t_κ=24 s (solid curve). The solid curve on right is the model prediction for a dry gel radius equal to 0.76 mm (■) using D_m=1.0×10^{-9} m^2/s, t_κ=24 s.

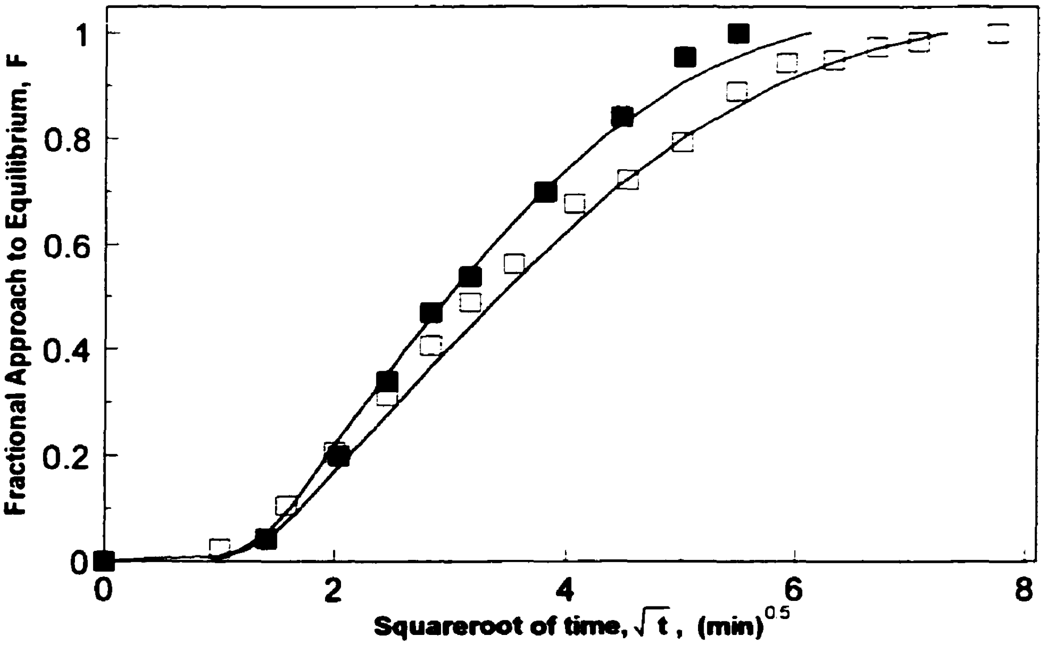

FIGURE 3.25. Best fit of model (the curve on left) to the swelling data for Sumitomo gels in water [Φ=550]. Dry gel radius=0.28 mm (■). D_m=8.3×10^{-10} m^2/s, t_κ= 24 s. The curve on right is the model prediction for a dry gel radius equal to 0.35 mm (☐) using the fitted values.

of the polymer network at the gel surface. The polymer molecules that form the gel are entangled as well as covalently crosslinked. When the gel is immersed in water, the molecules return to a "relaxed" state. One measure of the effective entanglement or crosslinking of polymers is the matrix elastic constant, *K*, discussed in Chapter 2. As pointed out in Section 2.4, the *K* values of Sumitomo and Stockosorb gels are nearly equal, thus the two gels should have similar t_κ values.

If the only difference between the surface of a crosslinked gel and that of a non-crosslinked gel in water is that the latter dissolves, then it is worthwhile to compare the value of t_κ with the time required by a non-crosslinked polymer particle to dissolve. A non-crosslinked polymer particle smaller than 100 μm diameter, requires 20-30 s to dissolve in a good solvent (Devotta *et al.*, 1993). This time range compares well with a t_κ of 24 s.

The fits with $t_\kappa = 0$ and $t_\kappa = 24$ s are different largely in the $F<0.2$ region. The ratio of the relaxation time constant to the swelling time constant is approximately equal to 0.02, thus indicating that relaxation is important in the first few minutes only. Using $t_\kappa = 24$ s, as opposed to $t_\kappa = 0$, changes the best fit values of D_m by 10%. Thus to obtain accurate values of D_m it is important to use the boundary time constant. In addition, accurate predictions for small values of *F* are required for soil applications in order to interpret the results of flow in gel-conditioned sand (Chapter 4).

3.6.3 FITTING THE MODEL TO DATA FOR GEL SWELLING IN SAND

First, the volume change model with $\Phi=100$ and the best fit values of parameters for gels in water ($D_m = 1.0\times10^{-9}$ m^2/s and $t_\kappa = 24$ s) was used to predict the swelling of Stockosorb gels. The predicted curves were much faster than the experimental curves. Next, using $D_m = 1.0\times10^{-9}$ m^2/s with adjustable t_κ, the model was fitted to the data. The slowed down the swelling but the fit was poor with a correlation coefficient equal to 0.833.

There are two important differences between swelling in water and swelling in sand: first, the equilibrium swelling ratio differs significantly for the two situations; second, as described in Section 3.3.3, sand slows swelling. The mechanism is related to the frictional nature of the surrounding sand. To account for the resistance to expansion of gel, the mutual diffusion coefficient in the extended Gel Volume Change model was replaced with an effective diffusion coefficient, D_{eff}, expressed by

$$D_{eff} = \omega D_m \tag{3.35}$$

where D_m is the mutual diffusion coefficient for swelling in water and ω is a retardation factor. In subsequent analysis, D_{eff} was adjusted along with t_κ.

Figure 3.26 shows the swelling data for Stockosorb gels in saturated sand. The left curve in the figure represents the best fit obtained with $D_{eff} = 3.0\times10^{-10}$ m^2/s and t_κ=24 s. The correlation coefficient was equal to 0.954. Note that t_κ is identical to the t_κ for water. With these best fit values the curve on the right was computed for a 0.76 mm radius gel sphere.

Figure 3.27 shows a similar analysis for Sumitomo gels (Φ=250). The curve on the right provides a good fit to the experimental points for the gel with an initial radius of 0.41 mm. The best fit values were $D_{eff} = 2.3\times10^{-10}$ m^2/s and t_κ=24 s. The correlation coefficient was 0.950. With the best fit values, the curve on the left was computed for a 0.36 mm radius gel sphere.

The data in Figure 3.28 are for fixed-volume-of-water experiments with a 0.76 mm Stockosorb gel. The curve in the figure was computed by using the best fit values obtained previously: $D_{eff} = 3.0\times10^{-10}$ m^2/s and t_κ=24 s. The fit is satisfactory with these values, which were obtained from experiments in water-saturated sand.

The values of ω for Sumitomo gels, swollen in 0.19 mm (water-saturated) sand, and for Stockosorb gels, swollen in 0.19 mm (water-saturated) sand, 0.19 mm (fixed-volume-of-water) sand, and 0.48 mm (water-saturated) sand were identical; ω was essentially equal to 0.3 for both gels. Gels are expected to

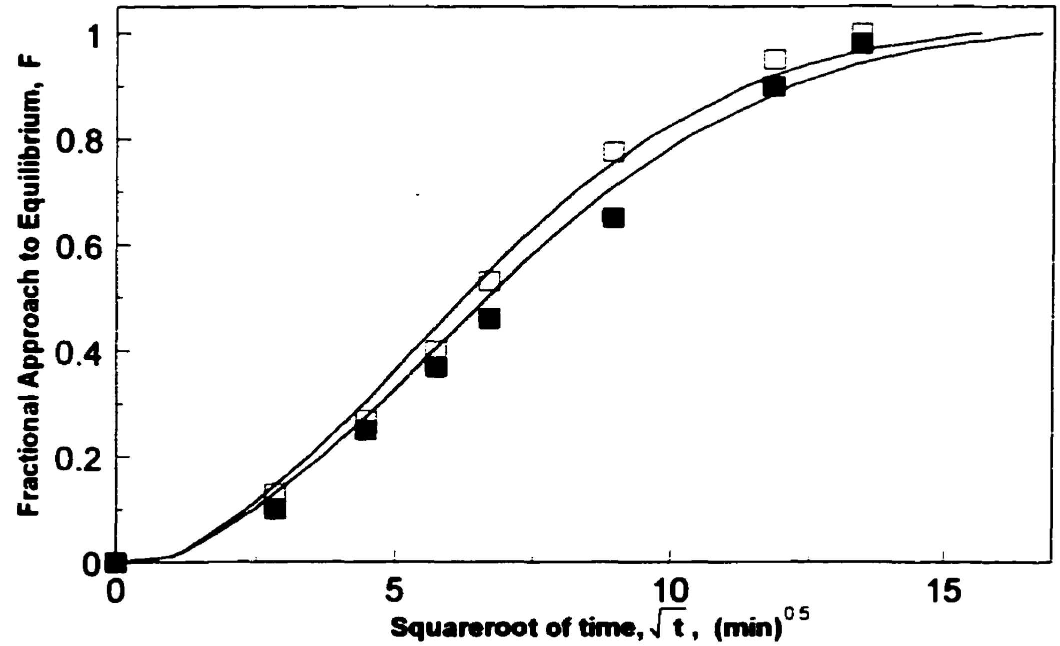

FIGURE 3.26. Best fit of model (the curve on left) to the swelling data for Stockosorb gels in saturated sand [Φ = 100]. Dry gel radius=0.71 mm (□). D_{eff}=3.0×10^{-10} m^2/s, t_r= 24 s. The curve on right is the model prediction for a dry gel radius equal to 0.76 mm (■) using the fitted values. Sand size: 0.19 mm. Depth: 1 cm.

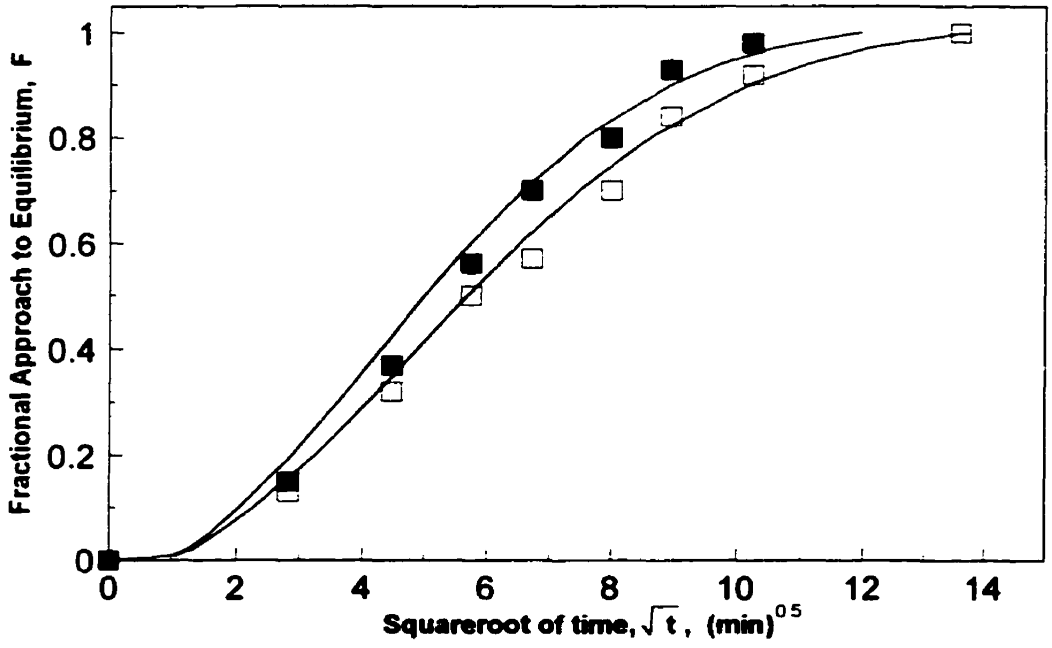

FIGURE 3.27. Best fit of model (curve on right) to the swelling data for Sumitomo gels in saturated sand [Φ=250]. Dry gel radius=0.41 mm (□). D_{eff}=2.3×10^{-10} m^2/s, t_r= 24 s. The curve on left is model prediction for a dry gel radius equal to 0.36 mm (■) using the fitted values. Sand size: 0.19 mm. Depth: 1 cm.

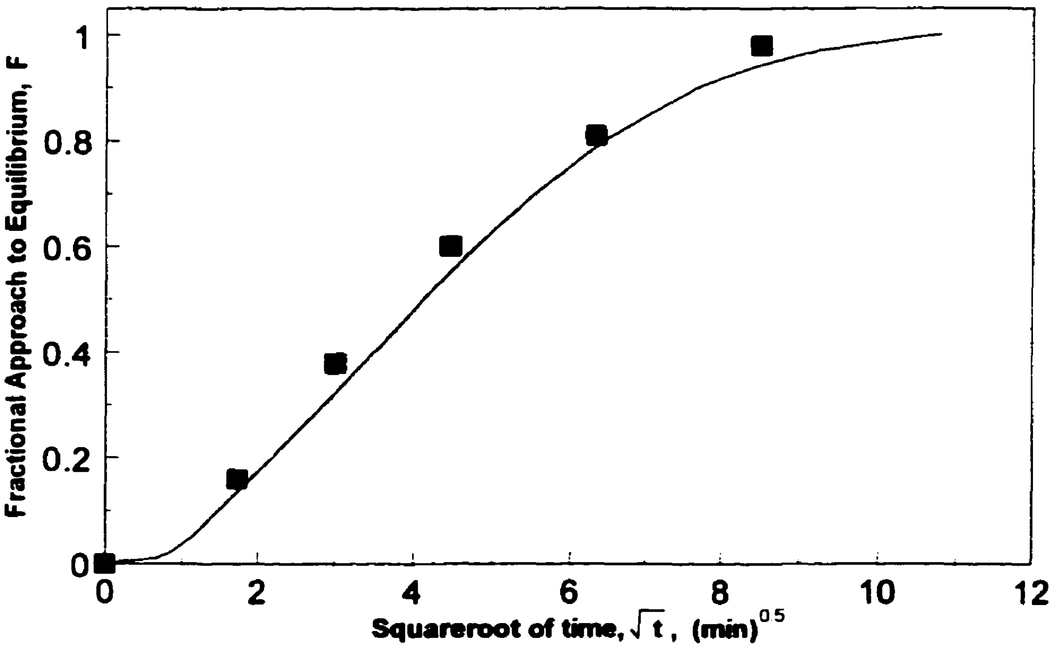

FIGURE 3.28. Model prediction of the swelling data for Stockosorb gels in fixed-volume-of-water sand [Φ = 27.7] using fitted values for swelling in saturated sand. Dry gel radius = 0.76 mm (■). D_{eff}=3.0×10^{-10} m^2/s, t_k= 24 s (the solid curve). Sand size: 0.48 mm. Depth: 1 cm.

swell with a different value of ω in real agricultural fields. In fields, owing to the absence of the wall effect of the cell (see Section 3.3.3), the value of ω is expected to be higher than 0.3 but much less than 1.

The values of diffusion coefficients for gels reported in the literature lie in the range 10^{-12}-10^{-9} m^2/s (Tanaka, 1985; Gehrke, 1993). The diffusion coefficients obtained here lie at the upper end of the reported values. It is interesting to note that the diffusion coefficients of the two gels in water are roughly a factor of two smaller than the self diffusion coefficient of water, which is 2.0×10^{-9} m^2/s (Cussler, 1984). The significance of this result is related to the definition of a self diffusion coefficient.

The self diffusion coefficient of water measures the mobility of the molecules, unlike the mutual diffusion coefficient which measures the rate at which the concentration gradients disappear. For a binary solvent-polymer solution there are two self diffusion coefficients (Vrentas, 1986):

$$D_s^* = RT\Lambda_s = RT/f_s \tag{3.36}$$

$$D_p^* = RT\Lambda_p = RT/f_p \tag{3.37}$$

where Λ_i is the mobility of component *i* and f_i is the friction coefficient, which is the product of effective viscosity of the medium and the effective diameter of the component *i*. Most molecular theories derive expressions for D^*_i rather than D_m.

An approximate relationship between the self-diffusion coefficients and D_m, based on the combination of statistical mechanics with the phenomenological theory of irreversible processes is (Loflin et al., 1969):

$$D_m = \left(\frac{\partial \ln a_s}{\partial \ln x_p}\right)_{TP} \left[D_s^* x_s + D_p^* x_p\right] \tag{3.38}$$

where a_s represents the activity of the solvent and x_i is the mole fraction of component *i*. Since the macromolecular D^*_p is generally much smaller than the small molecule D^*_s the above expression may be further simplified to the following form (Vrentas, 1986):

$$D_m = QD_s^* \tag{3.39}$$

where Q is a constant which is less than 1. Comparing Equation 3.39 to the fitted mutual diffusion coefficients for Sumitomo and Stockosorb gels and the literature value of self diffusion coefficient of water yields the value of *Q* equal to 0.5.

Chapter 4

FLOW IN GEL-CONDITIONED SAND

4.1. INTRODUCTION

In the previous two chapters, it became obvious that sand alters the swelling properties of superabsorbent gels. This chapter sets out to investigate how superabsorbent gels, in turn, modify the flow of water through sand.

The flow in uniformly gel-conditioned sand is illustrated schematically in Figure 4.1. When water is distributed over the surface of a dry bed, it leads to:

- the formation of a gel layer on the surface
- the formation of a wetting front which moves downward
- the upward movement of the surface in response to the swelling of the subsurface gel particles.

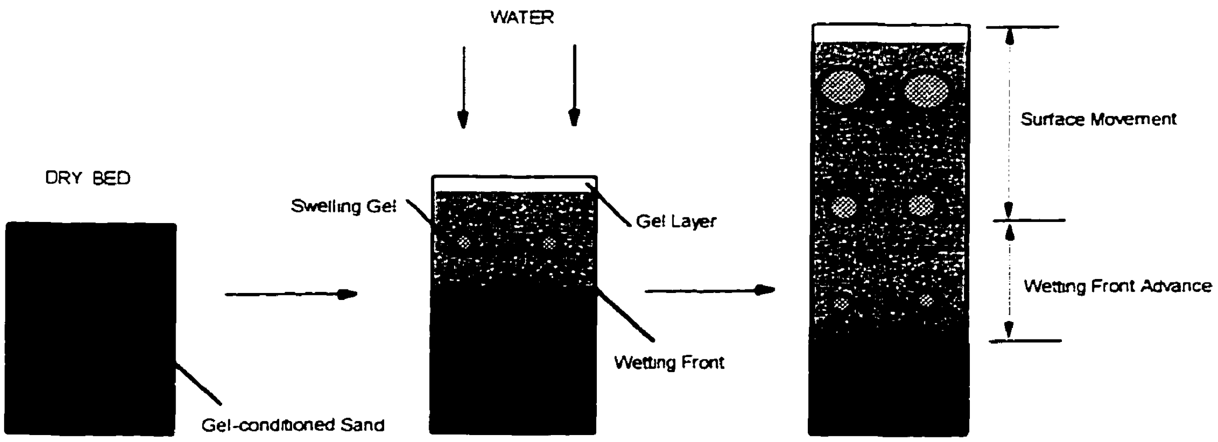

FIGURE 4.1. Schematic of flow of water through gel-conditioned sand.

The following section describes two-dimensional cell experiments which disclose the mechanism of formation of the gel layer at the surface. Column experiments to examine wetting front advance and surface movement are described next. Finally, two models are developed to describe the flow and fitted to experimental data.

4.2. GEL LAYER PHENOMENA

The formation of a gel layer has profound consequences for field soils. The gel layer may reduce the rate of penetration of water into the soil. A thick gel layer may become essentially impenetrable to water, thereby retaining irrigation water or rainfall on the surface, thus facilitating runoff. Such retained water evaporates quickly and is not available to plant roots which may be located up to 30 cm beneath the soil surface. The gel layer may also act as a seal against the entry of air. Another problem has to do with penetration of seedlings attempting to emerge after germination. On the other hand, for erosion control, for instance, the formation of a gel layer may be beneficial. On drying, the gel layer binds the sand particles by adhering the sand particles through polymer bridges.

MECHANISM OF FORMATION OF A GEL LAYER

Gel layer formation was observed in the two-dimensional cell described in Chapter 2. At the beginning of each experiment, uniformly-mixed gel-conditioned sand was packed into the cell. Next, water was distributed continuously from a height of 20 cm from the surface. The time evolution of the cell was video-recorded with the help of rear illumination. Video images of the cell interior over a spatial field of 14 cm wide by 10 cm high are presented in Figures 4.2 to 4.4.

The image of the dry cell at time zero is shown in Figure 4.2a. The dark region in the lower portion of the figure is dry gel-conditioned sand (190 μm). This region is dark because no light passed through the sand-gel mixture. The sand/air interface is located just below the horizontal line 5 cm from the bottom of the picture. The bright region above the sand surface, is occupied by air. This region has varying intensities of brightness depending on distance from the fluorescent lamp behind the cell.

Figure 4.2b, shows the cell 1 s after water entered from the top to disturb the sand-gel surface by the impact of its fall. The bright region of the image shows water swirling above the disturbed surface. In the dark region of the image a wetting front has formed between 2.6 and 3.9 cm from the bottom. Within the dark region there was a separation between the lighter wet zone above the wetting front and a darker dry zone below.

After 5 s, the wetting front was no longer visible because it has moved below the camera's field of view — see Figure 4.3a. The previously disturbed sand-gel surface became smoother. The space above the surface is completely filled by water. The bright spots inside the water are illuminated gel particles. These gel particles, initially located in the soil matrix, were set free by the disturbance caused by the impact of the water on the surface of the sand-gel mixture. The released gel particles, which had a specific gravity close to that of water, settled much less rapidly than the sand particles which were two-and-a-half times denser and thus the gel particles remained suspended in water for some time.

After 30 s, Figure 4.3b shows a bright area on the surface of the sand as a gel layer began to form. The gel layer formed as the water-borne gel particles settled on the sand surface. Below the sand surface, the light area between 2.5 and 4 cm from the bottom was caused by swelling gel particles beneath the surface. Gel particle swelling also caused the expansion of the soil matrix as a whole.

At 40 s (Figure 4.4a) the gel layer thickened further as more water-borne gel particles settled on the surface and as the individual gel particles swelled. Finally, one minute after the initial disturbance of the dry sand-gel mixture, all the water-borne particles settled on the surface to become a part of the swelling gel layer, as shown in Figure 4.4b.

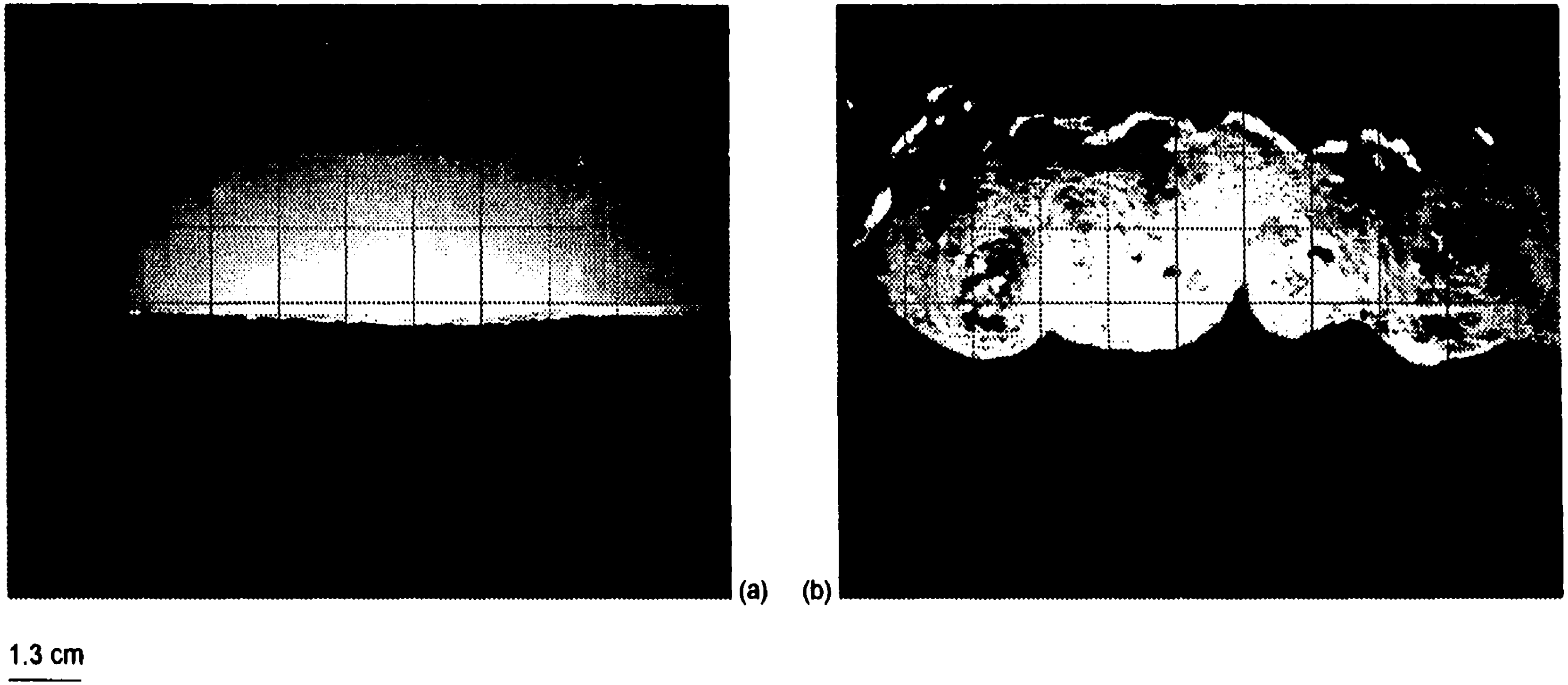

FIGURE 4.2. Images of gel layer formation inside a two-dimensional cell at (a) 0 s and (b) 1 s. Scale: one square equal to $(1.3\ \text{cm})^2$.

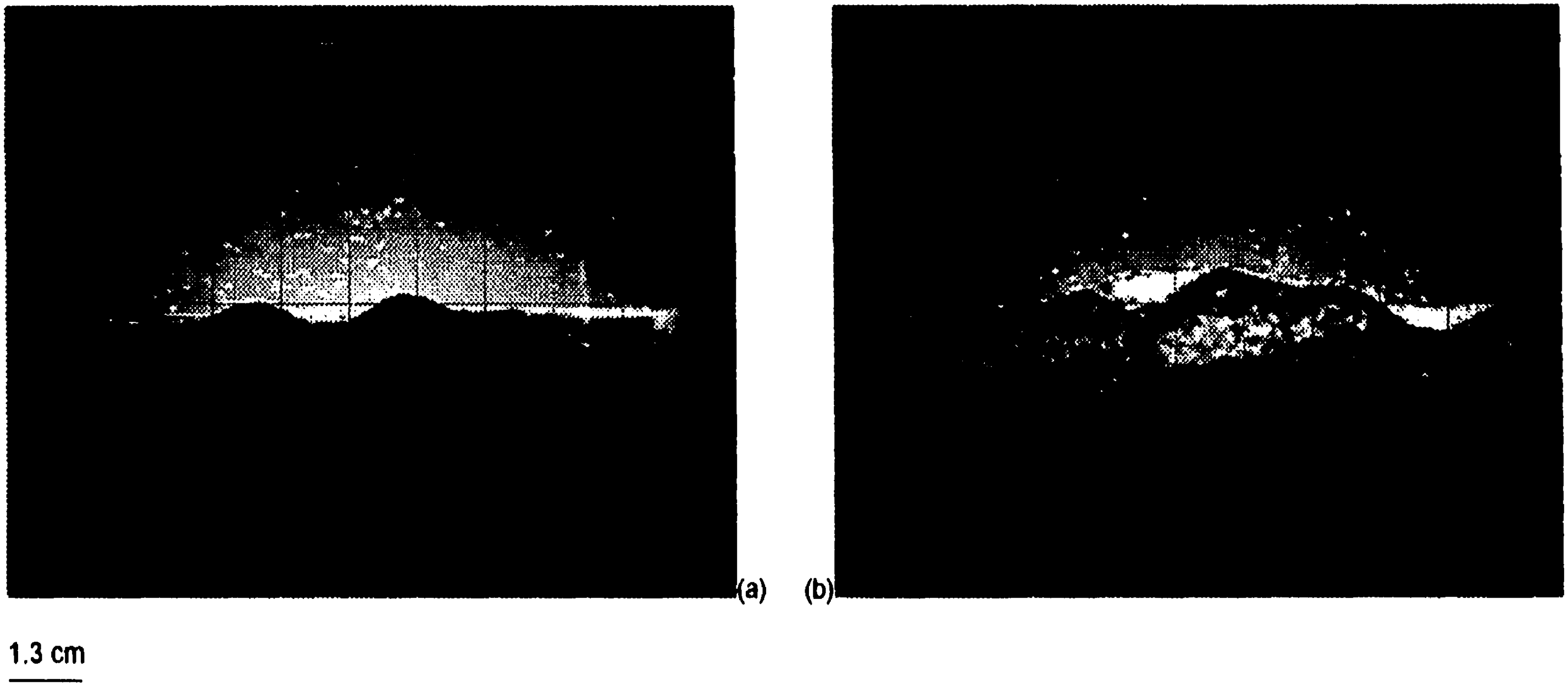

FIGURE 4.3. Images of gel layer formation inside a two-dimensional cell at (a) 5 s and (b) 30 s. Scale: one square equal to (1.3 cm)^2.

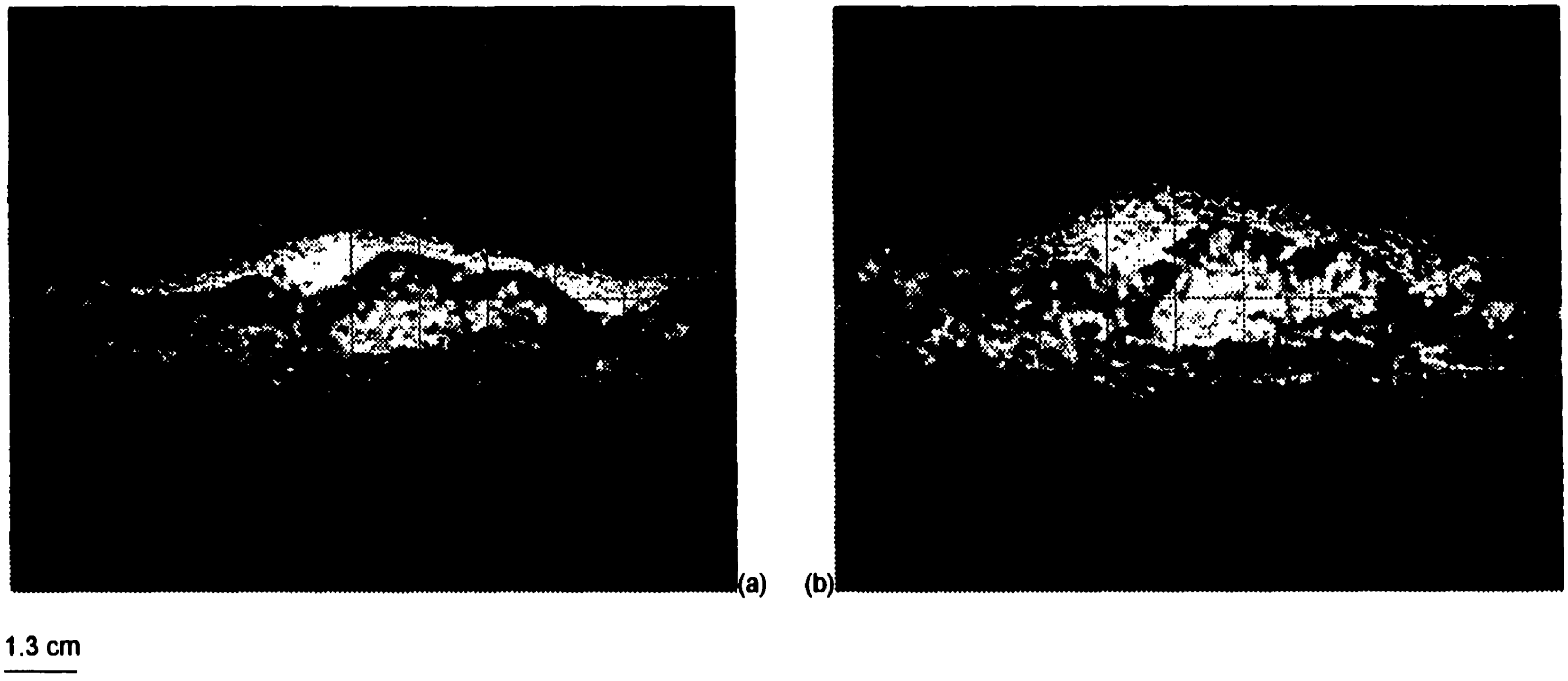

FIGURE 4.4. Images of gel layer formation inside a two-dimensional cell at (a) 40 s and (b) 60 s. Scale: one square equal to $(1.3\ \text{cm})^2$.

GEL LAYER THICKNESS

The thickness of the gel layer is dictated by sand size, gel type and size, and gel dosage among other variables. The video images at t=0 s and t=10 min for different gel types and dosages are shown in Figure 4.5. Average gel layer thicknesses measured from such images are tabulated in Table 4.1.

TABLE 4.1. Comparison of gel layer thickness for different gel types and dosages in different sands.

GEL DOSAGE	SAND SIZE	GEL LAYER THICKNESS
0.5 % Sumitomo	190 μm	1.0 cm
1.0 % Sumitomo	190 μm	1.2 cm
1.0 % Stockosorb	190 μm	0.4 cm
1.0 % Sumitomo	475 μm	2.5 cm

The gel layer was thicker for coarser sand. Large sand particles make it easier for gel particles trapped inside the soil matrix to rise to the surface. This is because large sand particles have fewer particle-to-particle contacts per unit volume of saturated sand than the smaller particles, thus they provide less resistance to the upward movement of a gel particle. As expected, the gel layer was thicker for higher gel dosage. The gel layer was also thicker for Sumitomo gels which swell more than Stockosorb gels. A higher swelling degree, a smaller size, and a smoother shape help Sumitomo gels form thicker gel layers than Stockosorb gels. A simple calculation shows that the gel particles, both Stockosorb and Sumitomo, which form the gel layer at the surface, come from a gel-conditioned sand layer approximately 1 cm thick. This 1 cm thickness may change if water is distributed onto the soil surface from a different height.

MOISTURE PROFILES WITH AND WITHOUT THE FORMATION OF A GEL LAYER

Experiments were performed to see how the formation of a gel layer affects the moisture profiles inside a gel-conditioned sand column. Plexiglas columns

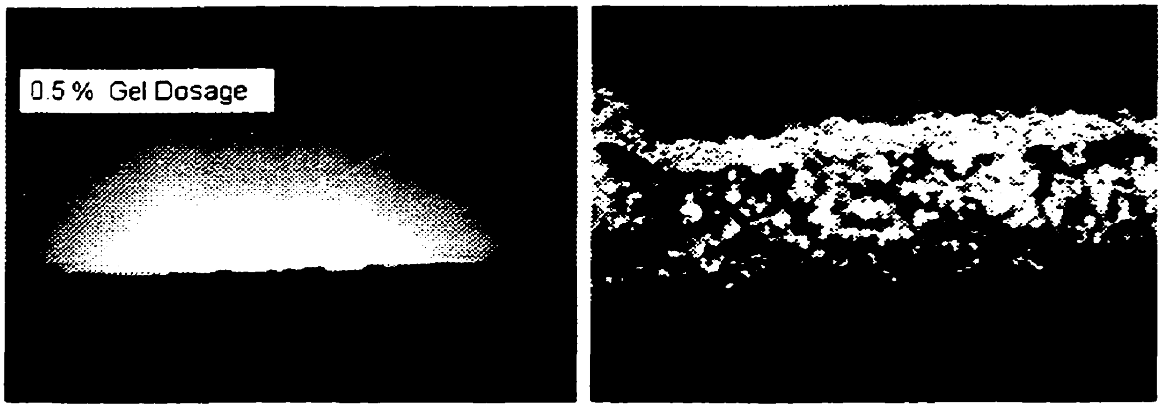

SUMITOMO

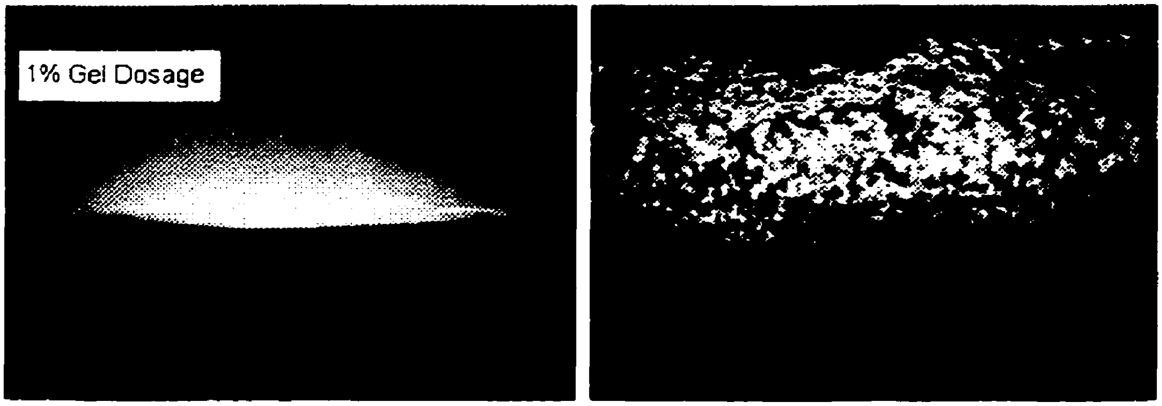

SUMITOMO

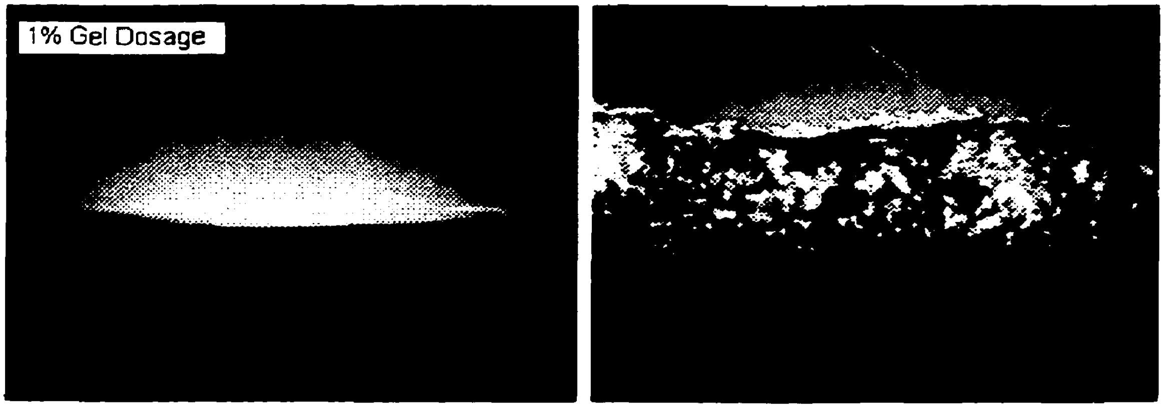

STOCKOSORB

FIGURE 4.5. Images of gel layer and surface expansion inside a two-dimensional cell at 0 and 10 minutes. Sand size was equal to 190 μm. The gel layer is the very bright area. Scale: ---- =1 cm.

— 6.9 cm in diameter and 30 cm long — with perforated bottoms were used for these experiments. Three columns were prepared: one with a uniform distribution of gel particles in sand, a second with a non-uniform distribution and a third with sand alone. The uniform distribution of gels particles was obtained by thoroughly mixing dry gel particles with dry sand particles and packing the resulting mixture into the columns to a height of 5 cm. The non-uniform distribution consisted of a 1 cm thick layer of gel-free sand above a 4 cm thick layer of uniformly gel conditioned sand.

Distilled water was distributed from a height of 20 cm above the surface and allowed to drain through the bottom of the column. Immediately after this, the columns were transferred to a larger container, 70 cm high and 12 cm in diameter, full of distilled water. The columns were held in a vertical position. The water level in the container was maintained at the level of the surface of the sand inside the inner column, thus ensuring complete saturation of the sand inside the columns. After 12 hours the columns were removed from the container, the bottom of each column was opened and the sand-gel mixture was gently pushed out with a piston. Samples in 3 mm lengths were sliced from the core and their water contents determined gravimetrically.

The moisture profiles in terms of mass fraction of water versus distance measured from the surface at time zero are shown in Figure 4.6. The data were reproducible within ± 3%. The difference between the uniform and the non-uniform gel distribution columns is reflected in the shape of their moisture profiles. For the uniform gel distribution, a gel layer is formed over the surface — compare Figure 4.7 (A) and (B).

On the other hand, the non-uniform column no gel layer is formed on the surface. In this column, the amount of water retained in the untreated upper sand layer is identical to that for saturated sand and the amount of water retained in the treated lower layer is similar to that for the uniform distribution column.

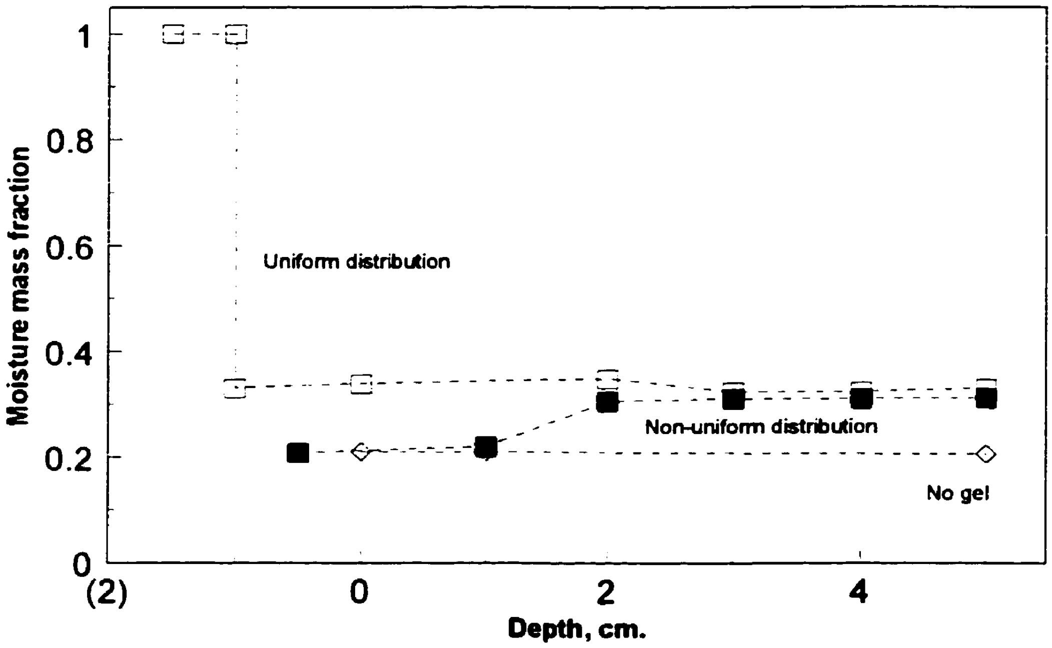

FIGURE 4.6. Moisture profiles for uniform gel distribution (□), non-uniform gel distribution (■), and no gel (◇) columns. Depth measured from original bed surface. Sand particle diameter equal to 190 μm.

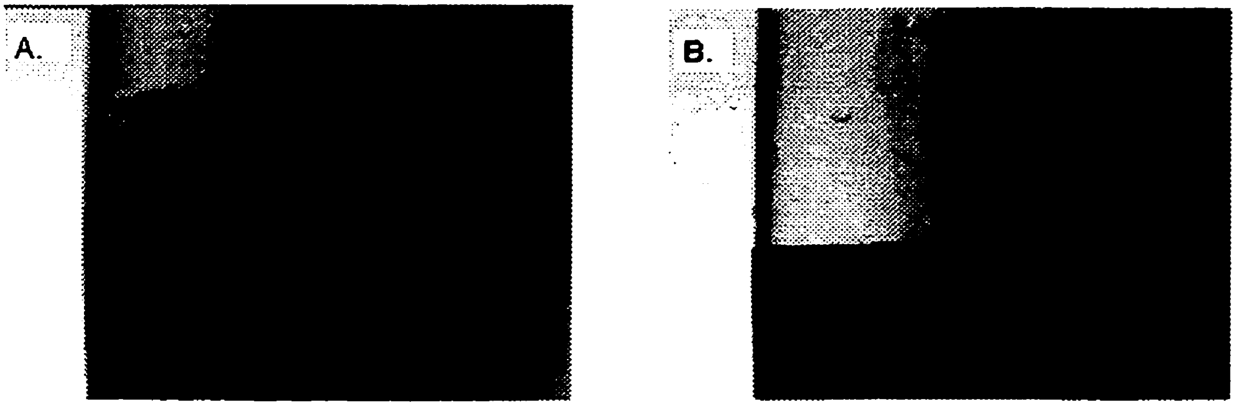

FIGURE 4.7. Images of surface layers in uniform (A) and non-uniform (B) distribution columns. The scale shown in the image A is in centimeters.

4.3 WETTING-FRONT ADVANCE AND SURFACE MOVEMENT EXPERIMENTS

PROCEDURE

The wetting-front advance and surface movement experiments were performed in Plexiglas columns: 6.9 cm in diameter and 132 cm long. The bottoms of the columns were perforated to retain the sand and to allow drainage. Dry sand of a given mesh size was mixed with a given dosage of gel particles in batches of 350 g. The column was packed in increments of 5 cm and the column wall was tapped 3 times after each increment. Sand or sand-gel mixture was poured into the column using a funnel. The funnel was raised 5 cm before pouring in the next increment. Sand or the sand-gel mixture was filled up to the 80 cm mark. Water was added through a distributor, installed at the top of the column, and dispersed evenly over the cross-sectional area of the cell. At time zero, the soil surface was ponded rapidly with water (approximate depth 5 mm). Thereafter, a constant depth of 5 mm (±1 mm) of water was maintained on the surface of the expanding bed. The wetting front advance and surface movement versus time were recorded manually. The position data were reproducible within ± 3%.

RESULTS

Figure 4.8 shows the position of the surface and the wetting front as a function of time for various Sumitomo gel dosages in 190 μm sand. The plot shows both the position of the upper surface of the bed and the position of the wetting front measured from the position of surface at time zero. The surface movement curve is above zero, whereas the wetting front advance curve is below zero. The surface movement increased with gel dosage. When no gel was present (0% dosage), the surface remained at its initial position, i.e. zero. The advance of the wetting front was impeded as gel dosage increased. The front moved fastest for 0% dosage. At a dosage higher than a critical value (above 0.63% for Sumitomo gel according to Equation 4.39) the wetting front

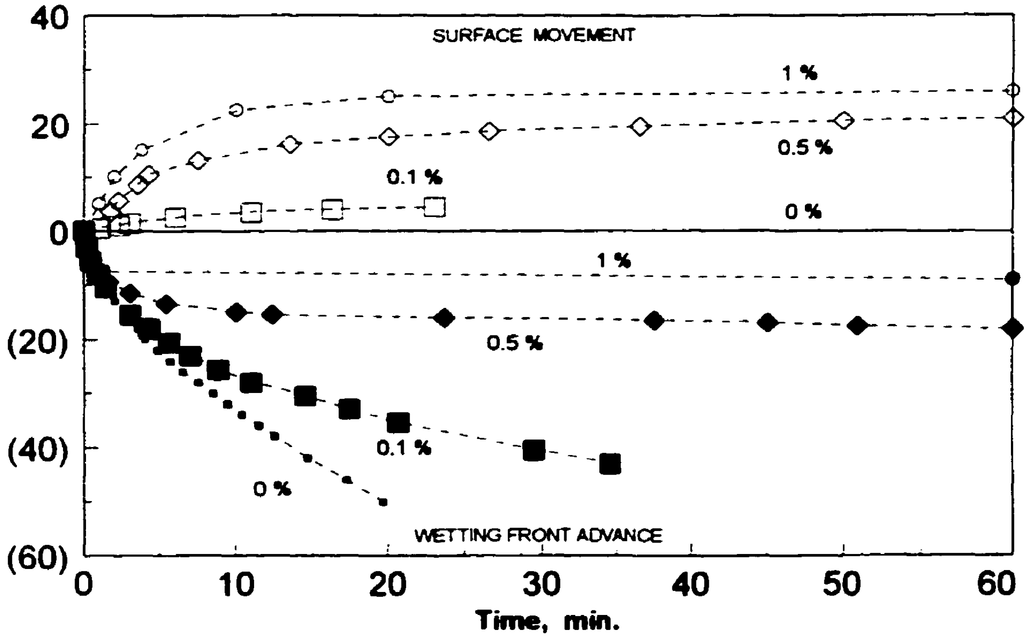

FIGURE 4.8. Surface movement and wetting front advance as influenced by different Sumitomo gel dosages in 190 μm sand shown on the same plot. (0%: •), (0.1%: □, ■), (0.5%: ◊, ◆), (1%: o,•). The dashed curves are drawn to guide the eye.

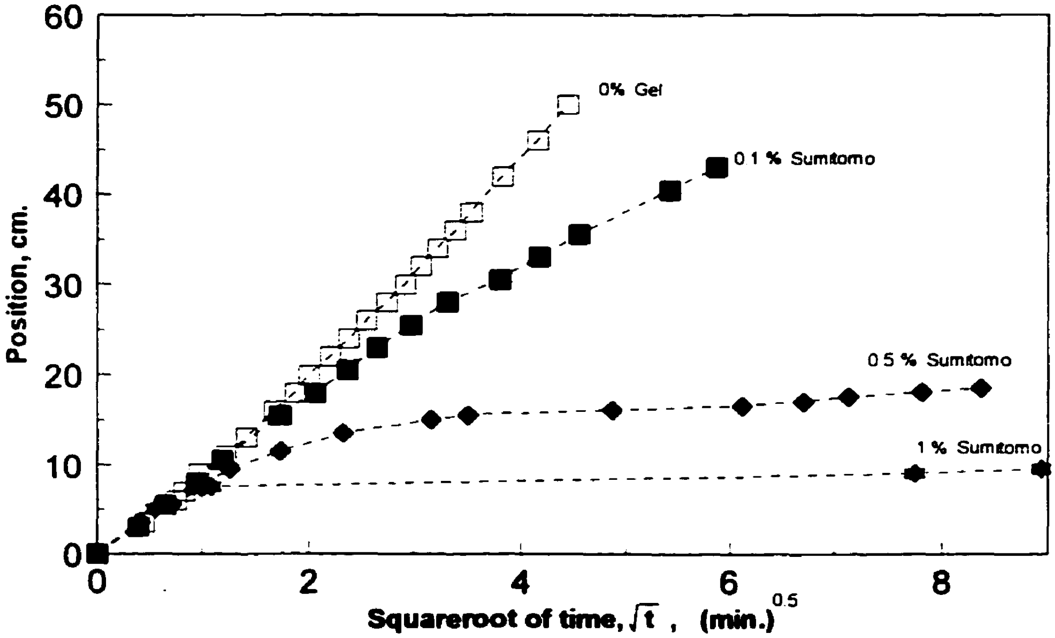

FIGURE 4.9. Wetting front advance for different Sumitomo gel dosages in 190 μm sand plotted as *Depth* vs $\sqrt{t}$. (0%: □), (0.1% Sumitomo: ■), (0.5% Sumitomo: ◆), (1% Sumitomo: ✱)

ceased to advance because the gel particles expanded to plug the cross section and prevent further downward flow of water.

Figure 4.9 presents the data for wetting front advance through Sumitomo gel-conditioned sand plotted as position measured from the position of surface at time zero, versus the square root of time in order to display the initial portions of the wetting front advance curves more clearly. On these coordinates the depth initially increased linearly with the square root of time for all dosages. The slopes were independent of dosage up for 1-2 minutes; thereafter the curves began to depart from the linear relationship with the departure occurring earlier for higher gel dosage. At a fixed time, the front advanced farther for lower dosages.

For all gel dosages, the wetting front advanced identically for the first few minutes because the gels, on coming in contact with water, do not start to imbibe large quantities of water immediately. As demonstrated in Chapter 3, the swelling of gels can be subdivided into early, middle, and late stages. Swelling is slow during the early stage, accelerates at the onset of the middle stage, and slows when approaching equilibrium. The wetting front advance is slowed as the gels enter the second stage of swelling. The rate of wetting front advance is fairly slow during this stage of increased gel swelling. The gel particles that form the gel layer on the surface of the bed impede the downward movement of water because flow is possible only through narrow interstitial spaces. The gel particles beneath the surface not only slow the wetting front by absorbing water but also occupy an increasing volume inside the column thereby further impeding the flow. At 1% gel dosage, the swollen gel particles stop the flow altogether. For dosages below the critical value, including zero dosage, the wetting front accelerates as it reaches the bottom of the column. The acceleration occurs because less air needs to be pushed out of the column by the wetting front now that it is closer to the bottom of the column.

Figure 4.10 shows the curves for both surface movement and wetting front advance plotted against time for Sumitomo and Stockosorb gels in 190 μm sand at a dosage of 0.5%. Sumitomo gels cause a larger surface movement and a smaller wetting front advance than Stockosorb gels. This is consistent with the equilibrium swelling results which show that Sumitomo gels swell approximately three times more than Stockosorb gels (See Table 2.2).

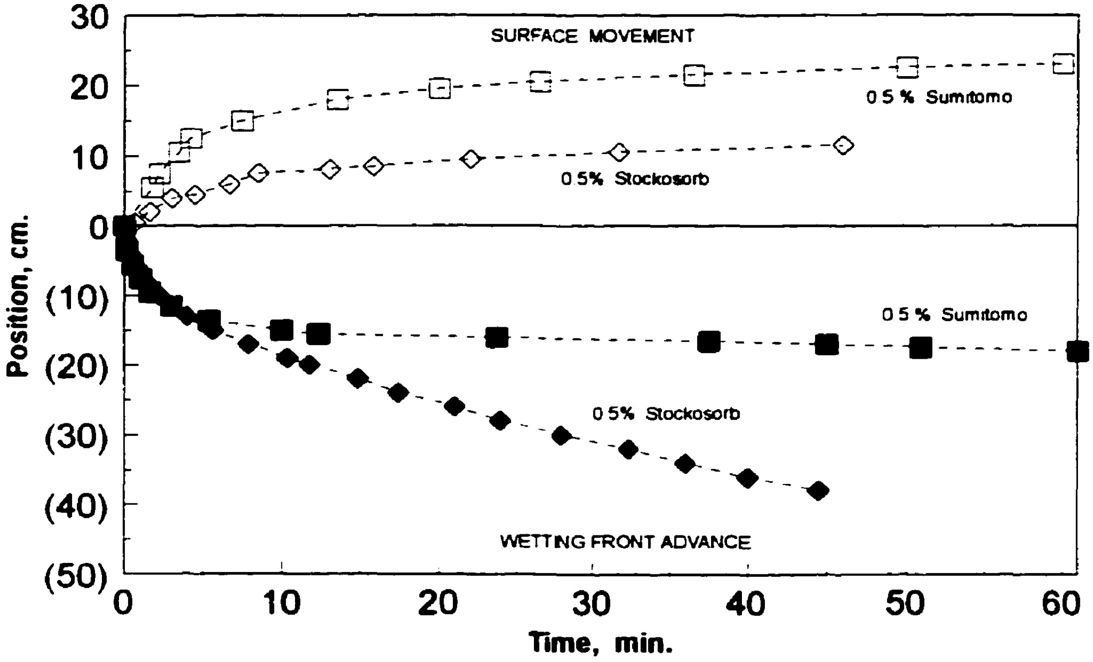

FIGURE 4.10. Surface movement and wetting front advance as influenced by different gel types, with identical dosage of 0.5% in 190 μm sand, shown on the same plot. (Sumitomo: □, ■) (Stockosorb: ◇, ◆)

For Sumitomo gels, the surface moved up more than the wetting front moved down for 0.5% dosage. At this dosage, although the gels did not plug the column completely, the gel volume fraction was sufficiently large to compete for most of the water as it infiltrated towards the bottom of the column. Because most of the available water diffused into the gel particles, which swelled to cause surface expansion of the bed as a whole, the rate of surface movement was higher than the rate of wetting front advance.

Figures 4.8 and 4.10 also show that the surface movement, unlike the wetting front advance, is initially more rapid for higher dosages. This is due to the formation of the gel layer. As discussed in Section 4.2, a gel layer forms in about 1 minute and its thickness depends on gel type and dosage.

4.4. MODELS

Two models are described below for flow in gel-conditioned sand: the Swelling Soil (SS) model and the Instantaneous Equilibrium (IE) model. The SS model considers gel swelling to be a function of time, whereas the IE model assumes swelling to be instantaneous. The SS model lumps the gel particles and the void spaces, whereas the IE model makes a distinction between the void phase and the gel phase. The model assumes the ratio of void phase volume fraction and the sand phase volume fraction to be a constant. Both SS and IE models make use of modified Darcy's law for flow through porous media which accounts for relative velocity of liquid with respect to solids. The IE model predicts the gel dosage for column plugging, whereas the SS model is unable to do so. Neither model includes the gel layer. This is not a shortcoming for situations with low gel dosages.

SWELLING SOIL MODEL

Flow through gel conditioned sand is similar to flow through clay soils; which expand as water infiltrates. The model of Philip (1969, 1972) for flow through unsaturated clay is extended to describe flow through gel-conditioned sand.

The actual gel-conditioned sand is replaced by a fictitious continuum. The continuum approach is useful because the variables and parameters averaged over a physical point or a representative volume which allow easy description of flow. In general, for porous media, as opposed to fluids, a coarser level of averaging is used – to the macroscopic level. Both gel-conditioned sand and clay can be classified as porous media, however, there is one essential difference. Clay is composed of swellable particles only. Gel-conditioned sand, on the other hand, is composed of discrete swellable gel particles uniformly distributed in non-swellable sand. The final size of a gel particle may be several times larger than the size of a typical pore space. To circumvent this difficulty, it must be kept in mind that the continuum approach applied to gel-conditioned sand involves a coarser level of averaging than the one for clay, and is thus two levels higher than the one used for fluids.

The soil medium is assumed to be composed of two phases: the solid phase (s) and aqueous phase (a) so that

$$\Theta_s + \Theta_a = 1 \qquad (4.1)$$

where Θ_i is the volume fraction of phase *i*. The gel particles are subsumed by the aqueous phase.

For one-dimensional nonsteady flow, assuming that the phases have constant densities, the continuity equation for each phase is

$$\frac{\partial \Theta_i}{\partial t} = -\frac{\partial}{\partial z}\left(\Theta_i \mathbf{u}_i\right) \qquad (4.2)$$

where *t* is the time, $\mathbf{u}_i$ is the velocity of phase *i*, and the product $\Theta_i\mathbf{u}_i$ is the volumetric flux density or the volume of phase *i* crossing a stationary unit area in unit time. The volumetric flux density is separated into two contributions: a convective flux at the velocity of the solid phase and a flux relative to the solid phase, $\mathbf{v}_r$.

$$\Theta_a \mathbf{u}_a = \mathbf{v}_r + \Theta_a \mathbf{u}_s \qquad (4.3a)$$

Darcy's law is applied to the flow of aqueous phase relative to the solid phase:

$$\mathbf{v}_r = -K_h(\Theta_s)\nabla\Psi \qquad (4.3b)$$

where K_h is the hydraulic conductivity, which is a function of the volumetric sand fraction, Θ_s, and $\nabla\psi$ is the gradient of total potential.

Water moves into an initially unsaturated gel-conditioned sand in response to a gradient of total potential. The total potential is composed of four components: the matric, over-burden, osmotic, and gravitational potentials. Assuming that the components of the overall potential are independent of each other and, hence, additive

$$\Psi = \Psi_m + \Psi_{ob} + \Psi_{os} + \Psi_g \qquad (4.4)$$

The component ψ_m, the matric potential, results from capillary and adsorption effects in soils due to interaction of water and solid soil particles. It is assumed to be a function of Θ_a alone. The overburden potential, ψ_{ob}, is related to the work performed to realize the movement of soil particles against gravity. It is equal to $g\gamma z\Theta_s$, where g is the acceleration of gravity, γ is equal to the ratio ρ_s/ρ_w, and z the elevation. The osmotic potential, ψ_{os}, is related to the swelling potential of the gels discussed in Chapter 2. This term ψ_{os} accounts for the presence of the gel. It is assumed to be a function of Θ_a alone. The gravitational potential, ψ_g, is the potential energy due to gravity and is equal to gz.

For one-dimensional flow in the z-direction, substituting Equation 4.4 in 4.3a yields

$$\mathrm{v}_r = -K(\Theta_s)\left[\frac{d(\Psi_m + \Psi_{os})}{d\Theta_s}\frac{\partial\Theta_s}{\partial z} + g(1-\gamma\Theta_s)\right] \qquad (4.3c)$$

or

$$\mathrm{v}_r = -\left[D_{soil}\frac{\partial\Theta_s}{\partial z} + \Omega_{soil}\right] \qquad (4.3d)$$

where

$$D_{soil} = K(\Theta_s)\frac{d(\Psi_m + \Psi_{os})}{d\Theta_s} = D^{\circ}_{soil}\Theta_s^{\alpha} \qquad (4.5a)$$

$$\Omega_{soil} = K(\Theta_s)g(\gamma\Theta_s - 1) = \Omega^{\circ}_{soil}\Theta_s^{\eta} \qquad (4.5b)$$

and D°_{soil}, Ω°_{soil}, α, and η are constants. It is customary to assume such simple composition dependence of the coefficients, which are difficult to determine experimentally (Smiles, 1986).

Combining Equations 4.1-4.3d and 4.5a-4.5b gives the following equation for water infiltration into a homogeneous medium of uniform initial moisture content

$$\frac{\partial\Theta_s}{\partial t} = D_{soil}\Theta_s\frac{\partial\Theta_s}{\partial z} + \frac{\partial(D_{soil}\Theta_s)}{\partial\Theta_s}\left(\frac{\partial\Theta_s}{\partial z}\right)^2 + \frac{\partial(\Omega_{soil}\Theta_s)}{\partial\Theta_s}\left(\frac{\partial\Theta_s}{\partial z}\right) \qquad (4.6)$$

For the infiltration of water into a homogeneous medium of uniform initial moisture content the boundary and initial conditions are

$$\text{at } t = 0, \quad \Theta_s = \Theta_s^{\circ} \quad \text{for } 0 \le z \le Z \tag{4.7a}$$

$$\text{at } z = Z, \quad \Theta_s = \Theta_s^{\infty} \quad \text{for } t > 0 \tag{4.7b}$$

$$\text{at } z = 0, \quad \frac{\partial \Theta_s}{\partial z} = 0 \quad \text{for } t \ge 0 \tag{4.7c}$$

The Equations 4.6-4.7c involve a moving boundary. They become much simpler by recasting them from their Eulerian form to Lagrangian form using a material coordinate based on the solid phase. This fixes the position of the boundary. Defining the material coordinate , *m* (*z*,*t*), such that

$$\frac{dm}{dz} = \Theta_s \tag{4.8a}$$

and using *M* as the initial position of the surface of the gel-conditioned sand given by

$$M = \int_0^{Z(0)} \Theta_s^{\circ} dz \tag{4.8b}$$

one arrives at the following transformed coordinate form of Equation 4.6:

$$\frac{\partial \Theta_s}{\partial t} = D_{\text{soil}} \Theta_s^2 \left[\Theta_s \frac{\partial^2 \Theta_s}{\partial m^2} + \alpha \left(\frac{\partial \Theta_s}{\partial m} \right)^2 \right] + \Omega_{\text{soil}} \Theta_s \left(\Theta_s + \eta \right) \left(\frac{\partial \Theta_s}{\partial m} \right) \tag{4.9}$$

The transformed boundary and initial conditions are

$$\text{at } t = 0, \quad \Theta_s = \Theta_s^{\circ} \quad \text{for } 0 \le m \le M \tag{4.10a}$$

$$\text{at } m = M, \quad \Theta_s = \Theta_s^{\infty} \quad \text{for } t > 0 \tag{4.10b}$$

$$\text{at } m = 0, \quad \frac{\partial \Theta_s}{\partial m} = 0 \quad \text{for } t \ge 0 \tag{4.10c}$$

INSTANTANEOUS EQUILIBRIUM MODEL

The bed is assumed to consist of sand, voids between sand particles, and gel particles — see Figure 4.11.

$$\varepsilon_s + \varepsilon_v + \varepsilon_g = 1 \tag{4.11}$$

where ε_s, ε_v, and ε_g are the volume fractions of sand, voids, and gel, respectively. Before water is added

$$\varepsilon_s^{\circ} + \varepsilon_v^{\circ} + \varepsilon_g^{\circ} = 1 \qquad (4.12)$$

where ε°_s, ε°_v, and ε°_g are the initial volume fractions of sand, voids, and gel, respectively.

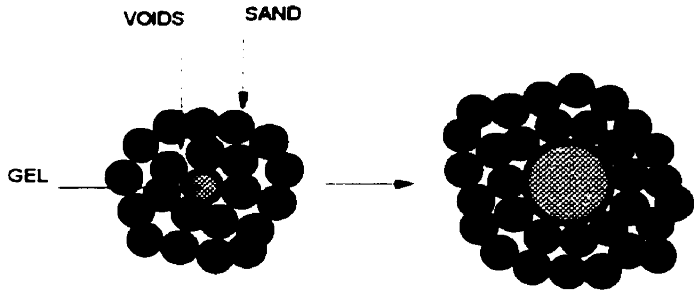

FIGURE 4.11 Three separate phases of a gel-conditioned sand element.

Assume that the gel particles swell instantaneously to their equilibrium size, Φ, as the wetting front (z=L) passes. Also assume that Φ is independent of position, hence there is no variation of ε_g, ε_s, and ε_v between z=-l and z=L. As shown in Figure 4.12, the original position of the surface is z=0; with downward movement considered as positive.

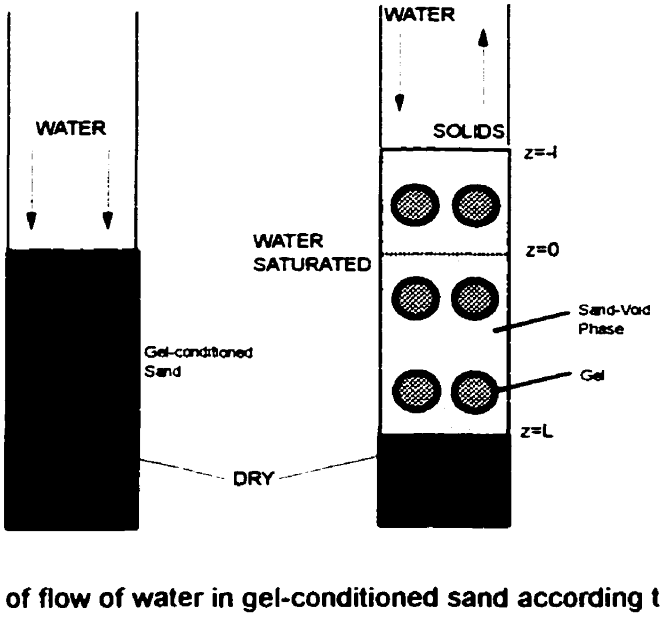

FIGURE 4.12 Schematic of flow of water in gel-conditioned sand according to Instantaneous Equilibrium model.

A water balance gives

$$\frac{Q}{A} = (\varepsilon_v + \varepsilon_g - \varepsilon_g^{\circ})\frac{d}{dt}(L + l) \tag{4.13a}$$

Neglecting the original volume of the gel because $\varepsilon_g^{\circ} << \varepsilon_g$ yields

$$\frac{Q}{A} = (\varepsilon_v + \varepsilon_g)\frac{d}{dt}(L + l) \tag{4.13b}$$

A sand balance gives

$$\varepsilon_s(L + l) = \varepsilon_s^{\circ} L \tag{4.14a}$$

$$L + l = (\frac{\varepsilon_s^{\circ}}{\varepsilon_s})L \tag{4.14b}$$

Assume the sand phase and the void phase have the same volume fraction ratio the had initially:

$$\frac{\varepsilon_v}{\varepsilon_s} = \frac{\varepsilon_v^{\circ}}{\varepsilon_s^{\circ}} \tag{4.15}$$

Combining 4.11, 4.12, and 4.15 gives

$$\frac{\varepsilon_s}{\varepsilon_s^{\circ}} = \frac{1 - \varepsilon_g}{1 - \varepsilon_g^{\circ}} \tag{4.16a}$$

Noting that $\varepsilon_g^{\circ} << 1$

$$\frac{\varepsilon_s}{\varepsilon_s^{\circ}} \approx 1 - \varepsilon_g \tag{4.16b}$$

Combining 4.13b, 4.14b, and 4.16b

$$\frac{Q}{A} = (\frac{\varepsilon_v + \varepsilon_g}{1 - \varepsilon_g})\frac{dL}{dt} \tag{4.17}$$

Now consider the gel

Final gel volume=V^{∞}=$(L$+l$)\varepsilon_g A$ (4.18a)

Initial gel volume=V°=$L\ \varepsilon_g^{\circ} A$ (4.18b)

where A is the cross-sectional area of the column.

The gel swelling ratio is given by

$$\Phi = \frac{V^{\infty}}{V^{\circ}} \tag{4.19}$$

Combining 4.18a, 4.18b, and 4.19 gives

$$\varepsilon_g = \frac{\Phi\varepsilon_g^{\circ}}{1+\Phi\varepsilon_g^{\circ}} \tag{4.20}$$

From 4.15, 4.16b, and 4.20

$$\varepsilon_v = \frac{\varepsilon_v^{\circ}}{1+\Phi\varepsilon_g^{\circ}} \tag{4.21}$$

Combining 4.17, 4.20, and 4.21

$$\frac{Q}{A} = (\varepsilon_v^{\circ} + \Phi\varepsilon_g)\frac{dL}{dt} \tag{4.22}$$

The volumetric flux density is separated into two contributions: a component of flux relative to the sand phase and a convective flux

$$\frac{Q}{A} = \frac{k\,\Delta P}{\mu(L+l)} - \varepsilon_v\frac{dl}{dt} \tag{4.23}$$

where k is the permeability of medium and μ is the viscosity of the fluid. Equation 4.23 is identical to Equation 4.3a. Assuming that the liquid head above the bed (i.e. above z=-l) is constant, ΔP is constant and

$$\frac{Q}{A} = \frac{\beta}{(L+l)} - \varepsilon_v\frac{dl}{dt} \tag{4.24}$$

where $\beta = \frac{k\,\Delta P}{\mu}$ is a constant.

From 4.14b and 4.16b

$$l = \frac{\varepsilon_g}{1-\varepsilon_g}L \tag{4.25}$$

or

$$\frac{dl}{dt} = \frac{\varepsilon_g}{1-\varepsilon_g}\frac{dL}{dt} \tag{4.26}$$

The initial condition is

at t=0, L=0 (4.27)

Combining 4.17, 4.24, 4.26, and 4.27 gives

$$L = \left[\frac{2\beta(1-\varepsilon_g)^2 t}{\varepsilon_v(1+\varepsilon_g)+\varepsilon_g} \right]^{1/2} \tag{4.28}$$

Substituting 4.20 and 4.21 into 4.28 gives

$$L = \lambda t^{1/2} \tag{4.29a}$$

where

$$\lambda = \left[\frac{2\beta}{\varepsilon_v^\circ(1+2\Phi\varepsilon_g^\circ)+\Phi\varepsilon_g^\circ(1+\Phi\varepsilon_g^\circ)} \right]^{1/2} \tag{4.29b}$$

If no gel is present ($\varepsilon_g^\circ = 0$) the above equation reduces to

$$L_\circ = \lambda_\circ t^{1/2} \tag{4.30a}$$

where

$$\lambda_\circ = \left(\frac{2\beta_\circ}{\varepsilon_v^\circ} \right)^{1/2} \tag{4.30b}$$

For the same time the ratio of distances without gel to with gel is

$$\frac{L_\circ}{L} = \left(\frac{\beta_\circ}{\beta} \right)^{1/2} \left[1+2\Phi\varepsilon_g^\circ + \frac{\Phi\varepsilon_g^\circ}{\varepsilon_v^\circ}\left(1+\Phi\varepsilon_g^\circ\right) \right]^{1/2} \tag{4.31}$$

In equation 4.31

$$\frac{\beta_\circ}{\beta} = \frac{k_\circ}{k} \tag{4.32}$$

where k_o is the permeability when no gel is present and k is the permeability with gel. If the only effect of the gel is to block a fraction (ε_g) of the cross-section, it is expected

$$\frac{k_\circ}{k} = \frac{1}{1-\varepsilon_g} = 1+\Phi\varepsilon_g^\circ \tag{4.33}$$

Finally from 4.31 - 4.33

$$\frac{L_\circ}{L} = \left(1+\Phi\varepsilon_g^\circ\right)^{1/2}\left(1+2\Phi\varepsilon_g^\circ+\frac{\Phi\varepsilon_g^\circ}{\varepsilon_v^\circ}\left(1+\Phi\varepsilon_g^\circ\right)\right)^{1/2} \tag{4.34}$$

GEL DOSAGE FOR COLUMN PLUGGING

As the gel dosage is increased, the volume occupied by the gels inside the column becomes greater, which decreases rate of water flow through sand. Thus a critical dosage must exist for complete plugging of the column.

Rearranging Equation 4.20 gives

$$\varepsilon_g^\circ = \frac{\varepsilon_g}{(1-\varepsilon_g)\Phi} \tag{4.35}$$

Assume that the column will become plugged only if ε_g° is greater than the value which gives ε_g corresponding to the closest packing of uniform spheres (which corresponds to ε_g=0.74).

Hence

$$\varepsilon_g^\circ = \frac{0.74}{0.26\Phi} = \frac{2.85}{\Phi} \tag{4.36}$$

Let f_g° be the mass fraction of gel corresponding to the volume fraction ε_g°.

$$f_g^\circ = \frac{\varepsilon_g^\circ\rho_g}{(1-\varepsilon_v^\circ-\varepsilon_g^\circ)\rho_s+\varepsilon_g^\circ\rho_g} \tag{4.37}$$

where ρ_s is the density of sand.

Since . $\varepsilon_g^\circ << \varepsilon_v^\circ$ and $\rho_s >> \rho_g$

$$f_g^\circ = \frac{\varepsilon_g^\circ\rho_g}{(1-\varepsilon_v^\circ)\rho_s} \tag{4.38}$$

Assuming ε_v° =0.4 and ρ_s/ρ_g= 2.5

$$f_g^\circ = \frac{1.9}{\Phi} \tag{4.39}$$

4.5. COMPARISON OF EXPERIMENTS WITH MODELS

FITTING SWELLING SOIL MODEL

Equations 4.9-4.10c were solved numerically by using the Crank-Nicolson central difference scheme. The discretization, and the convergence and accuracy of the numerical computations for similar, but not identical, equations are discussed in Singh (1993). Results are presented here as the distance from the position of the surface at time zero versus the time.

The four unknowns in the model are D°_{soil}, α, Ω°_{soil} and η. These parameters were estimated by minimizing the following objective function:

$$\Im = \sum_{i=1}^{n}\left[\text{Distance}_i^{exp} - \text{Distance}_i^{model}\right]^2 \qquad (4.40)$$

where n is the number of experimental points.

Figure 4.13 shows the fitting of Swelling Soil model with four parameters to the data for no gel, two Sumitomo (Φ=300) gel dosages, and one Stockosorb (Φ=100) gel dosage in 190 μm sand. The plot shows simultaneously surface movement and wetting front advance.

The curves represent the best fits which were obtained using parameter values listed in Table 4.2. The fits of the model to the experimental data were reasonably good. Lower gel dosages and gels with lower swelling ratio are associated with higher D_{soil}, and Ω_{soil}. This is consistent with the values of coefficients reported for sandy soils with varying clay content (Hillel, 1980). The values of K_h determined from the coefficient Ω_{soil} have the order of magnitude 10^{-4} m/s; which lies within the range of literature values of 10^{-7}-10^{-2} m/s (Bardett, 1997).

A 25% increase in the values of the parameters D°_{soil}, α, Ω°_{soil} and η makes the surface movement increase by 45%, 67%, 31%, and 22%, respectively, and makes the wetting front advance increase by 34%, 53%, 22%, and 14% respectively. Thus, both surface movement and wetting front advance are more sensitive to D_{soil} than Ω_{soil}.

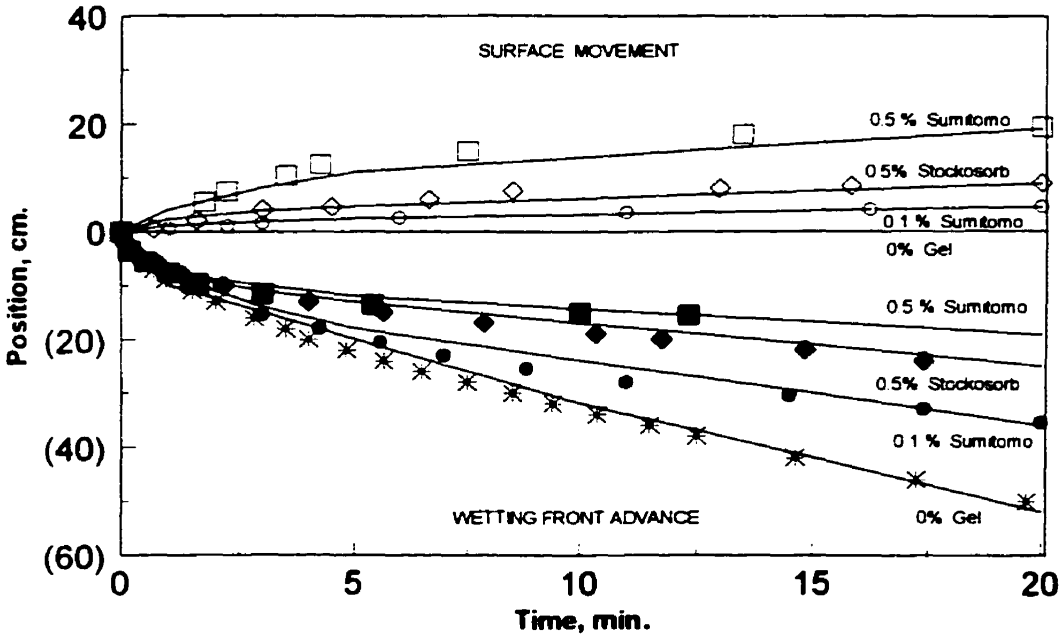

FIGURE 4.13. Best fits of Swelling Soil Flow model to the wetting front advance and surface movement data for different gels and gel dosages in 190 μm sand. (0% Gel: ✱), (0.1% Sumitomo: o,•), (0.5% Sumitomo: ☐, ■), (0.5% Stockosorb: ◇, ◆). The parameter values are listed in Table 4.2

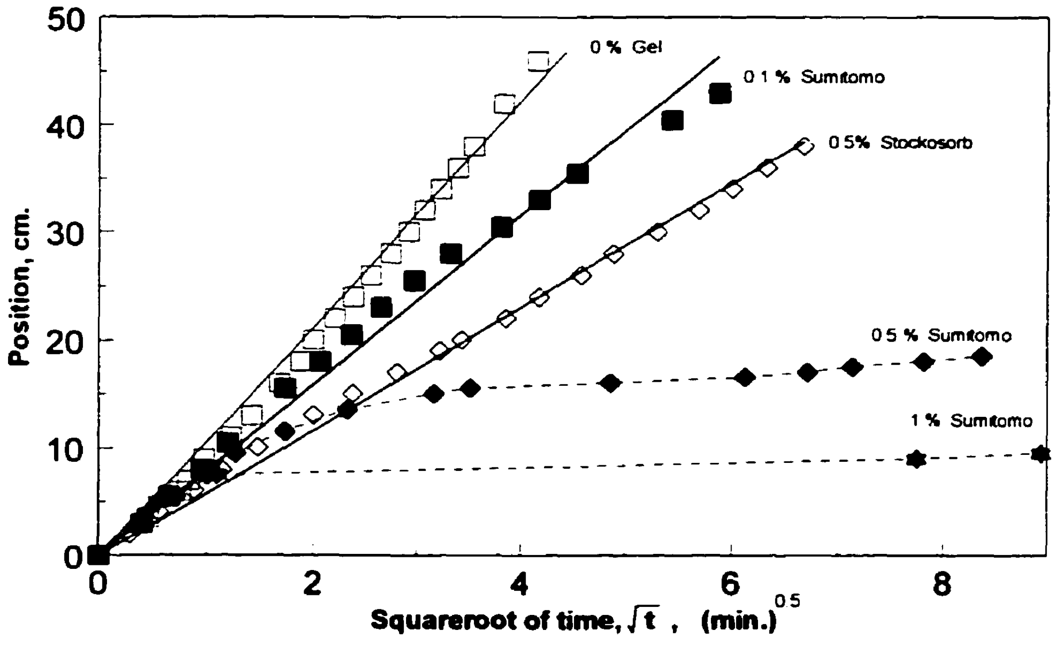

FIGURE 4.14. Best fits (bold lines) of Instantaneous Equilibrium model to the wetting front advance data for different gels and gel dosages in 190 μm sand. (0 %: ☐), (0.1% Sumitomo: ■), (0.5% Stockosorb: ◇), (0.5% Sumitomo: ◆), (1% Sumitomo: ✱). The dotted lines are drawn to guide the eye.

TABLE 4.2. Estimated parameter values in the Swelling Soil model for different gel dosages and types in sand.

DOSAGE	D^{o}_{soil}, m/s^2	α	Ω^{o}_{soil}, m^2/s^3	β
0%	1.2×10^{-5}	-0.5	0	0
0.1% (Sumitomo)	1.0×10^{-5}	0	1.6×10^{-3}	-1.5
0.5% (Stockosorb)	1.0×10^{-5}	0	1.6×10^{-3}	-1.4
0.5% (Sumitomo)	0.8×10^{-5}	0	1.6×10^{-3}	-1.1

FITTING INSTANTANEOUS EQUILIBRIUM MODEL

The value of permeability, k, varies widely for different soils. It is dependent on several factors: fluid viscosity, pore-size distribution, grain-size distribution, void ratio, roughness of mineral particles, and degree of saturation. Typical values of k for fine sand lie in the range 10^{-11}-10^{-7} m^2 (Das, 1985). The permeability, k_o, of gel-free sand was obtained from the slope of the wetting front advance curve in Figure 4.9. Its value was 4×10^{-10} m^2. The permeability, k, of gel conditioned sand was obtained from Equation 4.33.

The Instantaneous Equilibrium model with a single parameter, λ, was fitted to the data for various Sumitomo gel dosages in 190 μm sand as shown in Figure 4.14. The only unknown contained in λ was the instantaneous swelling ratio. The value of ε°_{v} was experimentally determined to be approximately equal to 0.4. The curves were generated by the model. The best fit values of λ for dosages of 0, 0.1, 0.5% were 10.6, 7.6, 2.4 cm/min$^{1/2}$, respectively. As expected from Equations 4.19 and 4.20, the curves follow a linear relationship with $\sqrt{t}$. These values correspond to an instantaneous swelling ratio of 100 and 150 for dosages of 0.1 and 0.5%, respectively. The best fit value for 0.5% Stockosorb gel dosage in 190 μm sand was 5.2 cm/min$^{1/2}$. This value corresponds to an instantaneous swelling ratio of 50. For 0.5% gel dosage for both Sumitomo and Stockosorb gels, the values of instantaneous swelling ratios obtained through fitting were a factor of 2 less than the average equilibrium swelling ratios obtained in Chapter 2.

For higher dosages the model is unable to capture the experimental curves at long times. However, it is able to predict the critical dosages required to prevent movement of the wetting front. Calculations based on this idealized model, which assumes instantaneous swelling of gel particles, predict the minimum value of gel dosage required for plugging the water flow at $\Phi=300$ is 0.63%. This is in good agreement with experimental data: A 0.5% dosage of Sumitomo gels with Φ equal to 300 slows the wetting front advance tremendously, whereas a dosage of 1% stops it completely.

Chapter 5

CONCLUSIONS AND RECOMMENDATIONS

5.1. CONCLUSIONS

Swelling equilibrium and kinetics of commercially available superabsorbent gel particles (Sumitomo's sodium polyacrylate spheres and Stockosorb's polyacrylamide-co-potassiumacrylate grains) were studied in water and in water-saturated sand at room temperature. Water flow in gel-conditioned sand was also investigated. Four narrowly sieved sand diameters were used: 720, 475, 300, 190 μm

Equilibrium experiments involved swelling gel particles at different depths in saturated sand columns packed with different sand sizes. The most striking feature of data on swelling was precipitous drop in swelling ratio near the sand surface. In the first centimeter, it dropped from 550 to 385 for Sumitomo gels and from 170 to 146 for Stockosorb gels. This behavior was much different from the action of hydrostatic pressure alone, which had a weak effect on the swelling behavior of both gels. When the gels were swollen in a water column the swelling ratio decreased, but the decrease was less than 13% at the 55 cm depth. With increasing depths, the swelling ratio in saturated sand, dropped further but much less rapidly. For instance, in case of Sumitomo gels in 190 μm sand size it dropped from 390 at 1 cm depth to 250 at 55 cm depth.

The sand particle size, over the range studied, had a little effect on the swelling ratio at depths close to surface, however, at increasing depths it had a stronger effect on swelling. For instance, for Sumitomo gels swelling at a 1 cm depth the swelling degrees were 395 and 390 for 720 μm and 190 μm sand particle diameters, respectively. In contrast, at a depth of 55 cm the swelling degrees were 330 and 250 for 720 μm and 190 μm sand particle diameters, respectively.

The shrinking of gels was not the reverse of swelling, although like swelling, shrinking was a function of sand particle diameter. For larger sand particle diameters, both gels underwent a small drop in swelling ratio in the first few centimeters of depth followed by little change in swelling at increasing depths. For smaller sand particle diameters, both gels underwent a precipitous drop in swelling ratio in the first few centimeters of depth followed by little change in swelling at increasing depths.

Both swelling and shrinking were performed in top loaded columns. Gel particles were buried at 1 cm below the sand surface beneath a steel cylinder of weight equal to 55 cm of saturated sand. In swelling experiments, the equilibrium swelling ratio was 40% below its value when buried 55 cm deep in saturated sand. In shrinking experiments, the equilibrium swelling ratio was close to its value when buried 55 cm deep in saturated sand. This unusual swelling and shrinking behavior is ascribed to the arching phenomenon.

The Flory-Cavity model was developed to describe the swelling equilibrium in saturated sand. The model was based on the Flory model for polymer gels and the Cavity Expansion model for frictional soil. The model was fitted to the data for Sumitomo and Stockosorb gels. The gel-elasticity parameter, K, was obtained by fitting the Flory model to the data for gel swelling in water. The polymer-water interaction parameter, χ, was obtained from the literature; the friction angle, ϕ, and the dilatation angle, ψ, were estimated from published correlations. The shear modulus, G, which was the only fitted parameter, which varied with the mean effective stress, P_o, according to $G = \gamma(P_o - P_{atm})^{\varepsilon}$; where γ and ε are constants and P_{atm} is the atmospheric pressure. The Flory-Cavity

Model provided a good fit to the experimental data for swelling in sand. The best fit values of γ were equal to 3.5 MPa and 2 MPa for 190 μm and 474 μm sand sizes, respectively. The exponent ε was equal to 1.5 for both sand sizes.

The Flory-Cavity model was also used to predict swelling ratios in columns of different diameters. These predictions extend the results of this work to gels swelling in fields, assumed as a column of infinite diameter.

Kinetic experiments were performed in a two-dimensional cell in order to visualize the swelling gel particles in sand. Both gel particle size and sand particle size were varied. Sand altered the swelling properties of gels. However, the relationship between the fractional approach to equilibrium (F) and the square root of time ($\sqrt{t}$) was sigmoidal for gel swelling in water and in saturated sand.

Gel Volume Change model was extended to describe the kinetics of swelling in water and in sand. The model was based on Fick's first law and accounted for the movement of the boundary of the gel. A simple form of time variation of surface polymer volume fraction was postulated, which used a single parameter: the boundary time constant, t_κ. Numerical computations for gel spheres were performed with a constant diffusion coefficient and a constant dimensionless boundary time constant, τ_κ. The fractional approach to equilibrium was a function of the dimensionless time τ, the volume ratio, Φ, and the dimensionless boundary time constant, τ_κ. The swelling curves with increasing τ_κ values lay to the right of the curve for $\tau_\kappa = 0$ for a given volume change or swelling ratio. In addition, increasing τ_κ made the sigmoidal portion increasingly pronounced.

Experimental data for both Sumitomo and Stockosorb gels in water and in sand were fitted by the model using two parameters. For swelling in water the two unknowns in the model were the diffusion coefficient, D_m, and the relaxation time constant, t_κ. The best fit values of D_m for Stockosorb and Sumitomo were 1.0×10^{-9} and 8.3×10^{-10} m^2/s, respectively. Both gels had an identical t_κ equal to 24 s. For swelling in sand the mutual diffusion coefficient was replaced with an effective diffusion coefficient, D_{eff}, expressed by the product of D_m and and ω, the retardation factor. The best fit values of D_{eff} for Stockosorb and Sumitomo gels were 3.0×10^{-10} and 2.3×10^{-10} m^2/s, respectively. Both gels had identical boundary time constants of 24 s. The retardation factor, ω, was equal to 0.3 independent of sand size, sand saturation, gel type, and gel size.

Flow experiments were conducted in columns as well as in two-dimensional cells. When water was distributed over the surface of a dry uniform sand/gel bed, it led to:

- the formation of a gel layer on the surface
- the formation of a wetting front which moved downward
- the upward movement of the surface in response to the swelling of the subsurface gel particles.

The gel layer formed because the gel particles, initially in the soil matrix, were set free by the impact of the water on the upper layer of the sand-gel mixture. The released gel particles, which had a specific gravity close to that of water, settled much less rapidly than sand particles and thus they remain suspended in the water for some time. One minute after the initial disturbance of the dry sand-gel mixture, the water-borne particles settled on the surface to form a swelling gel layer.

The thickness of the gel layer was dictated by several variables. It was thicker for coarser sand, higher gel dosage, and higher gel swelling degree. The gel particles, which formed the gel layer came from a gel-conditioned sand layer approximately 1 cm deep.

Gels modified flow in sand. The advance of the wetting front was impeded as gel dosage was increased. At 1% dosage the wetting front ceased to advance because the gel particles expanded to plug the cross section and prevent further downward flow of water. In contrast, surface movement increased with gel dosage. When no gel was present (0%) the surface remained at its initial position. For a dosage of 0.5%, Sumitomo gels caused more surface movement and less wetting front advance than Stockosorb gels.

Two models were developed to describe flow in gel-conditioned sand. Philip's Swelling Soil model for flow through clays was extended to describe flow through gel-conditioned sand by reinterpreting the osmotic potential term. The model was based on Darcy's law and accounted for the expansion of soil bed. Experimental data for both Sumitomo and Stockosorb gel conditioned sand were fitted by the model using four parameters. The Instantaneous Equilibrium accounted for the movement of sand particles and assumed instantaneous swelling of gel particles. Experimental data for both Sumitomo and Stockosorb gel conditioned sand were fitted by the model using an instantaneous swelling ratio. The model predicted a critical dosage for complete plugging of the column, equal to 0.63 %, which is close to the experimentally determined dosage which lies between 0.5 and 1 %.

5.2. CONTRIBUTIONS TO KNOWLEDGE

The contributions to knowledge resulting from this study are

- Observed the following phenomenon upon swelling of commercial gel particles in sand
    - rapid drop of swelling degree with depth with first few cms in saturated sand.
    - arching phenomena
    - the relationship between the fractional approach to equilibrium (*F*) and the square root of time ($\sqrt{t}$) in saturated sand was sigmoidal
    - formation of gel layer
- Elucidated the mechanism of the formation of gel layer at the surface of uniformly gel-conditioned sand.

- Combined the Flory model and the Cavity expansion model to describe swelling equilibrium of gels in saturated sand.
- Extended the Gel Volume Change model for kinetics of swelling of gels by including the effect of time variable surface boundary condition in order to describe swelling in sand.
- Extended the Swelling Soil model to describe water flow in gel-conditioned sand.
- Developed the Instantaneous Equilibrium model to describe water flow in gel-conditioned sand.

5.3. RELEVANCE OF THIS STUDY TO AGRICULTURAL APPLICATIONS

This work was conducted to answer some basic questions related to the ultimate use of superabsorbents as in-soil reservoirs in agricultural fields. Since the scientific study of gel conditioned soil as a biological system, involving plants, microorganisms, etc., is possible only after a good understanding of simpler systems, this study involved the simplest possible system, composed of gel particles, sand, and water. In this section the present results are related to the use of gels in agricultural fields.

While applying the swelling equilibrium and kinetics results, i.e. the results of Chapters 2 and 3, respectively, to real soils the following must be kept in mind:

- As shown in Chapter 2, the gels are expected to swell less in fields, when compared to swelling in sand columns, owing to the lowering of the silo effect.
- However, the gels are expected to swell more in fields than the predictions of Chapter 2 because of the lowering of the friction angle, which occurs due to the presence of other gel particles around a swelling gel particle.

- Gels are expected to swell faster in fields, when compared to swelling in sand in two-dimensional cells, owing to the absence of the wall effect and the lowering of the friction angle.

In fields, plants begin to wilt when they can no longer absorb soil water fast enough to replace moisture lost by transpiration. If soil water holding capacity is improved by using superabsorbents, the length of time to reach that critically low water level may be increased. Claims are often made by advertisers of commercially available superabsorbents that the use of these materials in soils actually leads to tremendous improvement in soil water holding capacity. Are these claims correct? If so, are the gels equally suitable for shallow (approx. 5 cm penetration) and deep (approx. 30 cm penetration) root systems? The answers to such questions are clear from this study. Even for the worst case scenario i.e. for gels buried 30 cm underneath the sand surface, the Sumitomo gels, for instance, undergo a depression in swelling degree close to 50%, from 550 in water to 300 in sand. A simple calculation shows that for an average swelling degree of 300, at an economically viable gel dosage of 1000 kg/ha, the water holding capacity increases by 300,000 kg/ha, which is a significant improvement.

The formation of the gel layer has profound consequences for field soils because the gel layer may reduce the rate of penetration of water into the soil. A thick gel layer may become essentially impenetrable to water, thereby retaining irrigation water or rainfall on the surface, thus facilitating runoff. Such retained water evaporates quickly and is not available to plant roots which may be located up to 30 cm beneath the soil surface. The gel layer may also act as a seal against the entry of air. Another problem has to do with penetration of seedlings attempting to emerge after germination. However, for erosion control the formation of a gel layer may be beneficial because it binds the sand particles.

Other question indirectly dealt by this study is how the gel type affects swelling in soil. Answers to this question are essential to tailor make gels for specific applications. This study reveals the interplay between the two major gel design variables: Ionic Content and Degree of Crosslinking. The degree of crosslinking of both Stockosorb and Sumitomo is not very different. However, the ionic content of Stockosorb is 40% less than Sumitomo, which makes it swell less in water and in saturated sand. Field soils would require a proper balance between these variables. Thus although it may not be possible to design a perfect superabsorbent polymer, it is possible to optimize products in a given application. This study also suggests that the design problems for gels meant for soil applications are different from the gels meant for the diaper-tampon industry. The major problem for soil gels is not preventing the absorbed water from being squeezed out under pressure; instead, it has to do more with overcoming the frictional forces due to soil particles so as to achieve higher absorbency.

In order to tackle other realistic problems like superabsorbents swelling in saline soils more experiments need to be performed. However, from free swelling experiments it is well known that gels swell less in salt solutions. Divalent cations such as calcium and magnesium inhibit swelling more than monovalent cations like sodium and potassium. This depression in swelling due to dissolved salts can be countered by increasing the gel dosage; if it were economical. Kazanskii and Dubrovskii (1992) mention the failure in employing polyacrylamide gels in sandy soils of the Russian Kara Kum desert. Due to excessive salinity of the Kara Kum soils the improvement of water holding capacity was only minor. The only way to counter such a depression in swelling degree by salts is to work with gels that swell independent of soil salinity. Attempts to make salt tolerant gel types from alternative raw materials have not been entirely successful because the new materials swell no more than 50 times the dry weight (Singh, 1993).

This study raises several important questions for future research. For instance, an important finding was that when a dry gel particle is swollen inside saturated sand, it is unable to swell as much as the particle swollen freely in water. However, when the freely swollen particle is transferred to saturated sand it does not shrink much. For real soil applications, under unsaturated or evaporating conditions, it is worthwhile to investigate whether the cavity surrounding the gel particle, would shrink along with the drying gel particle. If the cavity does not shrink while its gel particle shrinks, the depression in swelling due to the frictional nature of soil may be overcome. After shrinking to its dry state, the particle, in the presence of water, would reswell inside the cavity, thus achieving "free" rather than constrained swelling in sand. Perhaps the best technique of gel application might be injecting fully swollen gel particles below the soil surface, instead of applying them dry.

In case the gels are applied dry, particles much smaller than the size of a typical soil pores might be employed to overcome the frictional nature of soil. If the pores are larger than the fully swollen gel particles, the particles would swell without having to overcome the soil particle friction. In addition, the kinetics of swelling of small gel particles would be the same as the kinetics of swelling of the particles in water.

Another aspect which is sure to keep researchers occupied for years to come is the introduction of plants in the experiments. An improvement in soil water holding capacity is of no consequence if plants have limited access to additional water. To learn whether plant roots are actually able to remove moisture held by gel particles is a major question for agricultural scientists. Preliminary studies claim that more than 95% of the held water is removable in the range of moisture potentials common to plant growth (Kazanskii and Dubrovskii, 1992).

5.3. RECOMMENDATIONS

Although the potential of superabsorbents as in-soil reservoirs for large scale use in fields is clear, much remains to be done. As a follow-up to this work, some pertinent areas for further research would be:

- Investigate superabsorbents in biologically active soils rich in microorganisms and plants; also study the absorption of the gel-retained water by the plants
- Obtain drying data for the two gels studied in this thesis and compare the results.
- Investigate the swelling and drying for gel particles
    - sythesised from different polymer types with variations in polymer amount, crosslinking density, ionizable content, and exchangable ions.
    - of different shapes and size distribution
    - in soils of different pH and salt content.
    - in soils varying in composition, shape, and size distribution of particles
    - in soils with different initial gel distribution and soil water distribution
    - in soils utilizing different methods of water supply.
- Obtain cyclical swelling and drying data for superabsorbents-in-soils.
- Investigate whether the plant roots are actually able to remove moisture held by gel particles in soils.

References

Almdal, K., J. Dyre, S. Hvidt, and O. Kramer (1993). "Towards a Phenomenological Definition of the Term 'Gel'," *Polym. Gels Networks*, **1**, 5.

Al-Darby, A.M., Mustafa, M.A., and A.M. Al-Omran, A.M. (1990). "Effect of Water Quality on Infiltration of Loamy Sand Soil Treated With Three Different Gel-Conditioners," *Soil Techn.*, **3**, 83.

Al-Omran, A.M., Mustafa, M.A., and A.A. Shalaby (1987). "Intermittent Evaporation from Soil Columns as Affected by a Gel-Forming Conditioner," *Soil Sci. Soc. Am. J.*, **51**, 1593.

Al-Omran, A.M., Mustafa, M.A., Al-Darby, A.M., and A.A. Shalaby (1991). "Gel-Conditioned Barriers for Water Management of Sandy Soils," *Irrigation Sci.*, **12**, 7.

Anon (1975) "Super Slurper: Compound with Super Thirst," *Agricultural Research*, 7.

Azzam, R.A.I. (1980). "Agricultural Polymers: Polyacrylamide Preparation, Application and Prospects in Soil Conditioning," *Commun. Soil Sci. Plant Anal.*, **11**, 767.

Azzam, R.A.I. (1983). "Polmeric Conditioner Gels fore Dessert Soils," *Commun. Soil Sci. Plant Anal.*, **14**, 739.

Azzam, R.A.I. (1985). "Tailoring Polmeric Gels For Soil Reclamation and Hydroponics," *Commun. Soil Sci. Plant Anal.*, **16**, 1123.

Azzam, R.A.I. (1986). in Proc6 Tihany Symp on Isot and Rad Chem Siofok, **2**, 649

Bardet, J-P (1997). Experimental Soil Mechanics, Prentice Hall, NJ.

Bassiri, M. and S.N. Harikv (1986). "Soil Application of a Hydrophilic Conditioner in Relation to Moisture, Irrigation Frequency and Crop Growth," *Commun. in Soil Sci. Plant Anal.*, **17**, 573.

Berens, A.R. and H.B. Hopfenberg (1978). "Diffusion and Relaxation in Glassy Polymer Powders," *Polymer*, **19**, 489.

Bird, R.B., W.E. Stewart, and E.N. Lightfoot (1960). Transport Phenomena, Wiley, NY.

Bishop, R.F., Hill, R., N.F. Mott (1945). "Theory of Indentation and Hardness Tests," *Proc. Phys. Soc.*, **57**, 147.

Blodgett, A.M., Beattie, D.J., and J.W. White (1993) "Hydrophilic Polymers and Wetting Agents Absorption and Evaporation Water Loss," *HortScience*, **28**, 633.

Bolton, M.D. (1986). "The Strength and Dilatancy of Sands," *Geotechnique*, **36**, 65.

Brannon-Peppas, L. and R.S. Harland (1990). Absorbent Polymer Technology , (Eds.), Elsevier, NY.

Buchholz, F.L. (1994-a) "Keeping Dry with Superabsorbent Polymers," *Chemtech* 38.

Buchholz, F.L. (1994-b) "A Swell Idea," *Chemistry in Britain* 652.

Buckley, D.J. and M. Berger (1962). "Swelling of Polymer Systems in Solvents. II Mathematics of Diffusion," *J. Polm. Sci.*, **56**, 175.

Bulson, P.S. (1985). Buried Structures, Chapman and Hall, London.

Chadwick, P. (1959). "The Quasi-static Expansion of a Spherical Cavity in Metals and Ideal Solids" *Q. J. Mech. Appl. Math.*, **12**, 52.

Crank, J. and G. S. Park (1951). "Diffusion in High Polymers," *Trans. Faraday Soc.* **47**, 1072.

Crank, J. (1975). The Mathematics of Diffusion , Oxford University Press, London.

Cussler, E. L. (1984). Diffusion , Cambridge University Press, London.

Das, B.M. (1985). Principles of Geotechnical Engineering, PWS Engineering, Boston.

Dellavale, N.B. (1992) "Efficacy of DRiWATER: A Slow Water Release Substrate," *Commun. Soil Sci. Plant Anal.*, **23**, 2547.

Devotta, I., R.A. Mashelkar (1994). "The Life Time of a Dissolving Polymeric Particle," *Chem. Eng. Sci.*, **49**, 645.

El-Shafei, Y.Z., Al-Omran, A.M., Al-Darby, A.M., and A.A. Shalaby (1992) "Influence of Gel-Forming Conditioner on Water Movement in Sandy Soils Under Sprinkler Infiltration," *Arid Soil Research Rehabilitation*, **6**, 217.

Falatah, A.M.and W.A. Al-Mustafa (1993). "The Influence of Gel-Forming Conditioner on pH, pe, and Micronutrient Availability of Two Torrifluvents," *Arid Soil Research Rehabilitation*, **7**, 253.

Flory, P.J. (1979). Principles of Polymer Chemistry , Cornell University Press, Ithaca, NY.

Forrestal, M. J. and V. K. Luk (1988). "Dynamic Spherical Cavity-Expansion in a Compressible Elastic-Plastic Solid," *J. Applied Mech.*, **55**, 275.

Gehrke, S.H. (1986). Kinetics of Gel Volume Change and its Interaction with Solutes, Ph.D. Dissertation. University of Minnesota, U.S.A.

Gehrke, S.H. (1993). "Synthesis, equilibrium swelling, kinetics, permeability and applications of environmentally responsive gels," in Responsive Gels: Volume Transitions II, Advances in Polymer Science, **110**, (Ed. K. Dusek), Springer Verlag, N.Y.

Gibson, R.E. and W.F. Anderson (1961). "In-situ Measurement of Soil Properties with the Pressuremeter," *Civ. Engng. Pub. Wks Rev.*, **56**, 615.

Hemyari, P. and D.L. Nofziger (1981) "Super Slurper Effects on Crust Strength, Water Retention, and Water Infiltration of Soils," *Soil Sci. Soc. of Am. J.*, **45**, 799.

Hillel, D. (1980) Fundamentals of Soil Physics , Academic Press, NY.

Hopkins (1960). "Dynamic Expansion of Spherical Cavities in Metals," in Progress in Solid Mechanics, **1**, (Eds. S.I. Hunter and R. Hill), North-Holland, N.Y.

Hughes, J.M.O., Wroth, C.P. and D. Windle (1977). "Pressuremeter Test in Sands," *Geotechnique*, **27**, 455.

Illavský, M. (1982). "Phase Transition in Swollen Gels. 2. Effect of Charge on Polyacrylamide," *Macromolecules* **15**, 782.

Illavský, M., J. Hrouz, and I. Havlicek (1985) "Phase Transition in Swollen Gels. 7. Effect of Charge Concentration on the Temperature Collapse of Poly(N,N-diethylacrylamide) networks in water," *Polymer*, **26**, 1514.

Jacobson (1958). "On Pressure in Silos," in Proc. Brussels Conference on Soil Mehanics and Foundation Engineering, **1,** UNESCO.

Jansen, H.A. (1895). "Versuche uber Getreidedruck in Silozellen," *Z. Ver. Deut. Ingr.*, **39**, 1045.

Joshi, S. and G. Astarita (1979). "Diffusion-Relaxation Coupling in Polymers which show Two-Stage Sorption Phenomena," *Polymer*, **20**, 455.

Kazanskii, K.S. and S.A. Dubrovskii (1992) "Chemistry and Physics of 'Agricultural' Hydrogels," in Advances in Polymer Science, **104**, 97, Springer-Verlag, Berlin.

Koerner, R.M. (1970). "Effect of Particle Characteristics on Soil Strength," *J. Soil Mech. Found. Eng. Div.*, **96**, 1221.

Komori, T. and R. Sakamoto (1989). "On Tanaka-Fillmore's Kinetics Swelling of Gels," *Colloid Polym. Sci.*, **267**, 179.

Kudela, V. (1986). "Hydrogels," in Encyclopedia of Polymer Science and Engineering., **7**, 783, Wiley-Interscience, NY.

Lamb, T.W. and R.V. Whitman (1979). Soil Mechanics, John Wiley & Sons, NY.

Li, Y. and T. Tanaka (1990). " Kinetics of Swelling and Shrinking of Gels," *J. Chem. Phys.*, **92**, 1365.

Mazich, K.A., G. Rossi, and C.A. Smith (1992). "Kinetics of Solvent Diffusion and Swelling in a Model Elastomeric System," *Macromolecules* **25**, 6929.

Miller, D.E. (1979) "Effect of HSPAN on Water Retained by Soils after Irrigation," *Soil Sci. Soc. Am. J.*, **51**, 1593.

Moore, S. (1993) "Polymers Help Tame the Sahara," *Chem. Eng.*, June-48.

Mustafa, M.A., Al-Omran, A.M., Shalaby, A.S. and A.M. Al-Darby (1988) "Horizontal Infiltration of Water in Soil Columns as Affected by a Gel-forming Conditioner," *Soil Sci.*, **145**, 330.

Mustafa, M.A., Al-Darby, A.M., Al-Omran, A.M., and M. Mursi (1989). "Impact of a Gel-Conditioner and Water Quality upon Soil Infiltration," *Irrig. Sci.*, **10**, 169.

Ogawa, I., Yamano, H. and K. Miyagawa (1993). "Rate of Swelling of Sodium Polyacrylate," *J. Appl. Poly. Sci.* **47**, 217.

Orzolek, M.D. (1993) "Use of Hydrophilic Polymers in Horticulture," *HortTechnology*, **3**, 41.

Peppas, N.A. (Ed.) (1986). Hydrogels in Medicine and Pharmacy , CRC Press, Boca Raton, FA.

Peters, A. and S. Candau (1986). "Kinetics of Swelling of Polyacrylamide Gels," *Macromolecules* **19**, 1952.

Philip, J.R. (1969) "Hydrostatic and Hydrodynamics in Swelling Soils," *Water Resources Research*, **5**, 1070.

Philip, J.R. (1972) "Hydrostatic and Hydrodynamics in Swelling Media," Fundamentals of Transport Phenomena in Porous Media, Elsevier, Amsterdam.

Pieh, S.H. and O.A. El-Hady (1990) "Modified Polyacrylamide Hydrogels as Conditioners for Sandy Soils," *Egypt. J. Soil Sci.*, **30**, 159.

Rossi, G. and K.A. Mazich (1991). "Kinetics of Swelling for a Cross-linked Elastomer or a Gel in the Presence of a Good Solvent," *Phys. Rev. A.* **44**, R4743.

Rossi, G. and K.A. Mazich (1993). "Macroscopic description of the kinetics of swelling for a cross-linked elastomer or a gel," *Phys. Rev. E.* **48**, 1182.

Sassi, A.P., Blanch, H.W. and J.M. Prausnitz (1992). "Crosslinked Gels as Water Absorbents in Separations," in Polymer Applications for Biotechnology, (Ed. D. S. Soane), Prentice Hall, NJ.

Shalaby, A.A. (1993) "Impact of Gel-Conditioned Layer Depths and Water Quality on Water Movement in Sandy Soils," *Arid Soil Research Rehabilitation*, **7**, 281.

Siegal (1993). "Hydrophobic Weak Polyelectrolyte Gels: Studies of Swelling Equilibria and Kinetics," in Responsive Gels: Volume Transitions I, Advances in Polymer Science, **109**, (Ed. K. Dusek), Springer Verlag, N.Y.

Singh, J. (1993). Swelling of Polymer Gels, M.Eng. Dissertation, McGill University, Montreal, Canada.

Singh, J. and M.E. Weber (1996). "Kinetics of One-dimensional Gel Swelling and Collapse for Large Volume Change," *Chem. Eng. Sci.* **51**, 4499.

Smiles, D.E. and M.J. Rosenthal. (1968) "The Movement of Water in Swelling Materials," *Aust. J. Soil Res.*, **6**, 237.

Sparrow, E.M. and W. Chuck (1984). "An Implicit/Explicit Numerical Solution Scheme for Phase-Change Problems," *Numer. Heat Trans.* **7**, 1.

Sposito, G., Giraldez, J.V., and R.J. Reginato. (1976) "The Theoretical Interpretation of Field Observations of Soil Swelling Through a Material Coordinate Transformation," *Soil Sci. Soc. of Am. J.*, **40**, 208.

Swanson, C.L.W. (1953). "Soil Conditioners," *Scientific American*, August-36.

Tanaka, T, L.O. Hocker, and G.B. Benedek (1973). "Spectrum of Light Scattered from a Viscoelastic Gel," *J. Chem. Phys.*, **59**, 5151.

Tanaka, T. and D. Fillmore (1979). "Kinetics of Swelling of Gels," *J. Chem. Phys.*, **70**, 1214.

Tanaka, T., E. Sato, Y. Hirokawa, S. Hirotsu, and J. Peetermans (1985). "Critical Kinetics of Volume Phase Transition of Gels," *Phys Rev Lett* **55**(22), 2455.

Tanaka, T. (1986). "Gels," in Encyclopedia of Polymer Science and Engineering., **7**, 517, Wiley-Interscience, NY.

Tayel, M.Y. and O.A. El-Hady (1981). "Super Gel as a Soil Conditioner 1. Its Effect on Some Soil-Water Relations," *Acta Horticulturae*, **119**, 247.

Terzaghi, K. (1943). Theoretical Soil Mechanics, Chapman and Hall, London.

Vasheghani-Farahani, E. (1990). Swelling and Exclusion Behavior of Hydrogels, Ph.D. Dissertation, McGill University, Montreal, Canada.

Vasheghani-Farahani, E., J.H. Vera, D.G. Cooper and M.E. Weber (1991). "Swelling of Ionic Gels in Electrolyte Solutions," *Ind. Eng. Chem. Res.* **29**, 554.

Viollaz, P.E. and C. Suarez (1994). "An exact solution of the diffusion equation with shrinking," *Chem. Eng. J.* **55**, 135-138.

Vrentas, J.S. and J.L. Duda (1986). " Diffusion," in Encyclopedia of Polymer Science and Engineering , **5**, 36, Wiley-Interscience, NY.

Woodhouse, J. and M.S. Johnson (1991) "Effect of Superabsorbent Polymers on Survival and Growth of Crop Seedlings," *Agricultural Water Management*, **20**, 63.

Withers (1989). "Performance and Analysis of Cone Pressuremeter Tests in Sand," *Geotechnique*, **39**, 433.